POSITION MEASUREMENT

USING

GRATINGS AND CODED PATTERNS

John Thomas MacSween Stevenson

A Thesis Submitted for

The Degree of Doctor of Philosophy

to

The University of Edinburgh

1987

To my children,

Anne and John

ABSTRACT

The manufacture of metrological gratings and the design of associated moiré fringe reading heads is reviewed. The advantages of absolute, incremental and hybrid position transducers are discussed and the main types of linear position encoder are described. The use of optical position sensing in microfabrication is reviewed with emphasis on the problem of mask to wafer alignment during photolithography.

Novel designs of one-dimensional and two-dimensional optical position encoders, with a parallel fringe interpolation technique for additional accuracy, are introduced. Their practical implementation, both in small-scale instrumentation and on a larger scale in automated manufacturing systems, is described. Experiments on the use of reflecting gratings manufactured on silicon using microfabrication techniques are reported. The results are applied to the design of a dynamic alignment system using gratings and moiré fringe detection to measure mask to wafer alignment in a new design of 'flash-on-the-fly' wafer stepper. The results of measurements on a series of test wafers on a conventional wafer stepper are presented and recommendations on the future direction of research and development are made.

ACKNOWLEDGEMENTS

I wish to thank my employers, the University of Edinburgh, for allowing me to register as a part-time postgraduate student and for providing the laboratory facilities in which to do the work.

I am especially grateful to my supervisors Dr J.R. Jordan and Dr H.W. Whittington for their help and encouragement throughout the project. I am also indebted to many of my colleagues in the Department of Electrical Engineering who gave invaluable advice and assistance including: Alan Gundlach, Joe Gow, John Laurie, Graham White, Graeme Maxwell, Bob Holwill, Ron Mackie, Sandy Alexander, Stuart Anderson and Liz Paterson.

I wish to thank Professor Stephen Salter of the Department of Mechanical Engineering for recent help and encouragement in combining the dynamic alignment system with his design of scanning stage and for the use of his photocopier.

Finally, I would like to thank my wife and family for their support and tolerance during the preparation of this thesis.

CONTENTS

ABBREVIATIONS AND UNITS.

With the exception of chapters 2 and 3 where imperial units have been used when reporting the work of others, SI units are used throughout this thesis, with their usual abbreviations. In particular, the micrometre is abbreviated 'μm' and also as 'micron.' When referring to film thickness, the Ångström (abbreviated Å), has been used. 1 Å = 10^{-10} m. Although both the micron and the Ångström are not SI units, they have been included because they are in everyday use in metrology and microfabrication.

Unless otherwise stated in the text, symbols have the following meaning:-

λ	(lambda)	wavelength of light
f		frequency
g		index to scale gap
p		pitch of grating
s		second
V		volts
v		velocity

CHAPTER 1: INTRODUCTION.

The aim of this project was to investigate new methods of position measurement based on optical sensing of coded patterns and gratings. The use of metrological gratings and moiré fringe techniques in the measurement of mechanical position is well established with widespread applications in machine tools and instrumentation. A brief overview of the development of moiré fringe measuring systems is presented in chapter two with a review of the properties and manufacturing methods of general purpose metrological gratings. Lithography and etching processes for the production of diffraction gratings on silicon are also described.

The key feature of all moiré fringe systems lies in the fact that a grating can be used to generate an interference pattern by placing a similar grating against it. The moiré fringes thus formed are of a much coarser pitch than the lines on the gratings themselves and can therefore be detected by relatively simple optical methods. The sensitivity of the fringe pattern to mechanical movement is largely determined by the pitch of the gratings and not by the size of the photodetectors or the resolution of the optical system which detects the fringes. The formation of moiré fringes and the design of reading heads are discussed in chapter three and the historical development of electronic methods of fringe interpolation is reviewed.

Simple moiré fringe counters are purely incremental

systems which produce a count pulse for each unit of displacement relative to a datum or origin at which the display has been zeroed. Any interruption or corruption of the signal causes a loss of position information. In some applications, therefore, an absolute position encoder is more appropriate as it provides a unique code corresponding to each position in the operating range and can recover from an interruption of signal without having to re-establish the mechanical datum. The resolution of absolute systems is usually set by the size of the smallest element in the coded pattern but this can be improved upon by adopting a hybrid approach in which a coarse absolute encoder is combined with a moiré fringe reading head. The main types of absolute position encoder as applied to linear measurement are outlined in chapter four and the arguments for and against absolute, incremental and hybrid systems are presented.

The design of hybrid encoders for use in instrumentation is discussed in chapter seven and the results of experimental work are presented. It was also realised that the patterns could be implemented at a larger scale and a laboratory demonstration of a navigation system for automated guided vehicles is described.

It was felt that microfabrication techniques could be used to produce accurate metrological gratings on silicon for use in short-range, high resolution transducers. It was intended at the outset that the experience gained in optical sensing of patterns on silicon might be applied in new designs of equipment for the

manufacture of microcircuits. This is an area which has seen rapid development over the last 25 years and there is an increasing need for accurate, automatic position measurement in a wide range of fabrication equipment. One of the most demanding tasks in metrology is the accurate registration or overlay of patterns on successive process layers during the manufacture of a microcircuit. Since optical lithography is used to define the patterns, the use of optical sensing techniques to monitor alignment and registration is entirely appropriate. Chapter five reviews the use of moiré fringe techniques in microfabrication with special emphasis on the problem of mask to wafer alignment in photolithography.

The results of experimental work using reflection gratings on silicon with novel designs of reading head are presented in chapter six. The optical properties of vee-groove profile gratings were investigated and applied to both one-dimensional and two-dimensional measurement.

Chapter eight analyses the alignment requirements of future wafer steppers where the wafer stage may move continuously, with 'flash' exposure of the patterns using a 10 ns pulse from an excimer laser, thereby achieving an enormous increase in rate of throughput. A new design of dynamic alignment system is proposed, based on a two-dimensional grating pattern with moiré fringe detection. Experimental results from test wafers are presented.

A summary of results and conclusions is presented in chapter nine with an outline of further work which is

being carried out and recommendations for future directions of research and development.

CHAPTER 2: METROLOGICAL GRATINGS.

2.1 Overview.

The history of moiré fringe phenomena goes back over 100 years. In 1874 Lord Rayleigh [1] observed that the interference pattern of two superimposed diffraction gratings was a sensitive indicator of the quality and accuracy of their rulings. The fringes served to magnify the local differences in grating pitch and thus acted as indicators of mechanical misplacement of the lines. The principle of measuring the mechanical displacement of one grating relative to another by detecting moiré fringes was not implemented until 1950 when Roberts [3] used a pair of superimposed gratings between a lamp and a photodetector to convert mechanical movement into a periodic electronic signal. At about the same time the National Physical Laboratory (NPL) had produced suitable gratings {Merton (1949) [2], Dew and Sayce (1951) [4]} and a prototype measuring system for a numerically controlled machine tool was built and patented by Ferranti Ltd in 1953 {Williamson et al [5]}.

The interference patterns of crossed gratings were studied theoretically by Guild (1956) [7], (1960) [8]. Photographic replication techniques for metrological gratings were developed at NPL and at the National Engineering Laboratory (NEL) in the early 1960's and several industrial companies were subsequently licensed to produce replica gratings, thereby opening the way to

widespread industrial applications.

Since 1970, the superior resolution of laser interferometers has led to their widespread adoption wherever fine resolution is essential and cost is a secondary consideration. However, in some applications such as measurement under fluctuating ambient conditions, when it may be difficult to implement wavelength compensation on the laser, a moiré technique using grating scales can offer better stability at lower cost.

2.2 General Properties.

The gratings used in metrology differ from traditional spectroscopic gratings in several respects. In general, metrological gratings are about an order of magnitude coarser, with pitches ranging from 5 lines/mm to 250 lines/mm. The overall length of a single section of grating may exceed 1 m and sections may be joined end-to-end to achieve measuring ranges in excess of 10 m.

The accuracy of placement of individual lines is less critical than the overall systematic error over longer lengths. Typical errors have been quoted as 10-20 μm over a 1 m length [11]. Over longer range (L) the error (e) does not increase pro rata; a realistic estimate may be calculated using

$$e = \pm (a + b\sqrt{L})$$

where a is the short range error and b is an error

component proportional to the square root of the length. For commercially available gratings 'a' can have a value of 1-5 μm and b can be 5-20 μm/m. In a laboratory environment, accuracy of +/- 0.5 μm over a length of 1 m has been achieved by Purfit et al (1974) [12].

Both transmission and reflection gratings are used in metrology. For short range measurements using pitches finer than 50 l/mm, transmission gratings on a glass substrate are appropriate whereas reflection gratings on a steel substrate are normally used in the longer range applications on machine tools.

2.3 Manufacture of Master Gratings.

2.3.1 Outline.

Diffraction gratings have been produced by mechanical ruling engines of various types for over 100 years: the techniques have been reviewed by Hutley (1982) [13]. The requirements on accuracy of line placement and stability during ruling over periods of hundreds of hours make the design and construction of mechanical ruling engines one of the most challenging tasks in engineering.

The manufacture of metrological gratings may be divided into 2 stages:

(a) production of a master grating

(b) production of copies or replicas from the master.

To some extent, the production of master and copy are inter-linked by the technology of the replication process, since the master must be created in a form which is suitable for replication without a significant degradation in quality between master and copy and without causing significant wear or damage to the master itself.

2.3.2 Mechanical Methods.

The first successful metrological gratings were made using the Merton process [2] to create an accurate spiral groove on the surface of a metal cylinder. To minimise local pitch errors a two-stage process was used. Firstly, a fine-pitch leadscrew was made on a lathe, with every precaution being taken to optimise its accuracy. Secondly, this leadscrew was fitted with a long nut, faced internally with compliant material to provide elastic averaging of pitch errors. The leadscrew and nut was then used to drive a diamond cutting tool in the axial direction when cutting a screw thread of 2500 threads per inch (TPI) on the surface of a cylinder. By taking resin casts from the surface of the cylinder, using a transparent material, and then bonding the casts onto a glass substrate it was possible to produce replica prismatic gratings for use with spectroscopic reading heads (see section 3.2.6). The groove profile, which was determined by the shape of the diamond cutting tool, was chosen to optimise the energy in the first diffracted

order, i.e. the grating was 'blazed' for the first order.

2.3.3 Photographic Methods.

Short sections of metrological grating can be produced by photographic reduction of artwork. A realistic upper limit on the size of grating is about 50 mm due to imperfections in the reduction lens. Longer gratings have to be produced by abutting these short sections end-to-end in a step-and-repeat process. This principle was the basis of what become known as "NPL Method III" which is shown in figure 2.1 {Purfit et al (1974) [12], Hutley (1982) [13]}. This method of master grating generation has a number of interesting features. Essentially, the short section of grating or printing index is mounted on a moving carriage and the pattern is flash-exposed onto a blank photographic plate at intervals defined by the reference measuring system. The mechanical design of the bench and carriage ensures a smooth, repeatable scan at constant velocity. The effects of pitch, roll and yaw are kept to a minimum by eliminating Abbé offsets: the printing index and the reference measuring head are co-axial and the grating blank is mounted as close as possible to the reference measuring scale. The importance of the Abbé principle in the design of any metrological equipment has been explained by Bryan (1979) [31].

There is also provision for adjusting the grating blank parallel to the scan axis using a mounting

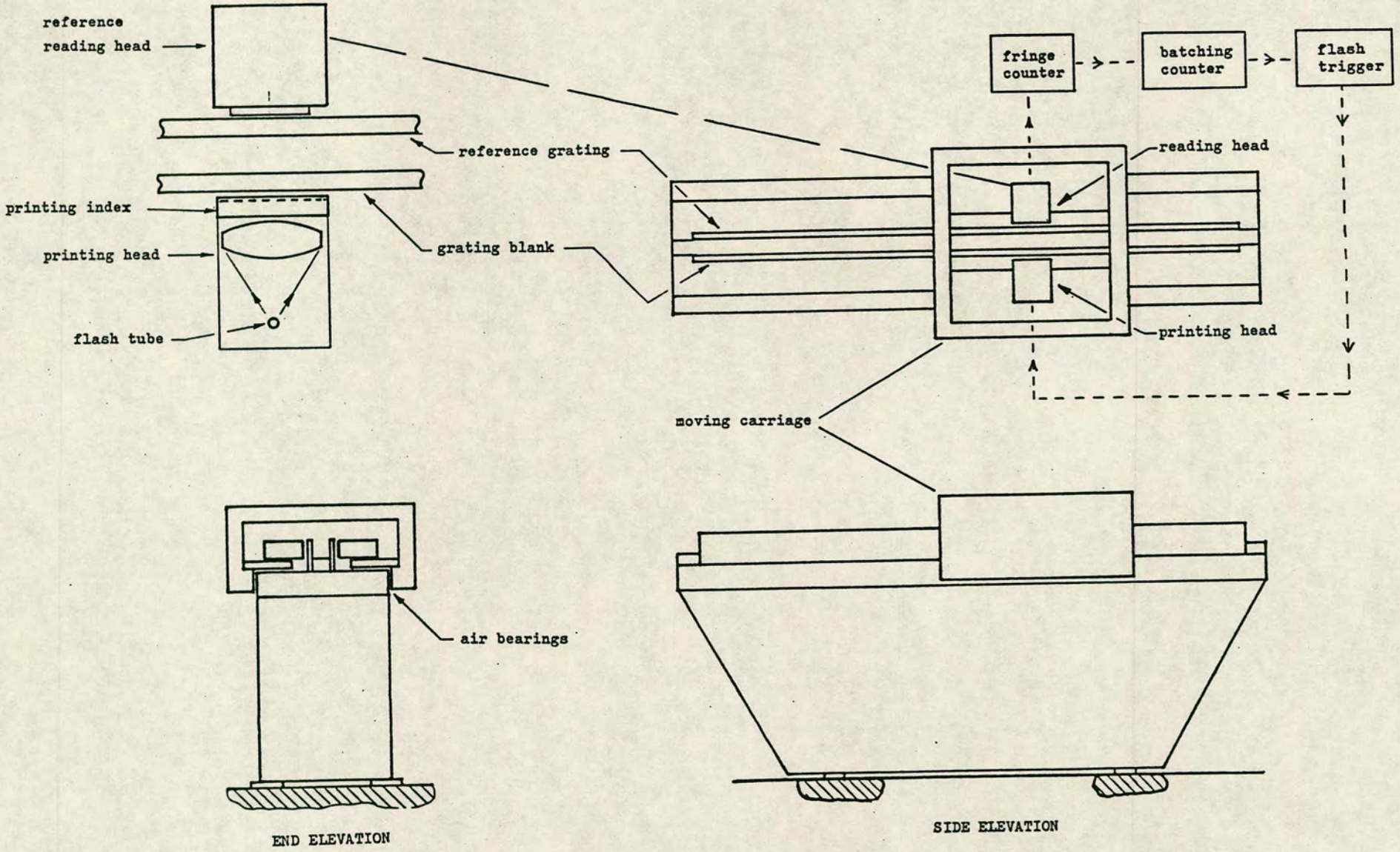

Figure 2.1 METHOD III PRINTING BENCH

arrangement which is referenced to the front face of the blank with clamps which are designed to avoid any mechanical distortion of the blank. The reference measuring system can be a laser interferometer or, more likely, a grating and moiré fringe reading head. If the systematic errors of the reference grating are known, they can be allowed for during printing by advancing or retarding the trigger pulses to the flash tube. Since the moiré fringe reading head samples an area about 10 mm square containing about 1000 lines, the error correction curve is a smooth function. In practice, the step interval between exposures is reduced to less than 1 mm so that multiple overlapping images of the short section of printing index are produced, thereby smoothing local variations in line placement and mark-to-space ratio.

The lines on the printing index are usually inclined at a bias angle of typically 20 milli-radian to the normal to the measuring direction, with a narrow reference line parallel to the measuring direction outwith the grating track, as shown in figure 2.2. When the finished grating is installed it is aligned such that the scale axis reference line is parallel to the measurement axis. It is sometimes necessary, however, to tilt the grating relative to the measurement axis in order to minimise the overall systematic error by the introduction of a deliberate 'cosine' correction. With a bias angle of, for example, 20 milli-radian this correction may be either positive or negative up to a maximum installed tilt of 20 milli-radian. It is rarely necessary to tilt the

grating by more than a fraction of this amount since the bias angle enhances the rate of change of cosine correction with tilt as shown in figure 2.2. Thus with a bias angle of 20 milli-radian, a tilt of 1 milli-radian would introduce a scale correction of 20 parts per million or 20 micron per metre.

The gap between the printing index and the surface of the blank is important. For coarse line structures with less than 25 lines/mm the pattern is shadow projected across the gap by the collimated source and the clearance between index and blank can be set to a sensible value in the range 50-150 μm. For line structures finer than 40 lines/mm the gap is adjusted so that the first Fresnel image of the printing index occurs at the surface of the blank (see section 3.2.6). This permits fine-line patterns to be printed with a reasonable working clearance: for a 100 lines/mm bar and space grating the Fresnel gap for printing with a wavelength of 500 nm onto photographic emulsion would be 50 μm. Experience of this method of grating manufacture has shown that the replica can be more accurate than the reference grating due to the averaging effect of the index grating on the reading head and the correction of systematic errors during exposure. Thus the replica could be used as the reference to produce an even better "second generation" replica. It is clear, however, that the ultimate accuracy will be determined by the stability and repeatability of the system. Even if the reference measuring system can be corrected to give perfect placement of trigger pulses, mechanical

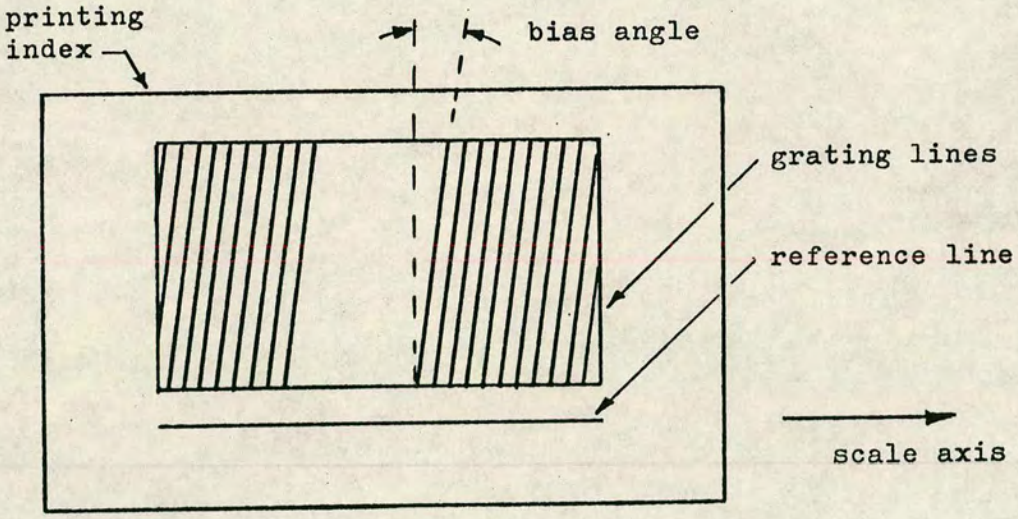

Effect of installed tilt on calibration.

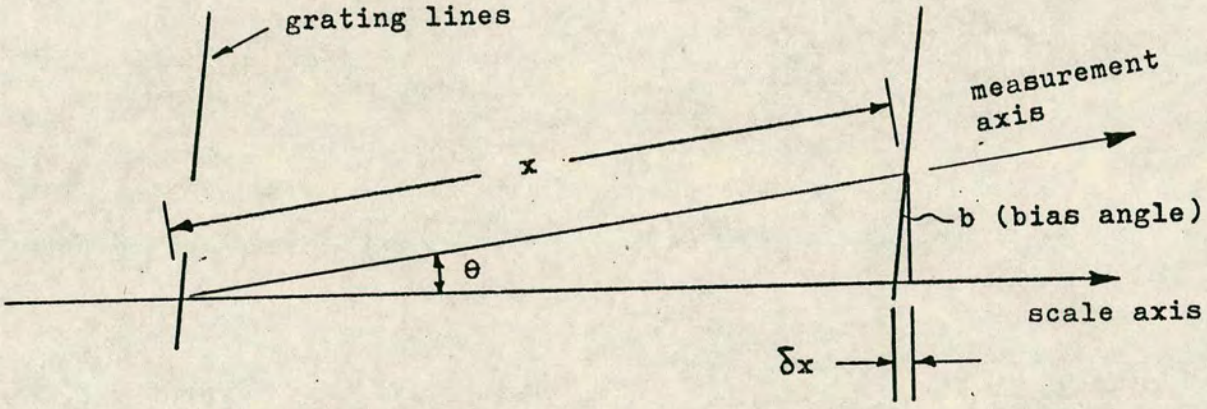

If the scale axis is tilted at a small angle θ to the measurement axis and if the lines on the scale are at a bias angle b, the correction δx due to θ is given by

$$\delta x = x \sin\theta . \tan b$$

and the correction per unit length is

$$\frac{\delta x}{x} = \sin\theta . \tan b$$
$$\simeq \underline{\theta . b} \quad \text{for small angles}$$

Figure 2.2 GRATING WITH BIAS ANGLE

repeatability and stability, in the presence of environmental changes such as temperature and vibration, will be the major factors in determining the accuracy of the final grating.

2.3.4 Interference Methods.

A grating may be generated by photographing the interference pattern of two intersecting collimated beams of coherent light as shown in figure 2.3. This has become known as a holographic grating because, although the technique was proposed by Michelson in 1927 [14] and some gratings were produced in the 1950's, it was not fully exploited until high powered, coherent laser sources became available in the 1960's. Holography was being developed at the same time and in fact an interference grating can be regarded as a type of hologram, hence the name. Holographic diffraction gratings are now an established alternative to mechanically ruled gratings for spectroscopic applications. The production methods and spectroscopic performance have been reviewed by Hutley (1982) [13].

Metrological gratings up to 15 inches square were produced holographically by Burch and Palmer (1961) [15], but the technique is best suited to smaller scale applications since the size of grating is determined by the aperture of the optical systems used to generate the interfering beams. The maximum aperture is limited by cost, mechanical stability and the difficulty of achieving

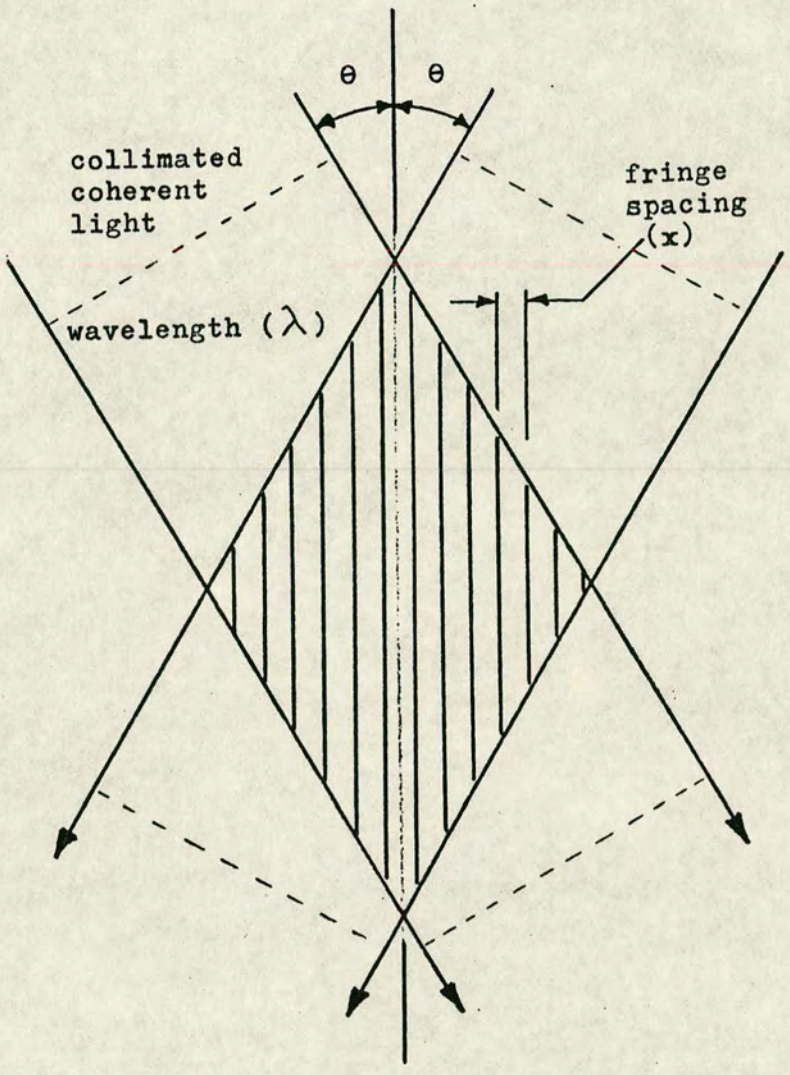

If coherent beams intersect at an angle 2 θ as shown, interference fringes are produced with a spacing x where

$$x = \frac{\lambda}{2\sin\theta}$$

e.g. taking λ = 458 nm and $\theta = 30^{\circ}$ produces fringes

with $x = \lambda$ = 458 nm

equivalent to about 2183 lines/mm.

Figure 2.3 INTERFERENCE (HOLOGRAPHIC) GENERATION METHOD

uniform intensity and wavefront accuracy over a large area. These large scale problems have been studied by Cowan (1984) [16]. On a more modest scale, a two dimensional holographic grating with a pitch of 0.8 micron has been used as the XY measuring element on a wafer stepper by Berger (1984) [9] and a one dimensional grating with a pitch of 0.83 micron over a length of 108 mm has been used in a linear displacement transducer by Iwoka and Akiyama (1984) [10].

To summarise, interference methods are suitable for the production of small sections of master grating, especially where a fine pitch is required, but large size metrological gratings can be generated more economically by mechanical scanning or by step-and-repeat methods.

2.3.5 Pattern Generators.

Computer controlled pattern generators have been developed to make the masks which are used in the fabrication of microcircuits. Accuracy of better than 1 μm over an area up to 150 mm square can be achieved with resolution in excess of 250 lines/mm and thus these machines can be used to produce short sections of metrological grating as reported by Milne et al (1978) [17].

2.4 Photographic Replication.

2.4.1 Contact Printing.

Simple line and space gratings may be replicated by contact printing from a transparent master. This is an effective, low cost method of transferring a pattern into photographic emulsion, or into photoresist, on samples up to about 300 mm square. The replica gratings may be of the transmission type on a transparent substrate or of the reflection type on a variety of substrates. The disadvantages of contact printing are fairly obvious. Mechanical contact between master and blank carries the risk of wear and damage to the master, leading to a steady decrease in the quality of the replica gratings. The clamping of master and blank face-to-face in a vacuum frame also introduces mechanical strain in both specimens, thereby degrading the accuracy of the replica pattern.

2.4.2 Proximity Printing.

The major drawbacks of contact printing may be eliminated by placing the surface of the blank in the first Fresnel zone of the master grating. This technique, sometimes known as Fresnel zone printing, was the basis of the "NPL Method I" apparatus for replicating gratings, described by Sayce (1972) [21]. The master grating and the blank were mounted face to face, separated by the appropriate Fresnel gap. A collimated light source was

slowly scanned along the length of the grating to transfer the line pattern onto the blank. Known errors in the master grating could be corrected by varying the angle of incidence of the collimated source during the scan using a tilting mirror coupled to a correction cam, but local line-to-line errors and defects would still be reproduced in the replica grating.

2.5 Gratings on Silicon.

2.5.1 Material properties.

The use of silicon as a substrate for the manufacture of metrological gratings offers a number of advantages. The thermal stability and mechanical properties of single crystal silicon compare very favourably with the traditional materials used in precision devices {Chetwynd (1987) [38]} and the standard techniques used in microfabrication may be adapted to produce metrological grating patterns. Thin films of silicon dioxide, silicon nitride, polycrystalline silicon, aluminium, aluminium-silicon alloy, aluminium-silicon-copper alloy and other materials with well characterised optical properties can be produced and etched on silicon wafers up to 200 mm in diameter. As in the case of microelectronic devices, mass production of gratings on silicon for use in short range transducers would be cost-effective. Although silicon is transparent at long wavelength it is more appropriate to use it as a substrate

for reflection gratings. Thin film interference gratings may be fabricated by etching patterns in the correct thickness of silicon dioxide or silicon nitride to minimise reflection at a particular wavelength whilst Al or Al-Si-Cu alloy may be deposited to give high reflectivity over a broad range of wavelengths, see Jenkins and White [39].

2.5.2 Etching of Grooves.

The surface of the single-crystal silicon may also be etched anisotropically to produce vee-grooves and other 3-dimensional structures where the etched shape is determined by the principal planes of the diamond cubic crystal structure. Diffraction gratings with a vee-groove profile have been described by Tsang & Wang (1975) [40] whilst more general descriptions of anisotropic etching of 3-dimensional structures have been published by Bassous (1978) [41], Bean (1978) [42] and Allen (1981) [43].

These methods are all based on wet chemical etchants which exhibit orientation-dependent etch rates. The three index planes most commonly used are (100), (110), (111) as shown in figure 2.4 and some of the etchants are listed in table T.2.4. Of particular note are the KOH solutions which etch in the (111) direction at less than 1% of the rate in the (100) direction. When this etchant attacks silicon through a rectangular window in a masking layer on the surface of a (100) wafer, a

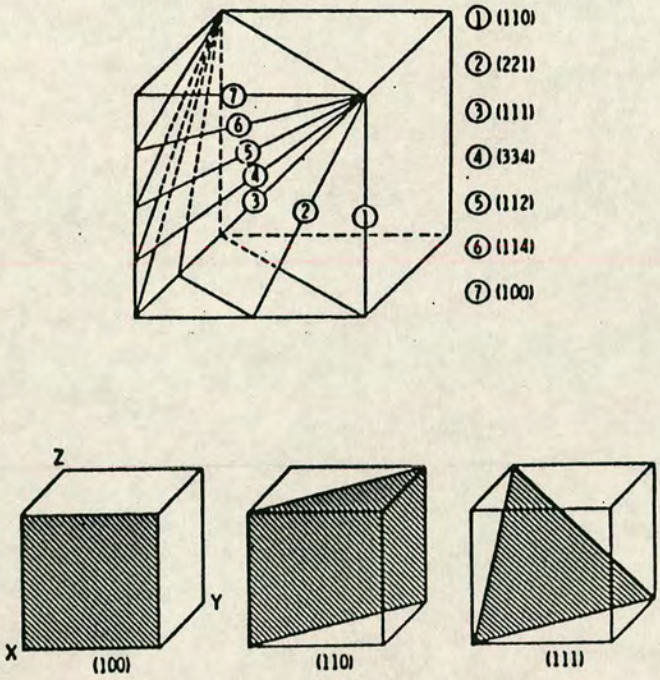

Figure 2.4 CRYSTALLOGRAPHIC INDEX PLANES OF SILICON

CHEMICAL ETCHING OF SILICON

ETCHES	CHARACTERISTICS	COMPOSITION	RATE AND REMARKS
PLANAR ETCH	ETCH UNIFORMITY	HF - HNO_3 - HAc ~8% ~75% ~17%	~5 μ/MIN (111) RT
1-3-10	ETCHES P^+ OR N^+ SILICON "STOPS" AT P^- OR N^-	HF HNO_3 HAc 1 3 10	~3 μ/MIN (100) RT
(100) ODE	ETCHES [100] ~100 X [111] DIRECTION	KOH - NORMAL PROPANOL H_2O	~1 μ/MIN AT 80°C IN (100) SILICON STOPS AT P^{++} INTERFACE
(110) ODE	ETCHES [110] 600 X [111] DIRECTION	KOH - H_2O	~.8 μ/MIN AT 80°C IN (110) SILICON
ETHYLENEDI-AMINE	ORIENTATION DE-PENDENT AND CONCENTRATION DEPENDENT	ETHYLENEDI-AMINE - CATECHOL - H_2O (HYDRAZINE)	~1.1 μ/MIN AT 100°C IN [100] . STOPS ETCHING AT P^{++} INTER-FACE. VERY SLOW ETCHING OF SiO_2

(from Bean ref. 42)

Table T.2.4 ORIENTATION DEPENDENT ETCHES FOR SILICON

rectangular pit is created with sloping sides formed by (111) planes. Etching continues into the wafer to a depth defined by the intersection of the (111) planes and thereafter the etching virtually ceases. Thus for practical purposes the etching process can be regarded as self-limiting and the quality of the reflecting (111) faces is independent of the photo-engraving process.

2.5.3 Photolithography - Fabrication of Gratings.

Fabrication of metrological gratings on silicon wafers is less demanding than fabrication of microcircuits since minor blemishes and defects on a grating are of little consequence. The tolerances achievable on masks have already been reviewed. The pattern transfer process, from mask to silicon wafer, may be done in several ways depending on the requirements of the pattern in terms of resolution, accuracy, and cost. Optical lithography using positive photoresist and exposure wavelengths around 400 nm is a well established technique which has been reviewed by Doane (1980) [44], Watts and Bruning (1981) [45], Wittekoek (1980) [46] and Stevenson and Gundlach (1986) [47].

For mass production of devices with geometries coarser than 2 microns on wafers less than 150 mm in diameter, whole wafer exposure using a 1:1 mask is the most appropriate technique. Contact printing has been superseded by the scanning slit projection imaging equipment first described by Markle (1974) [48] which

offers higher yield and longer mask life since there is no physical contact between mask and wafer. The trend to smaller geometries and larger diameter wafers has led to the introduction of direct step on the wafer machines. These are essentially step-and-repeat cameras in which a mask pattern is imaged directly onto the wafer surface with a reduction ratio of typically 5X or 10X. The image field is usually restricted to less than 20 mm square and the wafer is stepped and repeated on a high precision XY stage to expose the whole surface. The early wafer steppers were capable of resolution approaching 1 micron and image placement repeatability of about +/- 0.3 micron (3 sigma) as reported by Stover et al (1980) [49], (1981) [50], and Stevenson and Robertson (1982) [51]. Later machines, using a shorter exposure wavelength (365 nm) and lenses of higher numerical aperture have demonstrated better than 0.7 micron resolution, {Miller and Stover (1985) [52], Nuhn et al (1987) [53]}, whilst XY placement repeatability has been improved to +/- 75 nm (3 sigma), {Biesterbos et al (1987) [54]}.

Further improvements in resolution may be achieved by the use of shorter wavelength sources such as excimer lasers which have the additional property of a short duration output pulse, typically 10 ns. A 'flash-on-the-fly' method of exposure with a continuously moving stage was proposed by Markle in 1984 [55] but as yet no such system is available commercially. However, an existing wafer stepper has been retrofitted with a 248 nm KrF excimer laser and associated optics by Pol (1987) [56]

and, under favourable conditions, resolution down to 0.35 micron has been demonstrated.

To summarise, it is clear that current microfabrication techniques are capable of producing high quality metrological gratings with line structures as fine as 250 lines/mm and future developments will extend this capability to 1000 lines/mm. Since the practical limit for simple reflecting reading heads is 50 lines/mm it can be concluded that resolution is not a problem.

CHAPTER 3: OPTICAL DISPLACEMENT TRANSDUCERS.

3.1 Outline.

The term reading head is usually applied to the unit which converts relative movement of the scale grating and the index grating into an electronic signal which may be processed and displayed in a suitable form. Thus a reading head can be regarded as a transducer in the sense that it converts mechanical displacement into an electronic signal. The design must ensure reliable and accurate conversion of the measured quantity whilst taking account of the inevitable variations and perturbations which may occur under operating conditions.

Historically, the above requirements have been tackled in many different ways and, for the purpose of reviewing reading head designs, it is convenient to group them into three major categories, viz. transmission, reflection, and projection. This grouping is based on the optical arrangement, but certain principles which are common to all three categories will become apparent in the following text.

3.2 Transmission Reading Heads.

3.2.1 Moiré Fringe Formation.

When two coarse-pitch bar and space gratings of identical pitch are superimposed and viewed in

transmission, moiré fringes are formed as shown in figure 3.1. Relative movement of the gratings in the X direction causes the fringes to move in the Y direction. The spacing between fringes in the Y direction, s, for a given pitch of grating, p, is inversely proportional to the small skew angle, α , between the grating lines such that $s = p/\alpha$. When the gratings are adjusted so that the lines are parallel, s becomes infinite and the fringes are said to be "fluffed out." In this condition the total light intensity transmitted through the pair of gratings is a serrisoidal function of their relative position, X, with one cycle of intensity corresponding to a mechanical movement of one pitch of the grating. The intensity waveform depends on the mark-to-space ratio of the gratings: a symmetrical serrisoid is produced by identical gratings with a 1:1 mark-to-space ratio as used in most measuring systems, but the dark fringes may be sharpened for ease of visual observation by using gratings with complementary mark-to-space ratios, e.g. 1:2 superimposed on 2:1 as recommended by Luxmoore (1983) [11] and Vargady (1964) [18].

3.2.2 Vernier Fringe Formation.

When two gratings of slightly different pitch are superimposed with their lines parallel, vernier fringes are formed as shown in figure 3.1. These fringes may be regarded as spatial beats between the two slightly different spatial frequencies on the two gratings. Thus

MOIRÉ FRINGE FORMATION

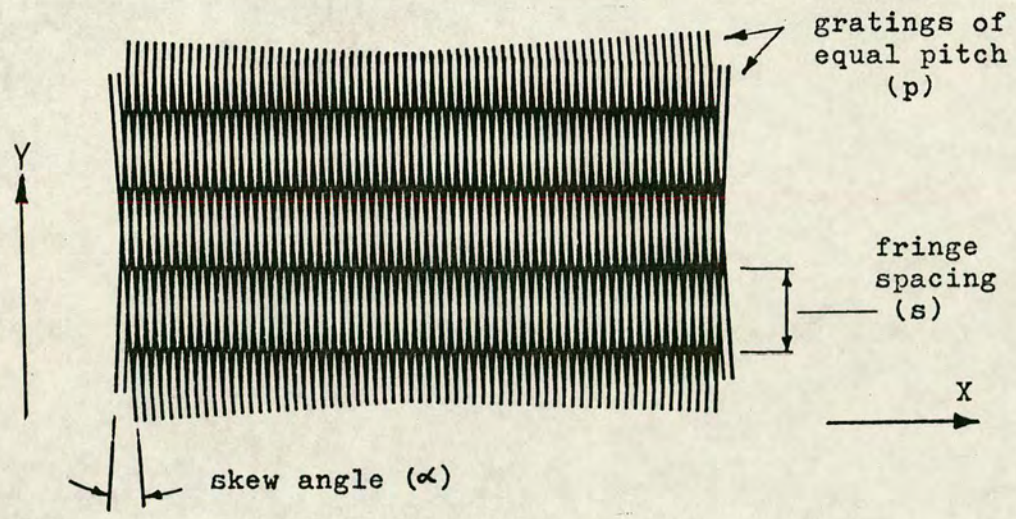

$$\text{fringe spacing } s = \frac{p}{\alpha}$$

VERNIER FRINGE FORMATION

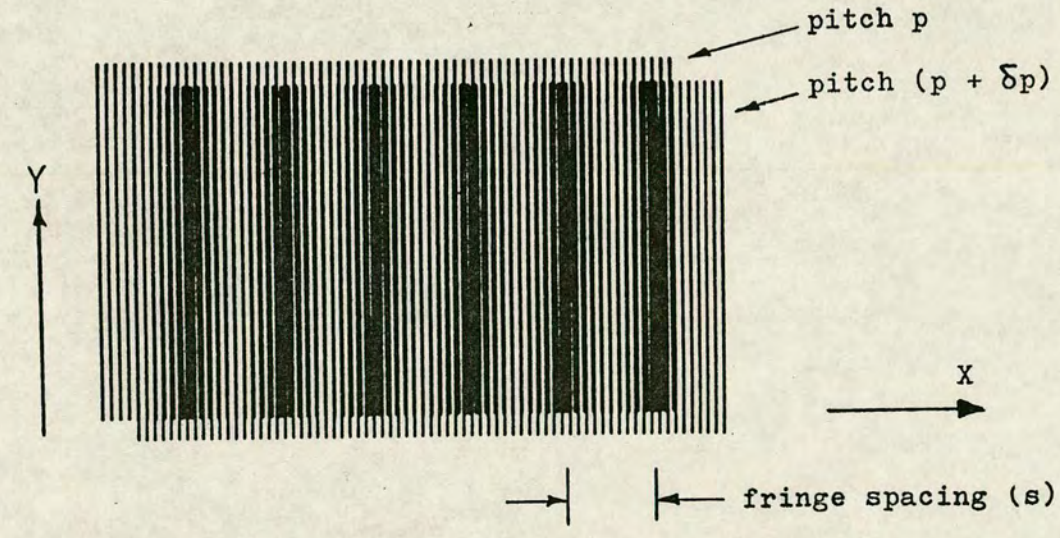

$$\frac{1}{s} = \frac{1}{p} - \frac{1}{(p + \delta p)}$$

$$s = \frac{p\,(p + \delta p)}{\delta p}$$

Figure 3.1 FORMATION OF FRINGES

the fringe spacing, s, is determined by the pitches of the two gratings and relative movement between the gratings in the X direction causes a greatly magnified movement of the fringes in the same direction. If the grating pitches are p and $(p + \delta p)$ then

$$s = \frac{p(p + \delta p)}{\delta p}$$

and the magnification, $$m = \frac{\text{(fringe spacing)}}{\text{(grating pitch)}} = \frac{p}{\delta p} + 1$$

It should be realised that although vernier fringes are capable of producing very high magnification of mechanical movement, the fringe pattern is susceptible to distortion by local line placement errors. The fringes have to be read by relatively narrow photodetectors to ensure good modulation and thus the potential gain in accuracy from averaging over a large number of grating lines is lost.

3.2.3 Detection of Fringes.

A bi-directional fringe counter requires two input signals which are in quadrature (90 degrees out of phase) in order to derive a direction signal. This can be achieved in a number of ways. In principle, two photocells can be arranged to collect the transmitted light from adjacent sections of the fringe pattern, i.e. at a spacing of $s/4$ to give signals in quadrature.

However, the intensity modulation due to movement of the gratings is superimposed on a d.c. level which depends on a number of factors such as the incident intensity and the optical density of the scale grating. It is not possible to a.c. couple the detectors as the system has to cope with stationary as well as moving patterns. To minimise the effects of variations in d.c. level, a four-channel arrangement was devised by Shepherd and Walker (1955) [6]. By connecting the photodetectors in pairs as shown in figure 3.2, the d.c. components of the photodetectors are cancelled at source whilst the modulated components are amplified to produce an output signal which is symmetrical about a stable d.c. level, usually zero volts.

3.2.4 Four-phase Index Grating.

By dividing the index grating into four sections, with the lines in successive sections out of phase by 1/4 of a pitch and by operating with the grating lines parallel, the constraints on the size and spacing of the photodetectors are removed. The phase relationship of the photodetector signals is built into the lines on the index grating and can be relatively insensitive to changes in the skew angle, α, between the grating lines. The layout shown in figure 3.3 achieves this stability of phase whilst making efficient use of the aperture of the collimating lens.

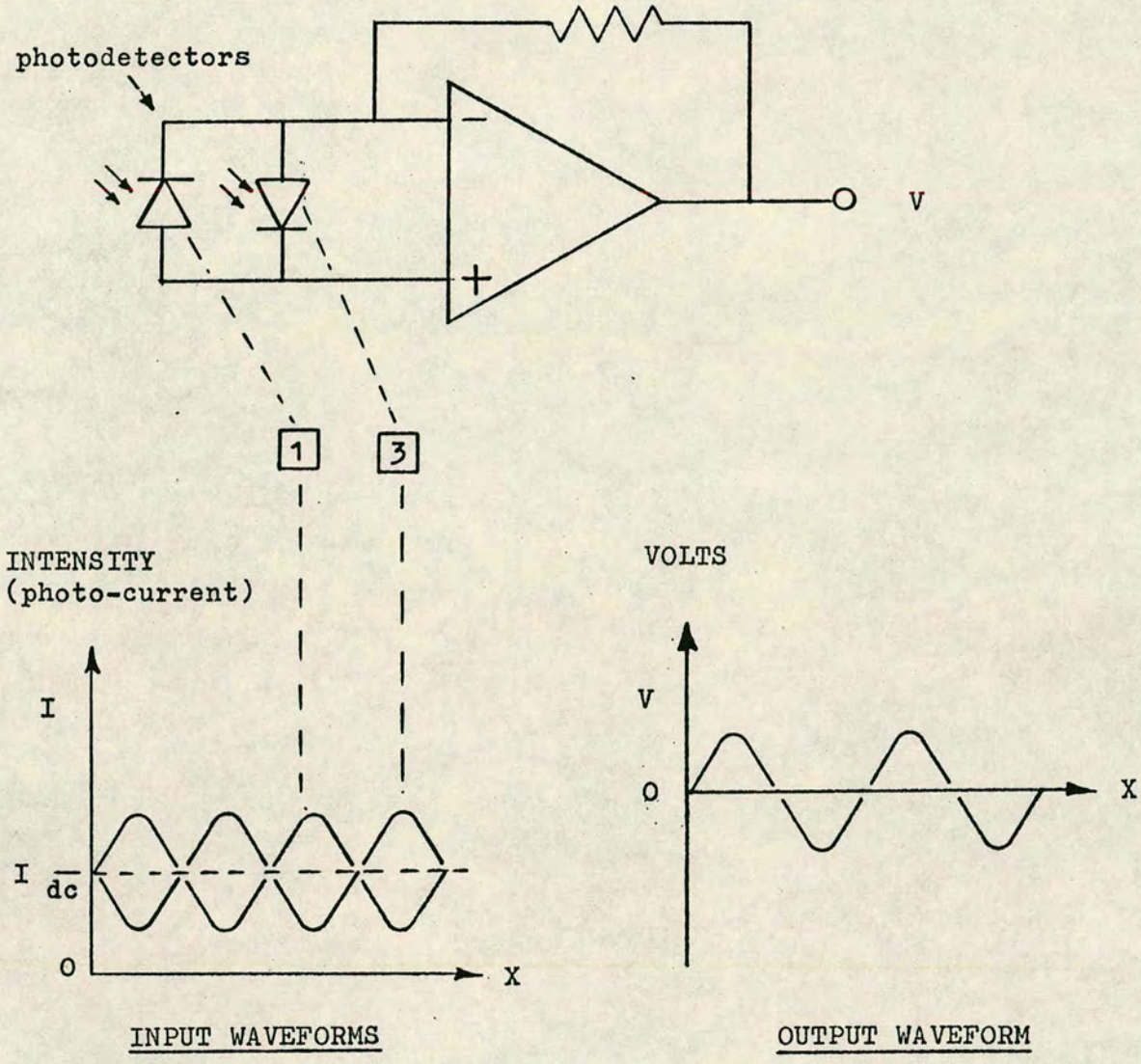

Photodetectors 2 and 4 are similarly connected to provide a signal in quadrature.

$$\text{Modulation} = \frac{I_{max} - I_{min}}{I_{max} + I_{min}}$$

Figure 3.2 PHOTODETECTOR SIGNALS

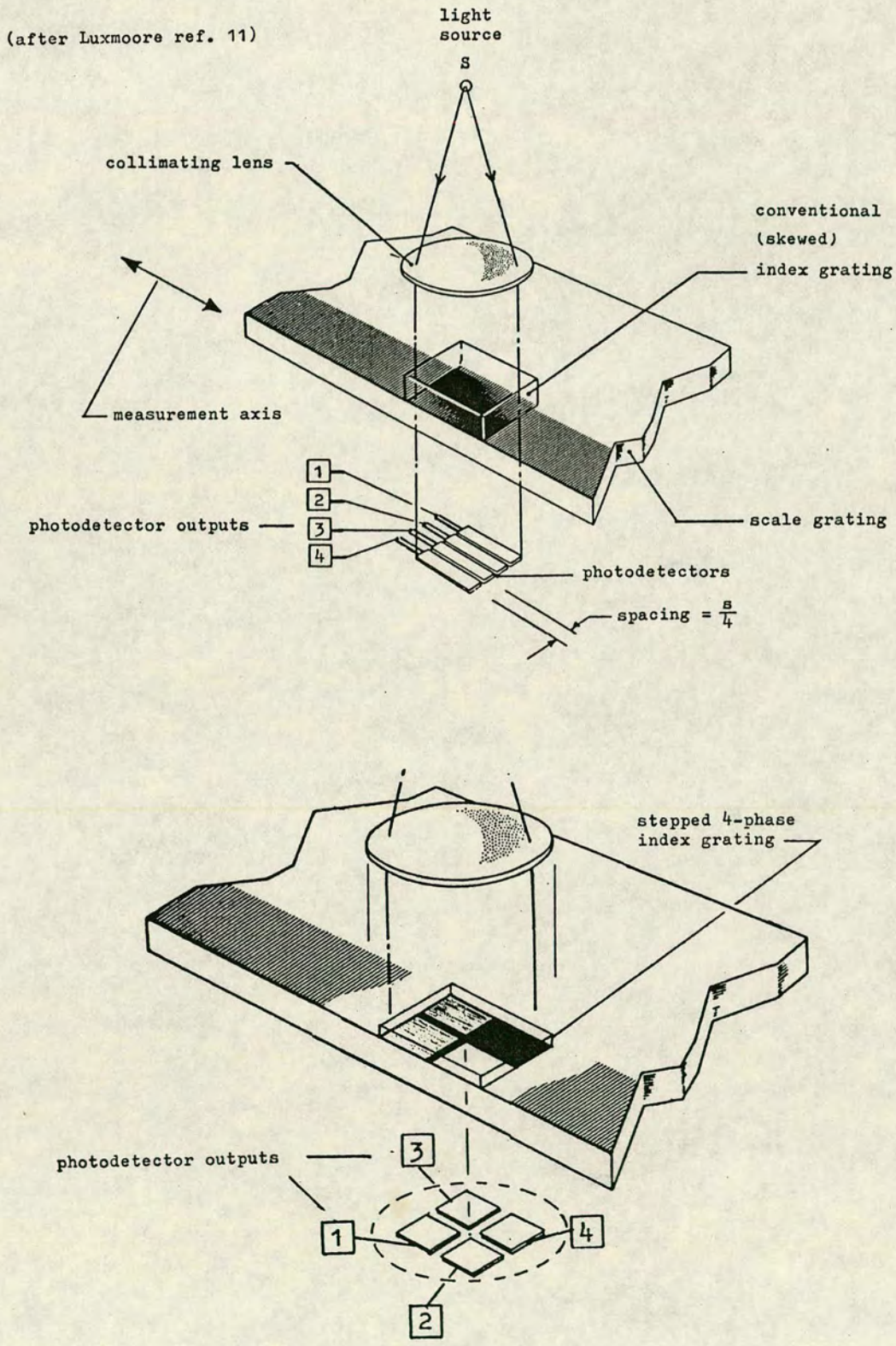

Figure 3.3 TRANSMISSION READING HEADS

3.2.5 Intensity Modulation.

The figure of merit in any reading head arrangement is the contrast or modulation of the photodetector signal, usually expressed as a percentage - see figure 3.2. In the ideal case of coarse-pitch transmission gratings in near contact, with perfectly collimated illumination, there should be virtually 100% modulation. In practice, the modulation is reduced because the grating lines have to be projected across a finite gap with imperfectly collimated light. The divergence or angle of smear of the illumination is given by w/f, where w is the width of the light source and f is the focal length of the collimating lens. In the limit, when the gap (g) between gratings of pitch (p) is such that p/g = w/f, one pitch of the grating subtends an angle at the index grating equal to the angle of smear and there is zero modulation. A practical limit on operating gap, corresponding to a 10% loss of modulation, has been found to be about one quarter of the maximum limit i.e g = 0.25pf/w. {Shepherd (1978) [22]}.

3.2.6 Fine-Pitch Gratings.

With gratings of 10 lines/mm and coarser the effects of diffraction may be ignored and the moire fringe properties may be predicted from simple geometrical considerations. At finer line structures the effects of diffraction become more significant until, at 50 lines/mm and finer, diffraction effects are the major factor in

determining fringe contrast.

Although the formation of fringes with fine-pitch gratings is easy to understand in a qualitative way, a full mathematical treatment of the theory to explain fringe formation in the various reading head configurations is somewhat complicated and tedious. It is not normally found in any of the standard textbooks on optics. The standard reference works on the subject are by Guild (1956) [7], (1960) [8], with a useful summary by Burch (1963) [20] and a more recent paper by Torii and Mizushima (1979) [19].

'Spectroscopic' Reading Head.

The practical aspects of the use of fine-pitch gratings in metrology have been covered by Burch (1963) [20], Sayce (1972) [21], and Shepherd (1978) [22]. A typical reading head arrangement is shown in figure 3.4 where phase gratings are used in a spectroscopic layout with only the first diffracted orders reaching the photodetectors. The gratings are blazed to optimise the energy in the first order and the working gap is chosen such that the first Fresnel image of the index grating occurs at the surface of the scale grating. When a fine-pitch phase grating is illuminated with collimated light, a series of images is formed behind the grating, known as Fresnel images. The first Fresnel image occurs at a gap given by

$$g = \frac{p^2}{2\lambda}$$

where p is pitch
and λ is wavelength

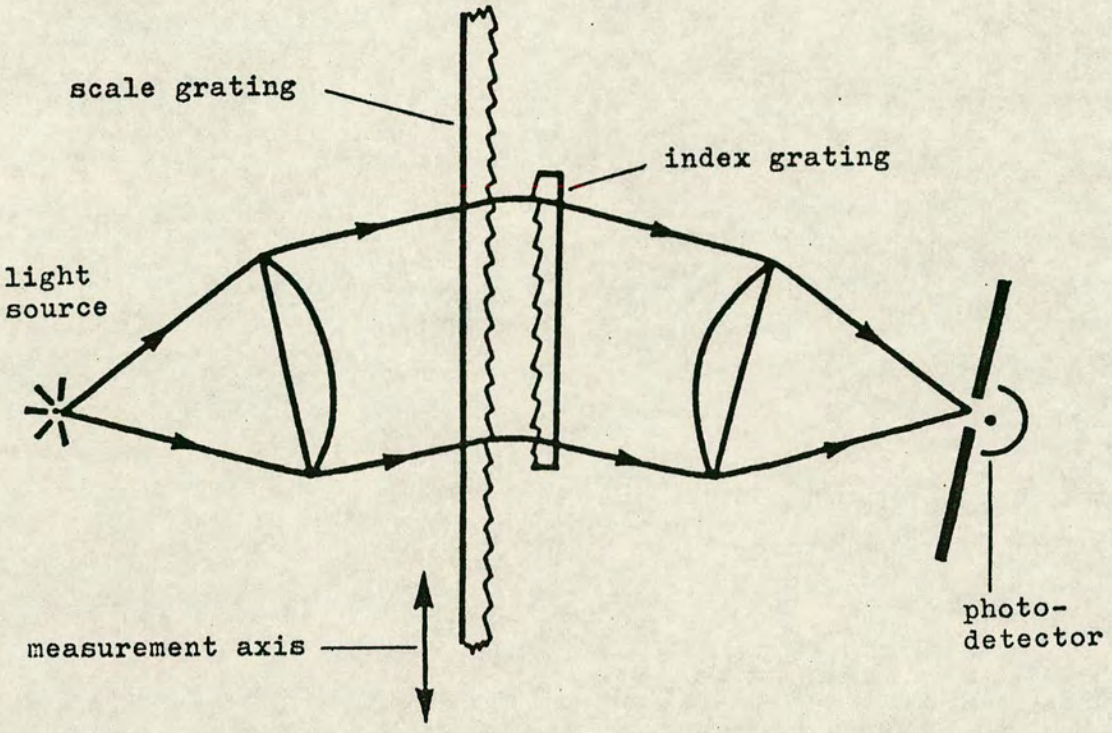

Note that the configuration is similar to a spectroscope in that the pair of gratings operate at 'minimum deviation' and only the first diffracted order groups are collected by the photodetector.

Figure 3.4 SPECTROSCOPIC READING HEAD

(after Sayce ref. 21)

and this is the gap which is normally used in fine-pitch reading heads. The limits and tolerances on working gap as a function of grating pitch are plotted in figure 3.5.

The index grating is usually formed by bleaching an image on a high resolution photographic plate to leave the 'image' of the grating lines as stripes of transparent gelatin on a clear substrate. The cross-section of the gelatin is a reasonable approximation to a prismatic line profile and, by careful control of the photographic processing, it is possible to optimise the line profile to maximise the energy in the first diffracted orders. This type of index grating improves the efficiency of the reading head and gives a higher signal level at the photodetectors.

3.3 Reflection Reading Heads.

A reflection reading head is convenient in some applications where it is desirable to have all the optics on one side of the grating, and it is essential when the scale grating is on an opaque substrate such as stainless steel or silicon. Typical reading head arrangements are shown in figure 3.6. As in the transmission types described above, two outputs in quadrature are derived from 4 photodetectors using an index grating which may be either a conventional moiré type, or a vernier, or a stepped 4-phase type. The major difference when operating in reflection is that the light has to pass through the index grating twice before it reaches the photodetectors.

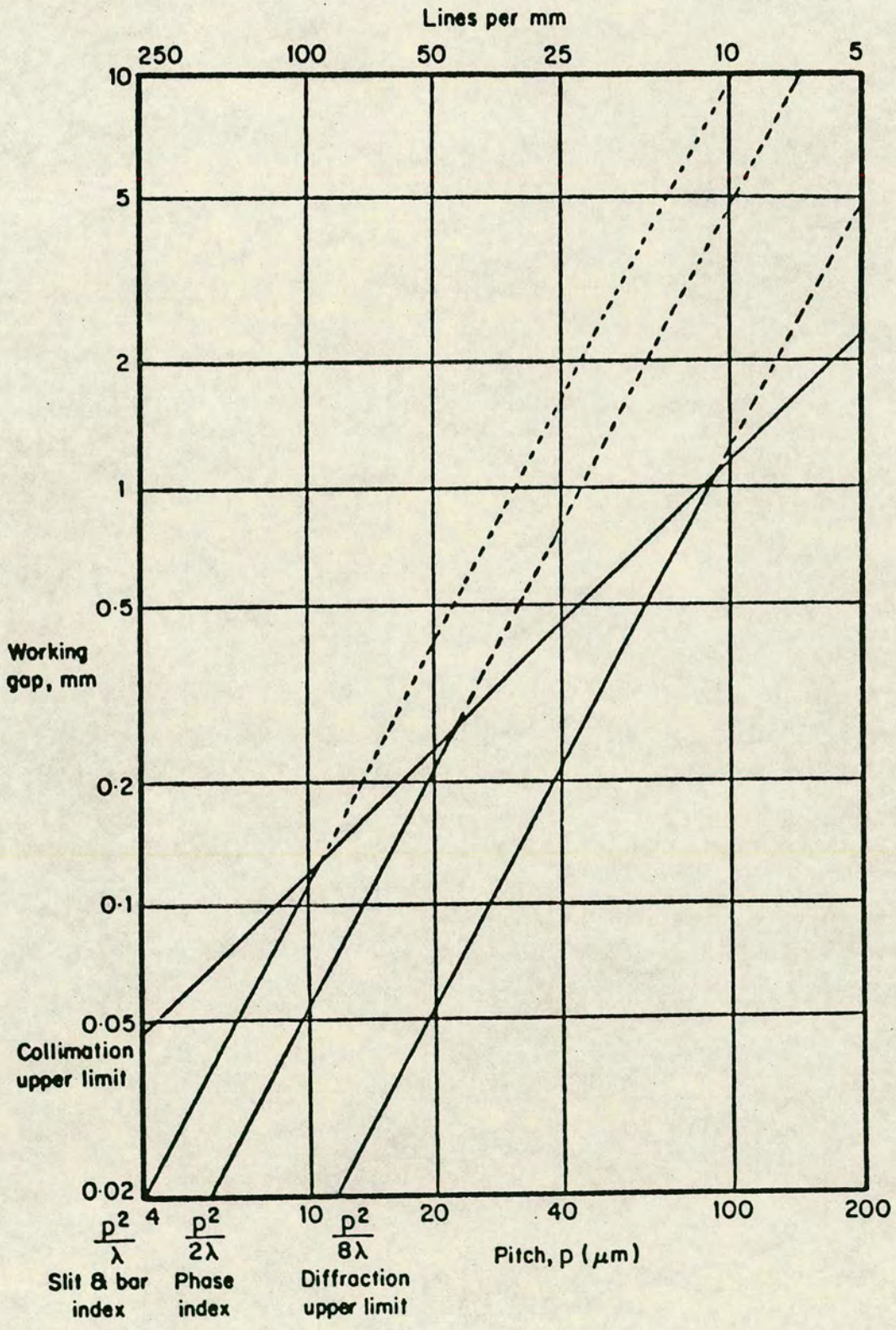

Figure 3.5 WORKING GAP v. GRATING PITCH

(from Luxmoore and Shepherd ref. 11)

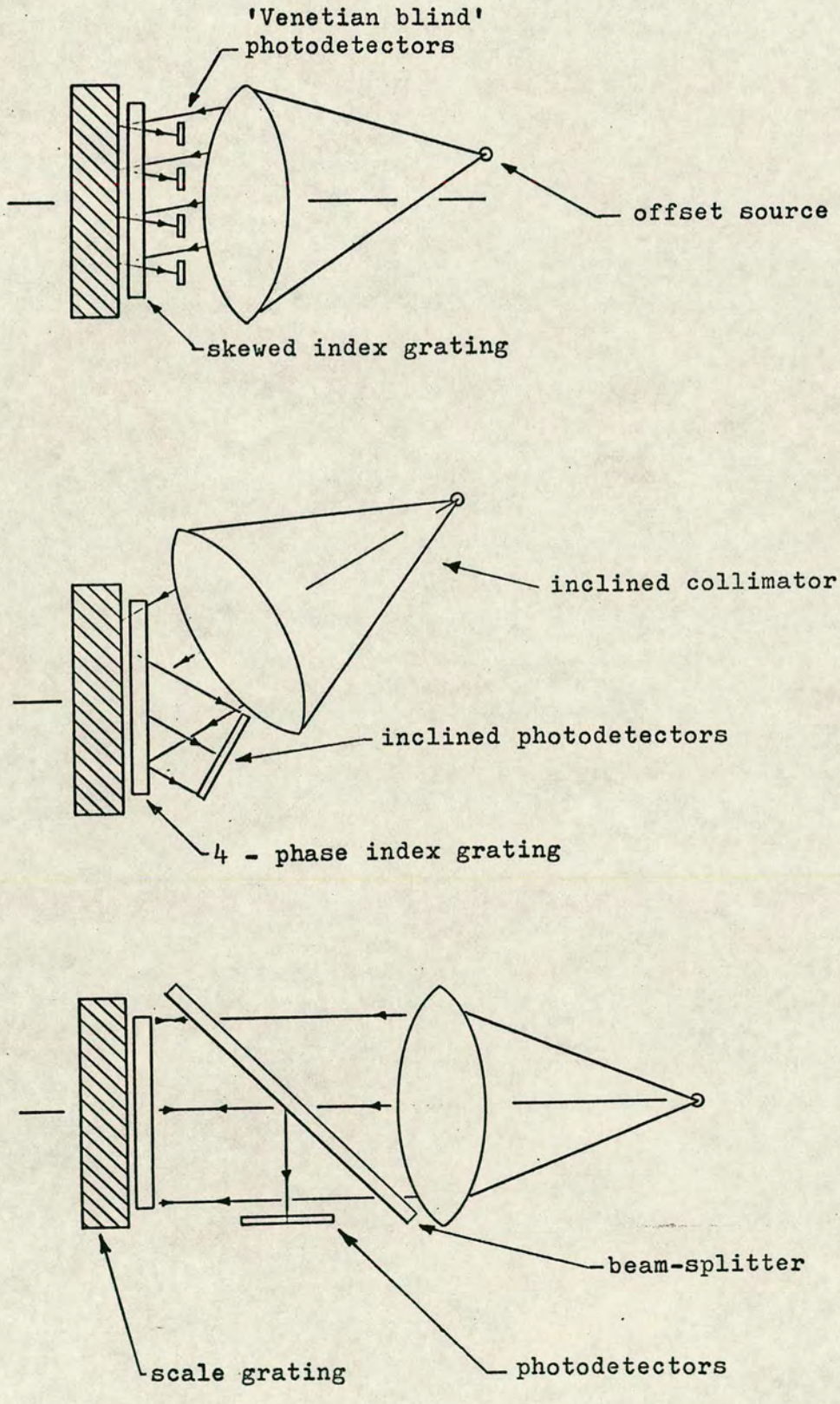

Figure 3.6 REFLECTION READING HEADS

Since the surfaces of the index grating are parallel to the surface of the scale grating, unwanted reflections from these surfaces contribute to an increased d.c. level at the photodetectors thus reducing the modulation depth. Also, the losses due to diffraction are more serious since the light interacts with 3 gratings in series.

Reflection reading heads are therefore more suitable for use with coarser gratings: at 25 lines/mm and coarser, index gratings of the bar and space (amplitude) type are used at working gaps set by the collimation limit whilst at 50 lines/mm a bleached (phase) index grating is used to give a working gap at the first Fresnel image of about 200 μm. Grating pitches between 20 lines/mm and 40 lines/mm are avoided in moiré fringe transducers because of the difficulties in formation and detection of the fringes. At a pitch of 100 lines/mm the working gap would be only 50 μm and the diffraction losses would be severe. For these reasons, the finest pitch of reflection gratings is usually 50 lines/mm and pitches of 20 lines/mm and 10 lines/mm are preferred because of the less demanding tolerances on adjustment and alignment.

3.4 Projection Reading Heads.

With all the simple reading heads described above, it is necessary to maintain a relatively small gap between the index grating and scale grating; the gap should remain constant and parallel over the working stroke of the transducer. In some applications it is not possible to

achieve this level of mechanical control and several designs of projection reading head have been devised to operate at a large working distance (of the order of 5 mm or more) with a correspondingly wider tolerance on variations in the working distance.

3.4.1 'Mirror Image' Projection.

Figure 3.7 shows reading heads in which there is no index grating: the scale grating is imaged back onto itself by a system of lenses and mirrors. Movement of the scale grating in the measuring direction causes its image to move by an equal amount in the opposite direction and thus the apparent pitch of the scale grating is halved e.g. with a 10 lines/mm scale grating (100 micron pitch) the photodetector output would go through one complete cycle for a scale movement of 50 μm. Reading heads of this type have been described by Palmer (1960) [24], Sayce & Jesperson (1970) [25] and De Lang et al (1969) [32].

The afocal reading head described by Shepherd (1976) [23], (1978) [22] used a two stage projection system to image one section of the scale grating onto an adjacent section as shown in figure 3.8. By using four sources and four detectors across the width of the grating a four channel output was obtained, in which all four detectors derived their signal from the same area of grating thereby maintaining d.c. balance in the presence of contamination. The 90 degree phase difference between channels was introduced by a special intermediate mirror

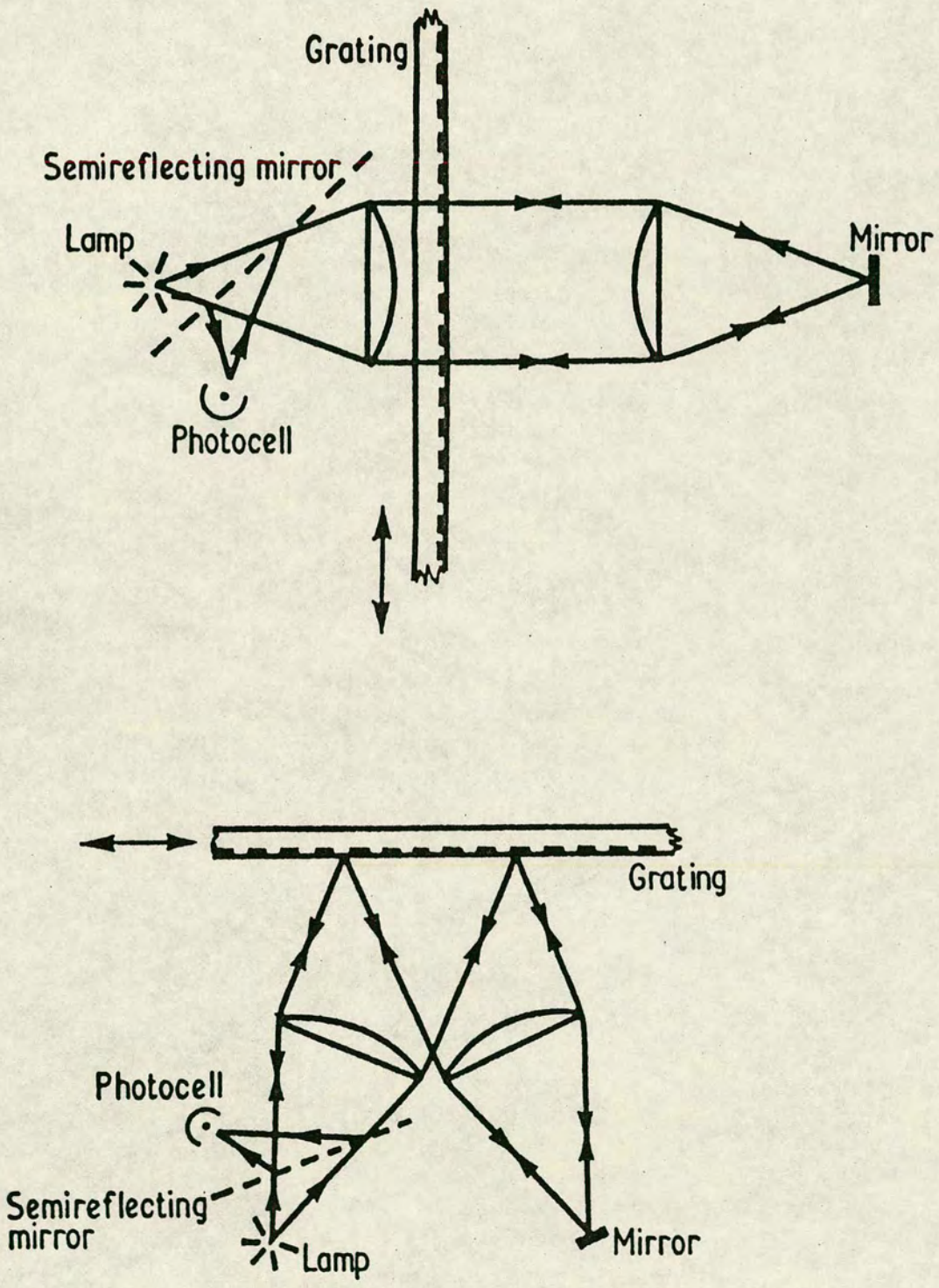

Figure 3.7 'MIRROR IMAGE PROJECTION' READING HEADS
(from Sayce ref. 21)

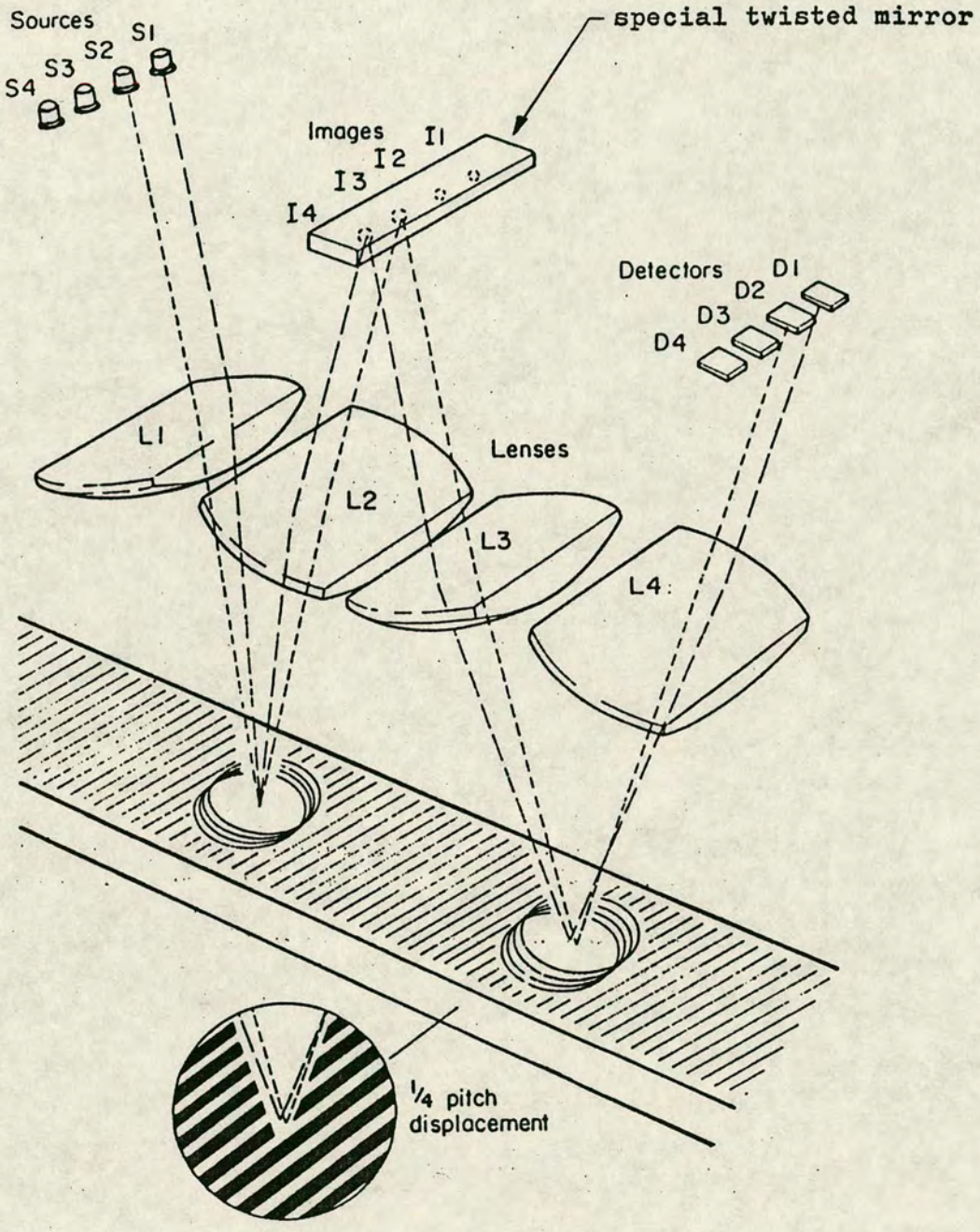

Figure 3.8 AFOCAL PROJECTION READING HEAD

(from Shepherd ref. 22)

between L2 & L3. This mirror was mechanically strained to produce a progressive twist along its length such that the projected image was progressively displaced by 1/4 of a grating pitch at the surface of the scale grating.

3.4.2 Direct Grating Imaging.

Where space is not at a premium or where a long working distance is required, the scale grating may be imaged onto a remote index grating or vice-versa using a projection lens. With a 1:1 imaging system, gratings of identical pitch can be used, but in some cases it may be more convenient to magnify or reduce the projected image. A projection reading head with a 13:1 magnification has been used on the stage measuring system of a wafer stepper by Dey & Johannsmeier (1980) [26].

The major drawback of direct imaging systems is the limitation on the use of fine-pitch gratings. To produce a reliable fringe signal, the lens must produce a high contrast image of one grating in the plane of the other. The tolerances on depth of focus, mechanical alignment and lens quality are thus determined by the pitch of the scale grating. Where mechanical alignment can be guaranteed and where lens cost is not a restriction, a line structure of 50 lines/mm could be regarded as an upper limit i.e. a similar limit to that imposed by the normal-incidence reflecting reading head. However, where mechanical variations and lens cost have to be taken into account, a line structure of 10 lines/mm is a more realistic limit.

3.4.3 'Three Grating' Reading Heads.

Reading heads which utilise the imaging properties of a periodic pupil, as analysed in detail by Pettigrew (1977) [27], can make use of fine-pitch gratings with less critical operating tolerances. The imaging process can be qualitatively explained by regarding the slits in the intermediate grating as an array of pinhole cameras. The imaging conditions were investigated in detail by Pettigrew and are summarised in figure 3.9. The most impressive features of the reflecting reading head, based on the diffraction image, are its small physical size and the insensitivity of the modulation depth to changes in the index to scale gap.

3.4.4 'Holographic' Reading Heads.

In this type of reading head there is no index grating. Instead, two intersecting collimated beams of coherent light create a series of interference fringes on the surface of the scale grating at a spacing which is chosen to match the lines on the scale. The resulting interaction between the patterns is similar to that which would be produced by an equivalent transparent index grating, but without some of the disadvantages. Control of the index to scale gap is no longer a problem as the projected pattern has a large depth of focus and line structures of more than 500 lines/mm can be generated

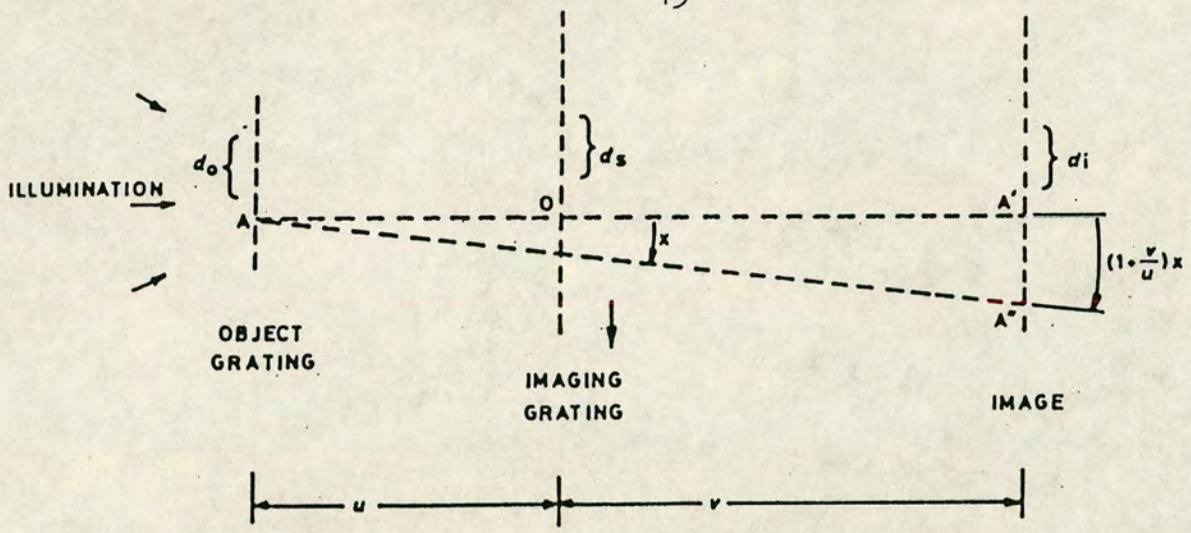

	GEOMETRIC IMAGE	DIFFRACTION IMAGE
a) IMAGING CONDITION	$d_o = d_s(1+u/v)$	$d_o = {}^1/_2\, d_s\,(1+u/v)$
b) IMAGE MAGNIFICATION	$d_i = v/u\ d_o$	$d_i = v/u\ d_o$
c) WAVELENGTH CONDITION	$u = n\,\frac{d_i\, d_s}{\lambda}$	NONE PROVIDED $v > \frac{d^2}{2\lambda}$

GRATING IMAGE FORMING CONDITIONS

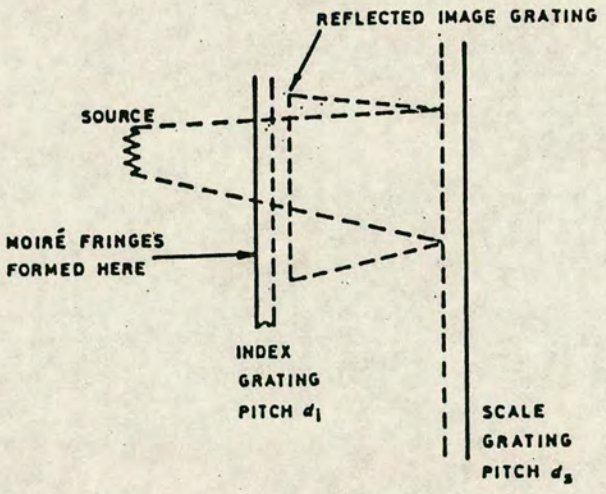

FOR GEOMETRIC TYPE TRANSDUCER $d_i = 2d_s$

FOR DIFFRACTION TYPE TRANSDUCER $d_i = d_s$

REFLECTION THREE GRATING SYSTEM

Figure 3.9 'THREE GRATING' IMAGING CONDITIONS (from Pettigrew ref. 27)

holographically and read successfully. A linear transducer based on this principle has been described by Iwoka and Akiyama (1984) [10] and a two-dimensional grating and reading head with a pitch of 0.8 micron has been used on a wafer stepper by Berger (1984) [9].

3.5 Processing of Photocell Signals: Fringe Interpolation.

3.5.1 'Divide by Four.'

It is clear from some of the limitations on grating pitch discussed above that it is usually necessary to interpolate within the grating pitch to give an acceptable least significant digit size. With the early d.c. coupled photocell signals the phase and quadrature waveforms were squared and then differentiated to generate count pulses at the transitions of the square waves thus producing four count pulses per grating pitch. The accuracy of interpolation depended on the square waves being symmetrical and in quadrature but was essentially independent of the shape of the input waveforms.

3.5.2 Analogue Divide by Ten.

The method of generating count pulses at the zero crossings of the input waveform was extended by Shepherd and McLaren (1964) [28] to sub-divide the pitch by a factor of 10. By connecting a tapped resistor network

across the 4 output phases from the reading head as shown in figure 3.10, with five output taps each connected to a squaring circuit and an inverter, ten square-wave output signals were generated. The difference in phase angle of 36 degrees between adjacent output taps was achieved by choosing the resistor values in each quadrant to be in the ratio of the tangent of the phase angle. The accuracy of subdivision depended on the input waveforms being sinusoidal and symmetrical about a zero volt d.c. level: problems such as clipping of the photocell signals or drift of d.c. level would produce cyclic interpolation errors. For these reasons, this type of analogue subdivision is usable only up to a maximum divide ratio of twenty.

3.5.3 Phase Modulated Carrier Systems.

Some of the problems of the d.c. coupled, analogue system described above can be avoided if the reading head is designed to modulate the phase of a continuous a.c. waveform. The foundations of phase sensitive detection methods in instrumentation have been described by Blair & Sydenham (1982) [36]. Phase comparison with a fixed reference waveform can readily detect differences of less than 1 degree so that linear interpolation to 1/100 of a grating pitch becomes feasible.

One of the earliest such reading heads {Barber and Atkinson (1959) [30]} used a rotating cylindrical grating to generate a continuously moving pattern of grating lines

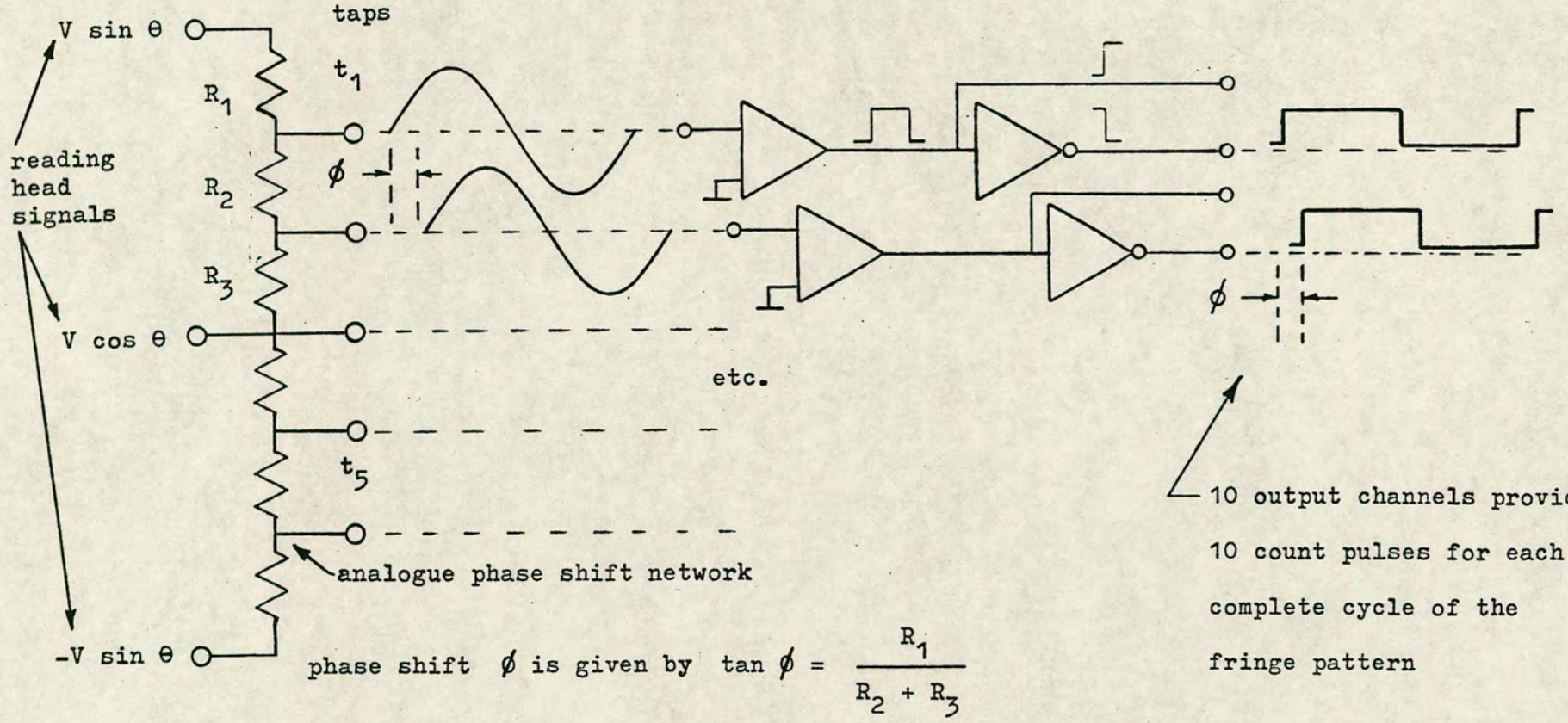

Figure 3.10 ANALOGUE DIVIDE BY TEN INTERPOLATION

which was projected onto the measuring scale and also onto a short section of reference or index grating within the reading head. A photodetector behind the fixed index grating provided a reference waveform against which the signal from another photodetector behind the movable scale grating was compared. A similar mechanical scanning reading head, using a spiral grating pattern on a rotating transparent disc, was used with 100 lines/inch reflecting gratings on the Ferranti MKIV continuous path control system. Other such systems have used vibrating galvanometer mirrors {De Lang et al (1969) [32], Sayce & Jesperson (1970) [25]}.

An alternative approach, involving continuous rotation of the plane of polarisation, was described by Jones & Forno (1975) [37]. A 3-phase index grating was used in a transmission arrangement where the total light transmitted by all 3 windows on the index grating was monitored by a single photocell. Each window had a polarising filter attached such that its polarising axis was at 120 degrees relative to the others. By illuminating the gratings through a continuously rotating polariser, the photocell in effect sampled the transmitted intensity from each of the windows in turn and the phase of the moiré fringe could be decoded from the output signal. With mechanical rotation of the polariser at 6600 rpm the fringe rate was restricted to only 2 fringe/sec but use of an electro-optic crystal to rotate the polarisation raised the fringe rate to 100 fringe/sec.

The first all-electronic phase-modulated reading

head was developed at Staveley Research by Davies et al (1960) [29]. The four photodetectors in a conventional reading head were sampled at about 2 KHz using a 4-phase clock as shown in figure 3.11. The clock phases overlapped and the four photodetector output signals were summed to produce a stepped temporal waveform with a periodic time equal to that of the clock, provided the fringe pattern remained stationary. Subsequent a.c. amplification and integration of this stepped waveform produced a signal which could be squared by a zero-crossing detector and then compared in phase with a reference signal derived from the clock. The phase difference between these TEMPORAL waveforms was a direct measure of the SPATIAL phase difference between the lines on the index grating and the scale: a relative mechanical displacement of 1/4 of a pitch would produce a temporal phase shift of 90 degrees. If the two gratings of pitch (p) had a relative velocity (v) the output waveform would have a frequency f_o, given by

$$f_o = f \pm \frac{v}{p}$$

where f was the frequency of the clock. Thus the upper limit on velocity was determined by the sampling frequency of the photodetector signals. To interpolate within a grating pitch by a factor of 100, clock pulses at a frequency of 100f were gated by the phase comparator circuit and counted to give a displayed resolution of 0.0001 inch from gratings with 100 lines/inch. The transistors available at that time limited f to about 2.5

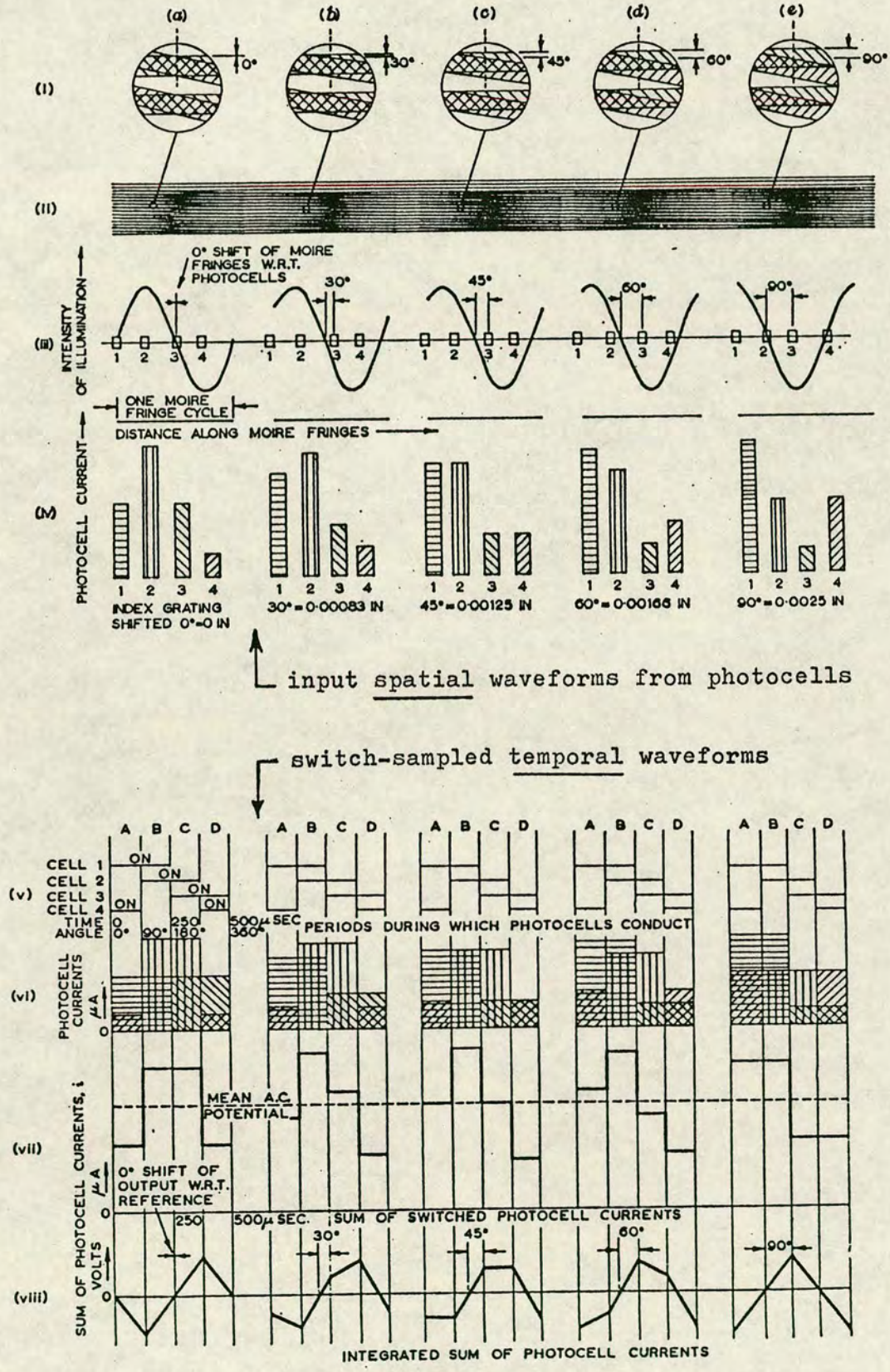

Figure 3.11 STAVELEY PHASE-MODULATED CARRIER SYSTEM
(from Davies et al ref. 29)

kHz, i.e. the count pulses occurred at intervals of 4 μs.

The Staveley system was a milestone in the sense that it provided reliable interpolation from a robust, relatively coarse-pitch reading head with a.c. coupling and digital signal processing.

A similar system was introduced more than ten years later by Ferranti, {Shepherd (1978) [22], [33]}. Advances in electronic component performance and LSI circuitry allowed operation at a clock frequency of 8 MHz with a corresponding improvement in the sampling rate and velocity limit. The phase modulated carrier signal was amplified with automatic gain control prior to filtering and digital phase comparison. Comprehensive checks on signal quality e.g. amplitude, frequency and quadrature of photodetector signals were included to provide warning of unreliable data.

It has been pointed out by Russell et al (1976) [34] that the use of a filter rather than an integrator prior to phase comparison can give rise to dynamic interpolation errors if the phase shift in the filter stage is a function of frequency.

3.5.4 Phase Locked Loop (PLL) Methods.

A multi-element linear array of photodiodes may be used to detect the fringe pattern instead of the four discrete photodetectors described above. If the fringe spacing is chosen to match the length of the array of diodes, repeated scanning of the array will produce a

continuous video output signal on which the amplitude represents the fringe intensity and the phase represents the fringe position. The phase of this video signal may be tracked using a phase locked loop which is inherently unlikely to introduce spurious phase shifts as it is a nulling system. The phase is measured by digital processing of the square wave VCO output signal. Russell et al (1976) [34] have shown that dynamic interpolation errors are typically less than 0.5% with a PLL and that the system can be made less sensitive to optical imperfections if the fringe spacing is reduced so that several fringes are sampled by the linear array.

McKeown and Bent (1979) [35], figure 3.12, used a PLL with a divide by N counter in the feedback loop between the VCO and the PSR. With the VCO operating at N times the array frequency, the VCO output will change in phase by 360 degrees when the array signal changes in phase by 360/N degrees.

3.6 Conclusion.

From the review of metrological gratings and optical displacement transducers it is clear that there have been considerable developments and changes in overall system design since the early 1950's. Although the early gratings were difficult and expensive to produce, the cost and complexity of the associated electronic fringe counters was probably even greater. It was essential to use fine-pitch gratings to get good resolution

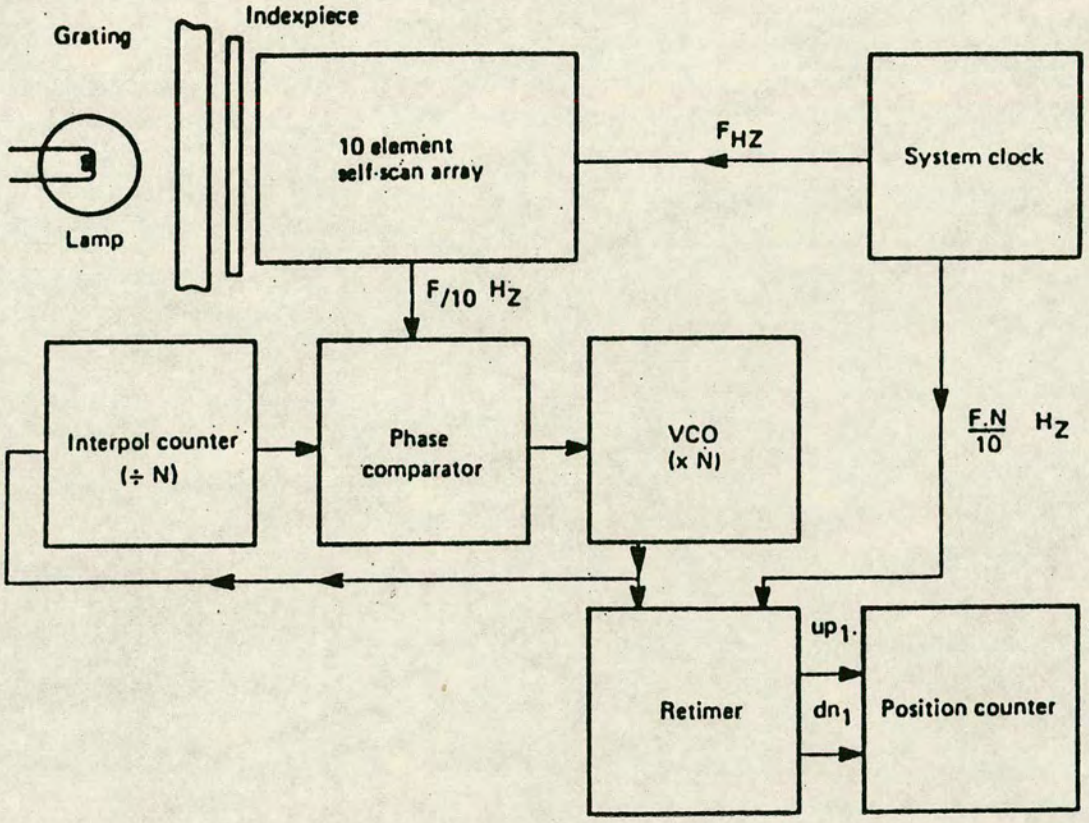

Figure 3.12 PHASE LOCKED LOOP : DIVIDE BY N SYSTEM
(from McKeown and Bent ref. 35)

and this imposed strict mechanical tolerances on the installation of the reading heads.

The introduction of the NPL Method III printing bench made a wider range of line structures available and improved the accuracy of gratings, especially over long lengths. Developments in fringe interpolation have reduced the need for fine-pitch gratings thereby easing the problems of reading head alignment and reducing mechanical and optical costs. The complexity has been transferred to the electronics where integrated arrays of photodetectors and digital signal processing are able to provide fringe interpolation and high speed counting at modest cost.

Fine-pitch gratings will still be required to provide the ultimate in resolution, especially in applications where it is not possible to use a laser interferometer. One such application is in detecting the misalignment between mask pattern and wafer in the fabrication of microcircuits. This will be reviewed in chapter 5.

CHAPTER 4: ABSOLUTE POSITION ENCODERS.

4.1 Introduction.

The techniques for digital measurement of mechanical position fall into two basic categories: incremental systems in which a pulse is produced for each unit of DISPLACEMENT and absolute systems in which each point on the axis of measurement is uniquely encoded as a pattern of bits which may be read and decoded to determine the absolute POSITION.

There is an on-going philosophical argument as to the pros and cons of the two types of system without any clear-cut answer emerging. The main features of each type have been summarised by Whitwell (1973) [82].

4.2 Multi-track Scales.

The most common example of the absolute transducer is the rotary shaft encoder in which the bit patterns are defined on a series of concentric tracks, the patterns being read by an array of detectors, one for each track, arranged in a radial line. The multitrack approach may also be applied to linear measurement but the need for fine resolution combined with large range requires a larger number of tracks and detectors with consequent increases in the cost of the scale and the complexity and alignment of the reading head. Examples of multitrack scales are shown in figure 4.1.

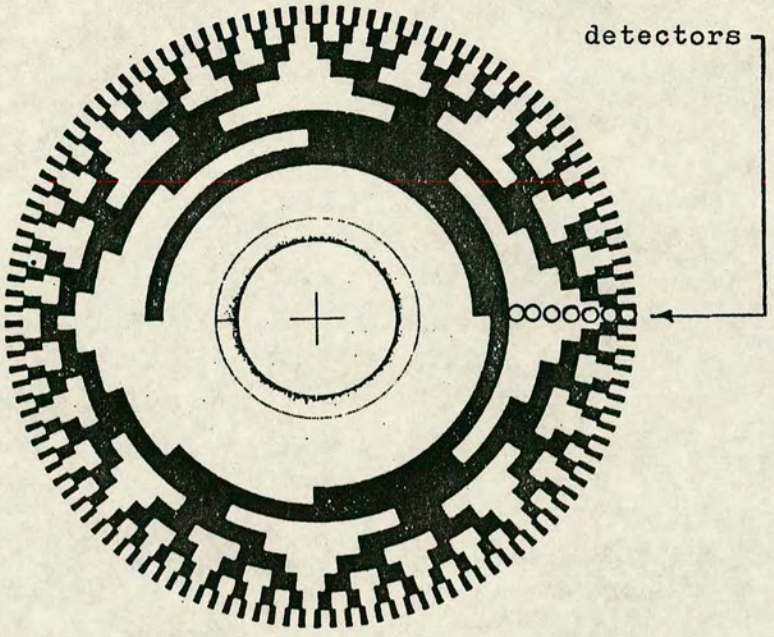

rotary shaft encoder

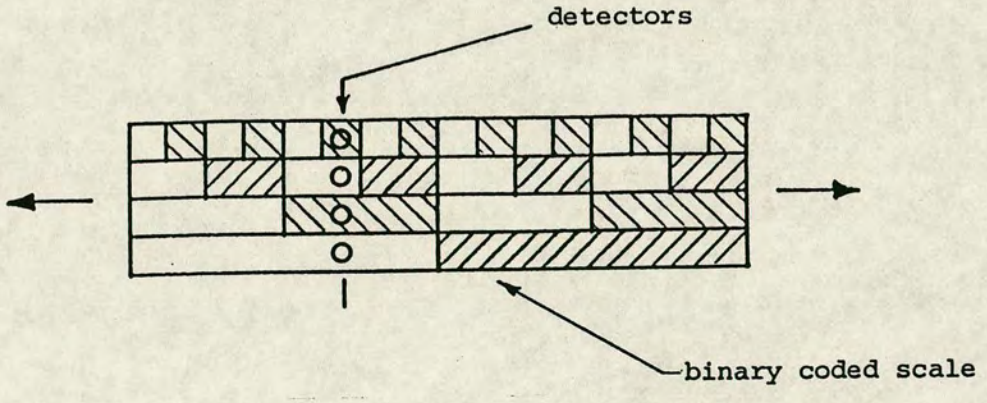

linear position encoder

Figure 4.1 MULTI-TRACK POSITION ENCODER SCALES

4.3 Electronic Signal Processing.

The conventional single-track grating transducer with a bi-directional fringe counter is a purely incremental system. The reading head is simple and the display may be reset to zero at any point in the travel. Experience has shown that such systems are convenient to use, cost effective and sufficiently reliable for use on machine tools and inspection equipment. On the debit side, any interruption in the power supply causes position to be lost and the datum must then be re-established. There is also the possibility of the position display being corrupted by electrical interference. Various measures may be taken to eliminate interference, including filtering of the transducer signals but care has to be taken not to restrict the bandwidth of the system if a high velocity capability is to be maintained. The count pulses may also be monitored so that a fault warning can be given if pulses outwith the acceptance envelope are detected.

It can be argued that absolute transducers need not have a high bandwidth and hence can have a higher velocity capability than the incremental type since the readout is a decoding operation at each position. This is true only if the measurements are being made in a static or quasi static mode with high velocity movement between the measurement points. If measurements have to be taken in a dynamic mode, i.e. on-the-fly, then the requirements on

bandwidth and in particular on phase lag are similar in both types of transducer.

4.4 Advantages of Absolute Transducers.

It is clear from the above that there are applications where absolute transducers can offer definite advantages. The key factor to be considered is the timescale over which the measurements are to be made. If this extends over days, weeks or longer and it is not possible to re-check the datum at regular intervals, some form of absolute transducer is required. Examples include the measurement of creep in material test specimens and the monitoring of settlement and deformation in civil engineering structures. Absolute transducers also offer the possibility of operating in a periodic sampling mode thus allowing multiplexing of multiple sensors and a saving of power since the unit need be switched on only when a reading is required.

4.5 Hybrid Systems.

Hybrid systems have been designed which seek to combine the best of both types. Russell (1966) [83] devised a system for use on machine tools in which an optical grating measured the linear movement of the tool-holder and a shaft encoder measured the rotary position of the leadscrew. The accuracy of tool positioning was determined solely by the optical grating.

The decoding of absolute position was done by hard wired interrogation of the fringe signals and the encoder outputs which were in a known, fixed relationship.

Another hybrid system, which evolved from the linear position encoder developed at NEL in 1966, was described by Whitwell [82]. A three-track grating with a decimal ratio between the tracks provided the three least significant digits of the readout with unambiguous, absolute information and decade counters were used for the more significant digits. In the event of power interruption or at switch-on, the more significant digits could be pre-set manually to the correct value whilst the fine position information from the grating made careful re-setting of the datum unnecessary. The difficulty of scale manufacture and reading head alignment limited the range of this method to a maximum of three tracks.

4.6 Single-Track Linear Position Encoders.

Absolute position may be encoded on a single track using a serial binary sequence or chain code, such that any group of a predetermined number, n, of consecutive bits in the sequence differs from any other such group and can therefore be decoded to determine its unique position within the sequence.

A twin-track scale with a code track alongside a linear grating was devised by Kennedy et al (1970) [84] as a hybrid system. The binary code was implemented as opaque bars on a transparent substrate. The reading heads

used a mechanical scanner to read both tracks simultaneously, the sample of n bits being scanned repeatedly at the same frequency as the moiré fringe from the grating. Phase comparison of the two signals allowed interpolation to 0.001 pitch, and thus with n=14 and a pitch of 1 mm the system could read out to 1 μm over a range of about 16 m. An arrangement of multiple photocells to read the coded pattern in a parallel manner was also described, as well as other methods of fringe interpolation.

A single-track scale with a parallel array of sensors arranged along the axis of measurement was also proposed by Silkin (1976) [85] who pointed out that the sensors need not sample a group of adjacent bits but could be more widely spaced along the scale provided the spacing corresponded to an integral number of bits.

The advantages of Pseudo Random Binary Sequences (PRBS) as maximal length codes for measuring scales were pointed out by Jones & Zia (1981) [86]. The maximum length of a PRBS of order n is 2^n -1 bits and hence, for any value of n, the maximum length of scale can be calculated once the physical length of an individual bit is established. The sequence may be generated using a n-stage shift register as shown in figure 4.2 or by a suitable computer program. The same program can also be used to decode the data from the transducer.

The displacement transducer described by Jones & Zia used a single detector for serial reading of the scale pattern into a microcomputer where it was decoded by

n - stage shift register with linear feedback

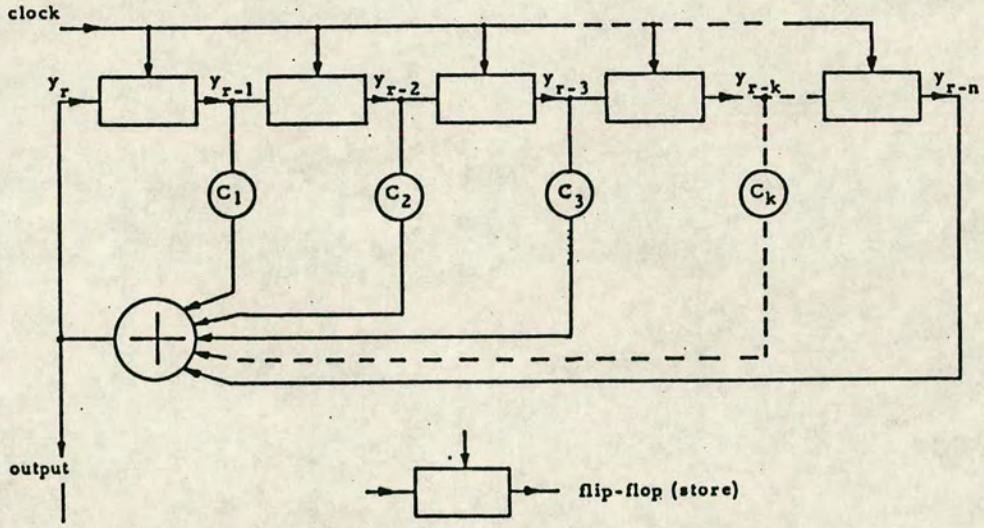

Shift register to generate PRBS
(from Jones & Zia ref.86)

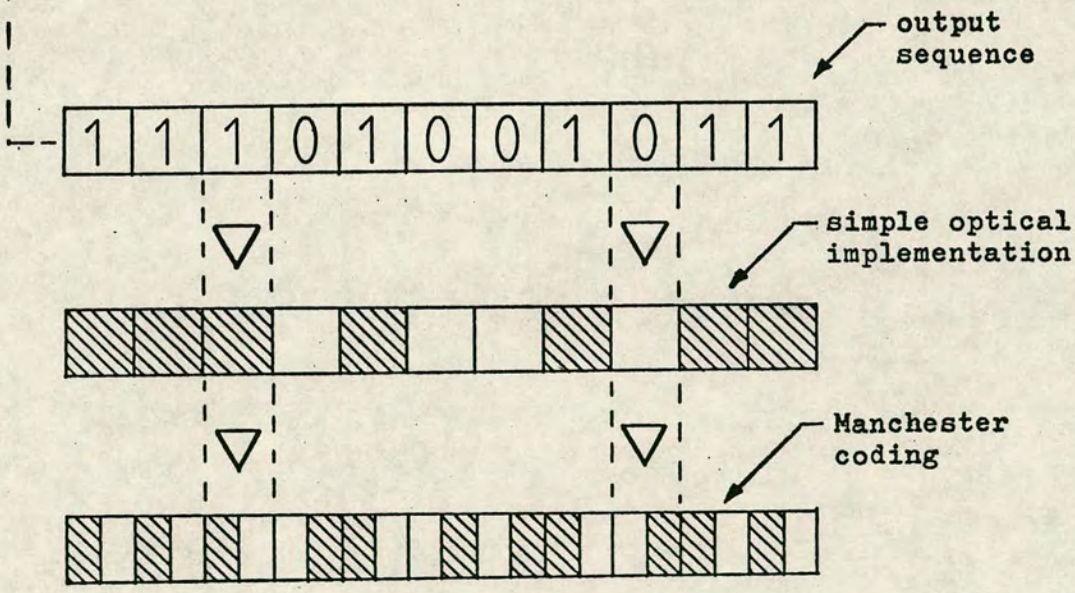

Figure 4.2 GENERATION AND IMPLEMENTATION OF PRBS CODES.

comparison with a similar pattern generated internally. Any serial reading head with a single detector requires an additional channel of information such as another detector in quadrature in order to determine direction of movement. In this case a separate track with an additional detector was provided. Another disadvantage of a serial reading system is the inability to determine position after switch-on until a displacement of at least n bits has occurred.

A parallel reading arrangement using a linear array of photodiodes was devised by Johnston (1983) [87], completely independently of the author. The implementation of the binary code on the scale was also identical to that chosen in this project in that each bit was encoded as a pair of adjacent bars as shown in figure 4.2, a method known as Manchester coding. This ensures that the overall optical density of the scale is uniform, irrespective of the proportion of 0's and 1's in the code, and that there are equal numbers of dark and clear bars in any sample from the sequence. The latter property could be used to prevent errors by detecting debris or defects on the scale. Further immunity to defects and errors was provided by the use of a digital correlator to find the best match between the transducer signal and the reference pattern. By choosing a detector spacing which was much smaller than the bars of the coded pattern, the position resolution was improved by locating the transition points in the coded pattern to the position of the nearest detector in the array. Thus the absolute position could

be determined to within +/- the width of 1 detector instead of to the nearest bit of the coded pattern.

4.7 Conclusion.

The main types of absolute position encoder have been reviewed and the advantages of hybrid systems have been discussed. The multitrack approach used in rotary shaft encoders is inappropriate to linear measurement where a single track scale has clear advantages. The reading of such scales is made easier by the availability of linear arrays of photodiodes thus enabling position to be read to within about +/- 20 μm. This is still too coarse for many applications. An additional track on the scale with a linear grating and moiré fringe interpolation is one solution. An alternative, which will be described in chapter 7 is to combine both absolute coding and a linear grating on a single track, thereby producing a 'universal' scale suitable for both absolute and incremental reading heads.

Serial coding of absolute position could also be applied in two dimensions to produce an XY position encoder plate. No reference to this approach has been found in the literature. The design and implementation of an XY position encoder is described in chapter 7.

CHAPTER 5: THE USE OF MOIRÉ FRINGE TECHNIQUES IN MICROFABRICATION.

5.1 XY Stage Measuring Systems.

Moiré fringe measuring techniques have been widely used in microfabrication equipment. The early optical pattern generators and step-and-repeat cameras used glass gratings as measuring scales on their XY stages, an example being that described by Milne et al (1978) [17]. More recently, laser interferometers have taken over this task in maskmaking equipment but it has been found that moiré fringe systems are less susceptible to the temperature fluctuations which occur in wafer fabrication areas. For this reason, the stage measuring system on the Optimetrix wafer stepper is based on a two dimensional grating or grid plate ruled with 50 lines/mm on a quartz substrate, {Dey & Johannsmeier (1980) [26]}. The stepper described by Berger (1984) [9] used a two dimensional holographic grating with a pitch of 0.8 micron. The reading head operated in reflection using coherent illumination in a holographic configuration to give a least significant digit of 0.1 micron. A similar system with additional analogue interpolation to 1 nm on a one dimensional scale has been described by Iwaska and Akiyama (1984) [10], and commercial transducers based on holographic techniques are available from Holograf [57].

5.2 Mask to Wafer Alignment - General.

Production of microcircuits involves several stages of layer deposition and patterning. At the second and at all subsequent stages, the mask pattern must be aligned to the existing pattern on the wafer prior to exposure. The alignment tolerance is usually a function of the smallest dimension on the pattern and all circuit designers aim for a device layout which is tolerant of misalignment without sacrificing packing density. On MOS devices the most critical patterns have to be aligned to within about one fifth of the smallest dimension, {Broers (1985) [58]}.

For various reasons both technical and economic, critical dimensions are being reduced whilst wafer sizes are being increased - trends which make the task of layer-to-layer registration increasingly difficult. Although the rate of miniaturisation is slowing down, Broers (1985) [58] has predicted that by the early 1990's lithography equipment will have to be capable of defining features of 0.5 micron with an overlay accuracy of +/- 0.15 micron (3 sigma). This overlay requirement is comparable with the line placement accuracy on traditionally ruled diffraction gratings. It is most unlikely that any whole-wafer projection system can achieve this level of accuracy on 200 mm diameter wafers and thus a step-and-repeat system with direct referencing of the reticle to the wafer pattern will be essential.

5.3 Wafer Steppers.

5.3.1 Alignment Strategy.

There is no agreed standard on the type of alignment mark and associated detection technique for use on wafer steppers: there are as many systems as there are makes of stepper. The marks vary from simple crosses to Fresnel zone targets and grating patterns, and the detection systems range from simple photodiode and slit arrangements to video cameras with complex image processing. However, all these systems have some factors in common:

(a) the wafer is globally aligned in x, y, z and θ prior to stepping. Thus the surface of the wafer is levelled in the image plane of the optics and the overall pattern is aligned parallel to the XY axes of the stage

(b) the marks for site alignment are usually placed in the scribe channels

(c) the marks are fairly small in area, usually less than 200 μm square, and are intended to be used when the stage is either stationary or moving slowly near each exposure site to update the local site co-ordinates

(d) the local site corrections can be confined to small xy adjustments unless the wafer stage exhibits significant yaw error in which case local adjustment of θ may be required.

5.3.2 Blind Stepping.

Before describing the alignment systems on steppers in detail, it is useful to consider the different philosophies and options available. Irrespective of the techniques employed, the wafer must be globally aligned in x, y, z, and θ prior to exposure, see figure 5.1. The initial Z adjustment or wafer levelling is done using the automatic focus sensors to align the top surface of the wafer in the image plane of the lens. Thereafter, the wafer is aligned in θ, y, x with respect to the main XY stage and optical column. The early steppers used an off-axis microscope to view and adjust the global alignment of the wafer and then exposed each site by moving the stage to the nominal x, y co-ordinates after allowing for the baseline or offset between the optic axis of the microscope and optical column. This mode of operation is known as blind stepping since there is no re-checking of alignment at each site. The overlay accuracy clearly depends on:

(a) the initial reticle alignment relative to both the optical column and the axes of the wafer stage
(b) the initial global wafer alignment
(c) the stability of the baseline
(d) the repeatability of the x,y stage
(e) the amount of wafer distortion during the process.

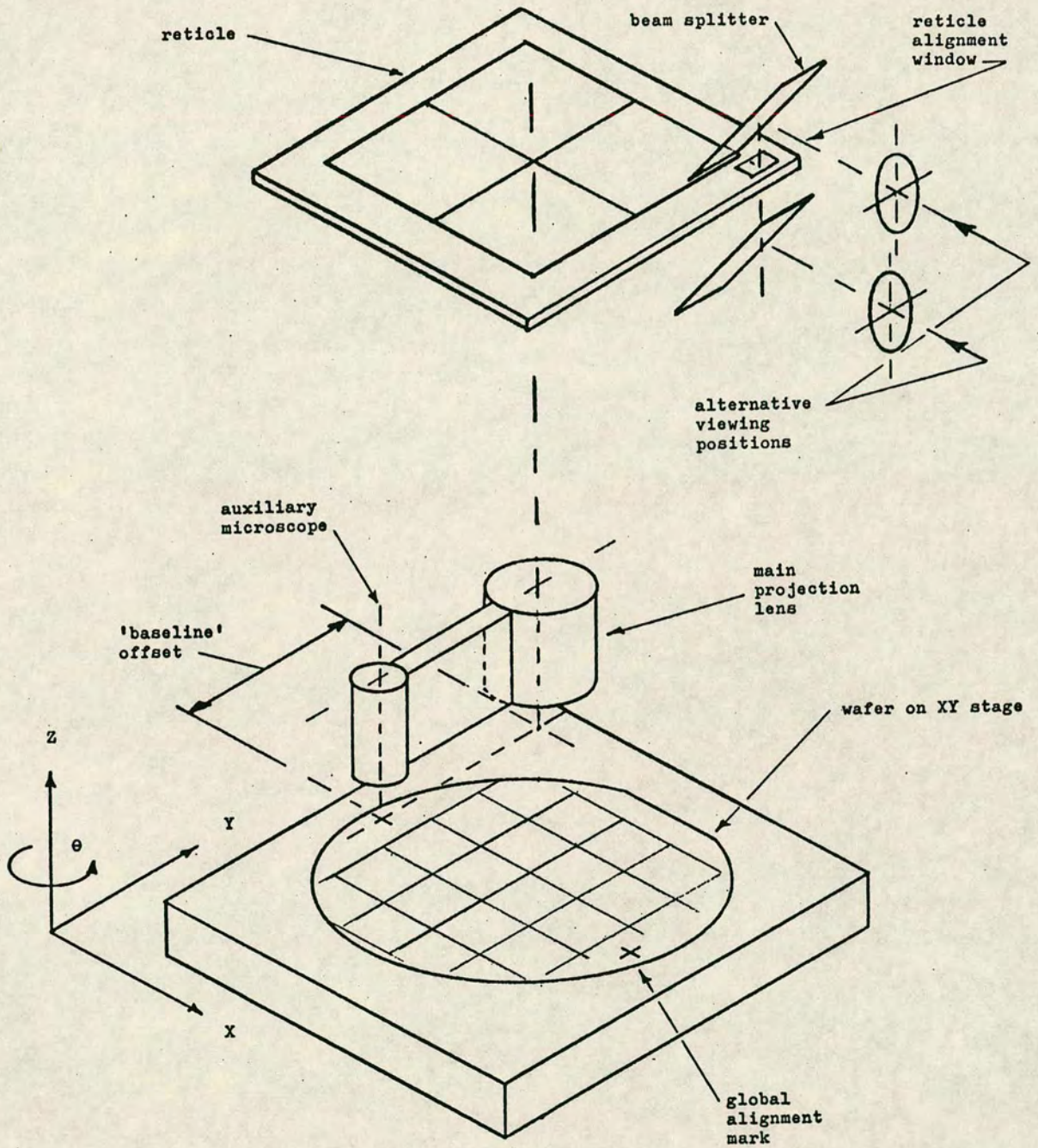

Figure 5.1 WAFER STEPPER ALIGNMENT OPTIONS

The errors from (c) and (e) can be reduced by frequent checking of the baseline and by measuring the actual separation of the global marks on each wafer. Any departure from nominal can be applied as a linear scale factor to the blind step co-ordinates. A typical value for wafer distortion is 10 parts per million or 1 micron across a 100 mm diameter wafer.

5.3.3 Die-by-Die alignment.

The ideal alignment system would refer a target on the wafer directly to the corresponding target on the reticle using the main projection optics and thus re-check alignment at each die site prior to exposure, without any baseline offset. The advantages of such a "direct-reticle-referenced die-by-die alignment system" have been analysed by Lavine et al (1985) [64]. Several designs of die-by-die alignment system have evolved, using a variety of techniques. The essential feature of all direct-reticle-referenced systems is an alignment detector which operates through the main projection optics.

5.4 Detection of Alignment Marks.

5.4.1 Outline.

The approaches to alignment detection fall into three main categories:

(a) video systems which capture an image of the wafer and reticle targets

(b) simple bar (on wafer) and slit (on reticle) targets where the combined reflected intensity is detected directly or where the wafer target is scanned by a laser spot and the reflected light is detected

(c) targets in the form of gratings or Fresnel zone plates which diffract light in a structured way and where both the phase and the amplitude of the reflection from the target are used to derive the alignment error signal.

5.4.2 Video Methods.

A video image of the superimposed reticle window and wafer mark may be obtained by introducing a beam splitter and camera optics either above the reticle or between the reticle and the main projection lens, as shown in figure 5.1. Both configurations are in use on existing steppers: above the reticle viewing is used by ASET [59], [65], whereas below the reticle viewing has been used by GCA [64] and Optimetrix [26]. Ideally, the alignment mark should be illuminated using the actinic wavelength for which the projection lens is corrected. This illumination will expose the photoresist and it is essential, therefore, to either limit the intensity and time of the illumination or to mask off the rest of the reticle during alignment viewing and to use a separate mask for each

layer.

5.4.3 Visibility of Marks.

When viewed from above, the alignment window on the reticle is seen in reflection and will appear as a dark aperture containing the image of the wafer mark, with a bright surround. Conversely, when viewed from below, the reticle image is projected through the main lens onto the wafer mark and the superimposed patterns are then projected through the main lens again onto the camera tube, see figure 5.1. Thus the light from the reticle window passes through the main lens twice in this configuration. This is of little consequence if the lens is aberration free but if, for example, the alignment wavelength is different from the exposure wavelength the focus shifts and aberrations due a double pass through the lens will be difficult to correct. Correction optics can introduce lateral image offsets leading to alignment errors. In general therefore, alignment and exposure at the same wavelength will produce a more accurate result.

However, recent developments in photoresist technology such as anti-reflection coatings (ARC), contrast enhancing layers (CEL), absorbing dyes in the resist and the trend to shorter exposure wavelengths have made the task of alignment at the actinic wavelength much more difficult. The optical absorption of the resist can be so high that the underlying alignment mark is invisible, see figure 5.2. If the topography of the mark,

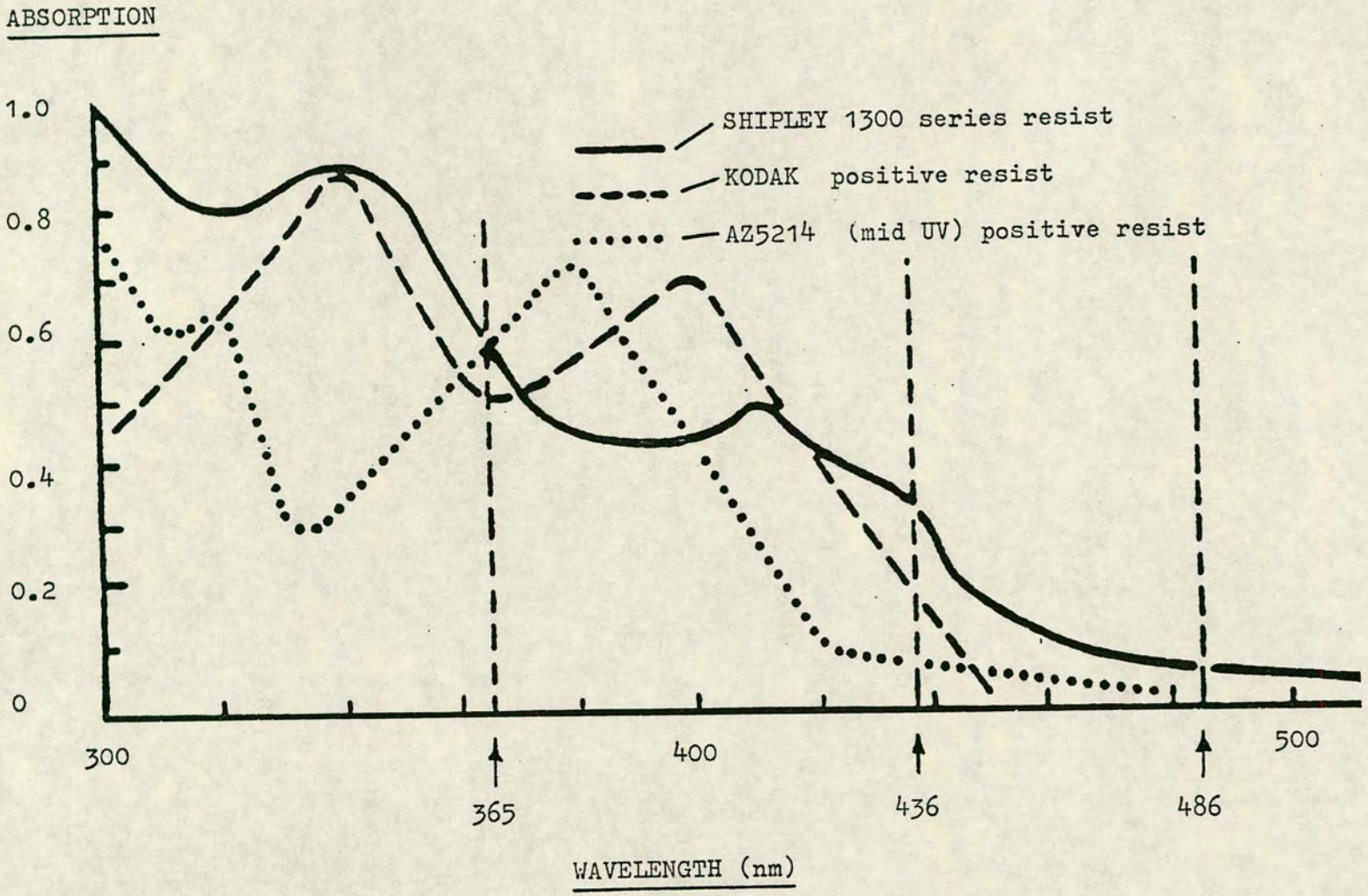

Figure 5.2 ABSORPTION SPECTRA FOR PHOTORESISTS
(after Yao ref. 65)

either trench or mesa, is replicated on the surface of the resist, the edges may be detected using dark field illumination or other methods based on light scattered from the edges of features. Unfortunately there is a general trend in semiconductor processing towards planarisation which, if totally successful, would defeat such systems.

Various solutions to this problem have been devised. The resist covering the mark may be exposed and developed away in an additional, separate, photolith operation or it can be ablated or blasted away by a high energy pulse from an excimer laser. Pre-exposure of the area to cause bleaching of the resist prior to alignment has also been used. These methods can reduce the throughput of the stepper to unacceptable levels and hence the use of a longer non-actinic wavelength to which photoresists are transparent, with appropriate correction optics, has been adopted by ASET [65] on a stepper which exposes at 365 nm. Alignment is done at 514 nm with a bandwidth of 40 nm to minimise thin film interference effects. Several other manufacturers have also adopted longer wavelengths for alignment such as CENSOR (yellow/green) and ASM-L (633 nm He-Ne laser).

5.4.4 Video Image Processing.

The video image of the superimposed alignment marks may be captured, stored and then processed in various ways. The penalty for digital processing of video images

is the time taken to deal with the large amount of data in addition to the time taken to capture and store the image. The main methods have been reviewed by Lavine et al (1985) [64], who pointed out that the choice of algorithm is somewhat arbitrary and intuitive. Noise suppression is usually achieved by averaging over a number of line scans or over several complete frames, in addition to any conventional electronic filtering. Edge detection of mask and wafer features could, in theory, be achieved by threshold triggering but experience has shown that differentiation of the video signal gives a more reliable result and is more tolerant of variations in reflectivity and contrast.

5.4.5 Correlation.

The enhanced video image is usually correlated with the 'ideal' pattern corresponding to perfect alignment. The wafer-to-mask alignment is adjusted until the output of the correlation operation is maximised. This sequence requires repeated correlation of a pair of two-dimensional patterns, each of which might contain up to 256K elements. To reduce the computing time, alignment marks in the form of chevrons can be used to derive both X and Y alignment information from a one-dimensional line scan. Such patterns as used by 'Optimetrix' [26] are shown in figure 5.3. In principle a single line scan and a one-dimensional correlation algorithm would suffice but in practice a number of line scans are averaged to reduce

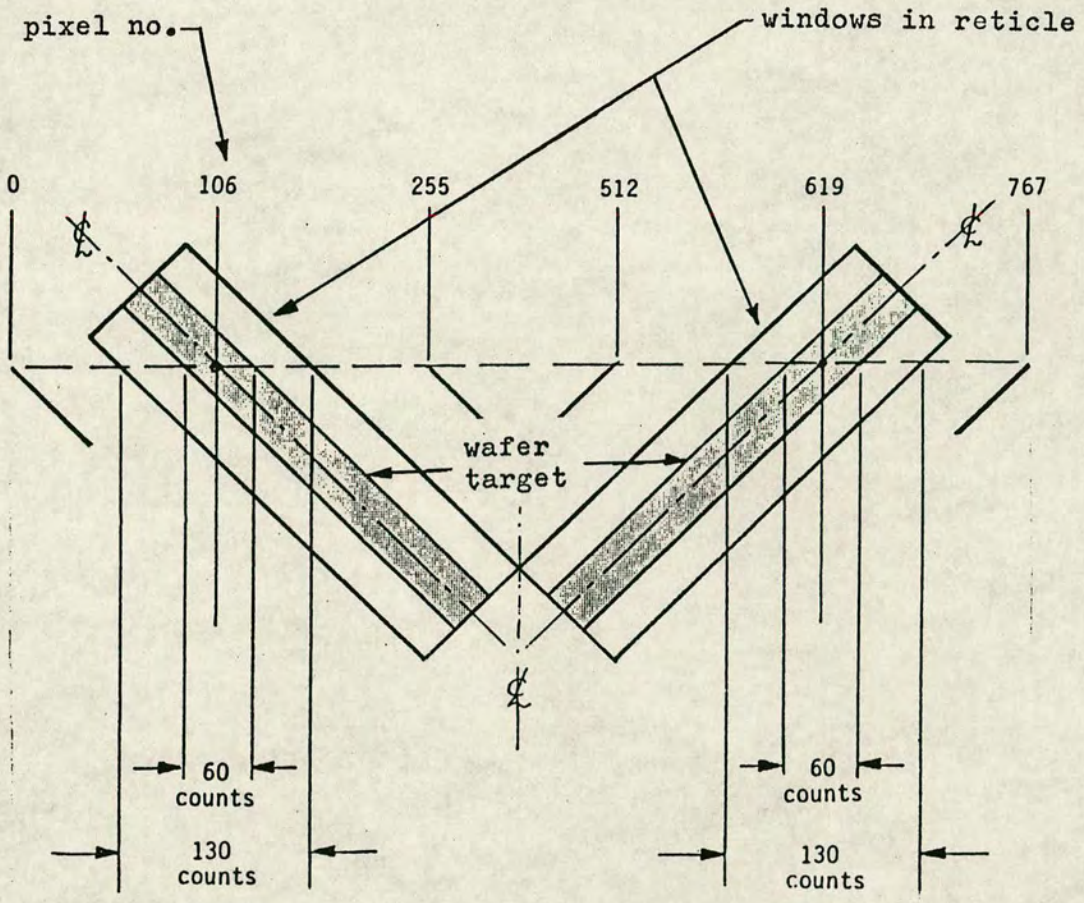

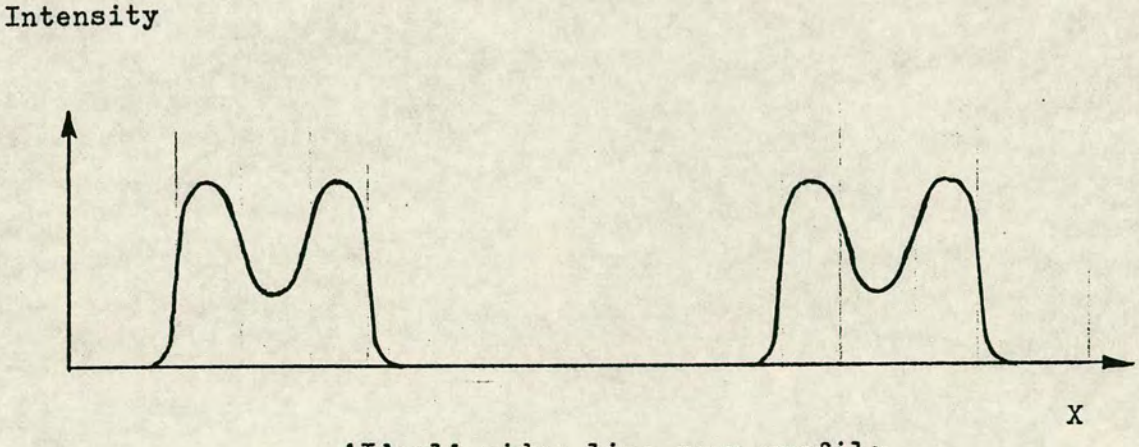

'Ideal' video line scan profile

Figure 5.3 'OPTIMETRIX' ALIGNMENT MARKS

noise and uncertainty of edge position.

It is likely that video processing methods will see significant improvements in the near future as the cost and availability of parallel computing hardware such as the transputer improve, thereby reducing the time penalties. However, all direct video viewing systems are limited in performance by the optics between wafer and camera tube and are thus unlikely to match the resolution and process tolerance of interferometric methods based on gratings and other periodic structures.

5.4.6 Bar and Slit Targets.

If the width of the window or slit on the reticle is reduced until it matches the width of the trench or mesa on the wafer, the correlation of the bar image with the reticle slit may be achieved using a single photodetector to measure the reflected intensity as a function of the relative position of wafer and reticle. The photodetector signal will exhibit either a sharp maximum or a sharp minimum when the two are in alignment, depending on whether the bar appears light or dark. Thin film interference effects can cause the contrast of the bar image to reverse, sometimes between one die and the next, thereby creating difficulties in alignment detection.

It was realised in the late 1970's that dark field illumination of the wafer target could give a more reliable signal, independent of any interference effects within the deposited films. Light scattered from the

edges of the target is collected by a photodetector which always exhibits a maximum at the ideal alignment position, {Wilczynski (1979) [67]}. A dark field system using a single cross as the alignment target was designed by Hershel (1979) [68] and is now in widespread use on the 'Ultratech' 1:1 wafer steppers. The low light levels available from dark field illumination demand the use of photomultiplier detectors as it is not desirable to increase the intensity of illumination above that set by the sensitivity of the photoresist. Reliable detection of the alignment point involves locating the peak of the photomultiplier signal which may vary in amplitude from one die to the next.

The Ultratech method is shown in figure 5.4. The wafer stage is scanned through the alignment position at slow speed in the -X direction whilst the detector signal is monitored. A peak detector senses Vo and sets a trigger threshold of 0.5Vo so that the X position of the stage, X1, is sampled from the laser interferometer on the trailing edge of the detector output. The sequence is repeated with the stage moving in the +X direction to find X2 and thereafter the stage makes a blind step to the exposure position, Xo. The bi-directional scan ensures that any systematic phase lags in the system do not affect the accuracy of determination of Xo.

Hershel also proposed a target in the form of a single 45 degree cross, as also shown in figure 5.4, to determine both Xo and Yo from a bi-directional scan in the X direction. Although this method is potentially fast and

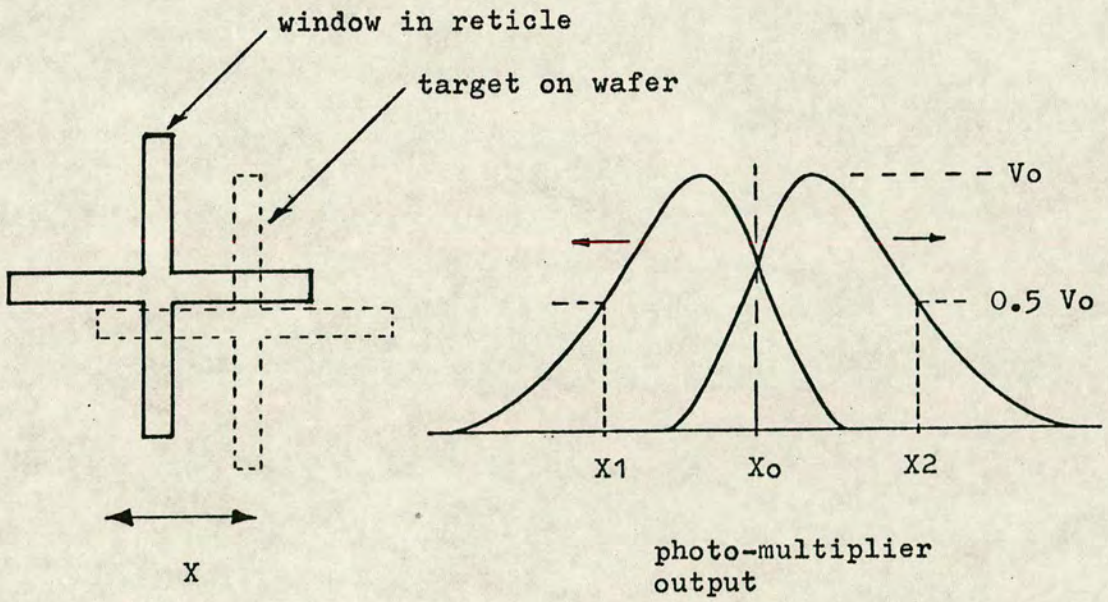

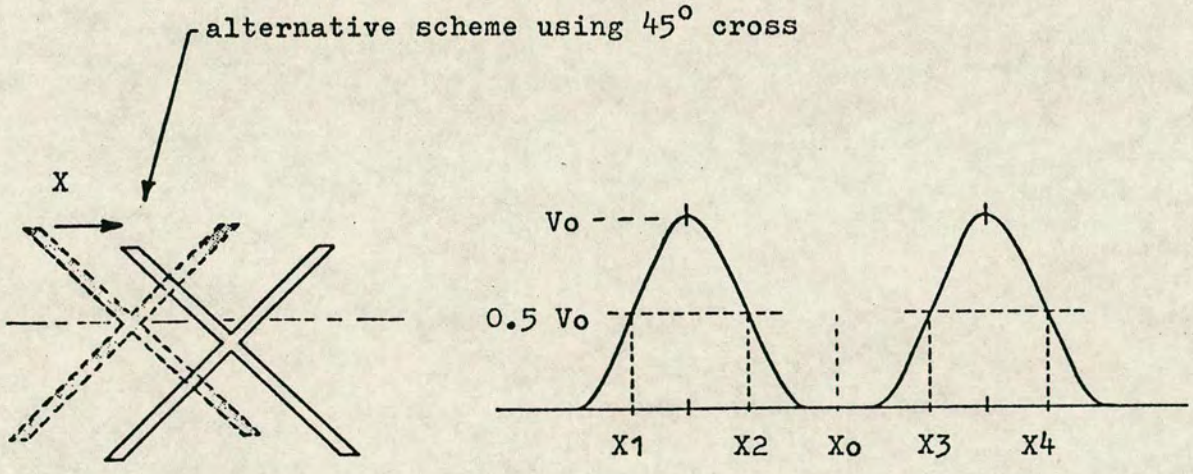

$$X_o = \frac{1}{4}(X1 + X2 + X3 + X4)$$

$$Y_o = \frac{1}{2}\left[\frac{1}{2}(X3 - X1) + (X4 - X2)\right]$$

Figure 5.4 'ULTRATECH' DARK FIELD ALIGNMENT SCHEME

(after Hershel ref. 68)

just as accurate as two separate scans in X and Y, it requires a deliberate Y offset during scanning to separate the signals from the two arms of the cross so that all four X co-ordinates can be sampled using a common trigger threshold. Thus it is still necessary to move the Y axis and, in practice, orthogonal crosses are used with separate scanning in the X and Y directions.

User experience has shown that the dark field system on 'Ultratech' steppers is one of the fastest and most consistent automatic alignment systems currently available, with good immunity to variations in process layers. As with any dark field system, planarisation of the substrate is likely to cause alignment failure, unless alternative methods are adopted.

5.5 Gratings as Alignment Aids.

5.5.1 Proximity Alignment.

Diffraction gratings have been used as alignment targets and also as sensitive visual indicators of the actual alignment errors achieved experimentally on patterns which have been aligned and exposed using other methods.

The use of moiré fringes as visual position indicators in general metrological applications has been reviewed by Vargady (1964) [18] and their use in mask to wafer alignment in proximity has been reported by many others including King & Berry (1972) [60], Flanders et al (1977) [61], Kleinknecht (1979) [62] and Lyszczarz et al (1981) [63].

The patterns used by King and Berry were circular gratings with pitches in the range 2 to 4 microns. The fringes were observed visually using a low magnification microscope with low numerical aperture so that the fine grating lines were not resolved. This enhanced the visual contrast of the fringes by restricting the number of diffracted orders in the image, as recommended by Guild [7] [8].

Flanders et al [61] used linear gratings (which are much easier to generate on maskmaking equipment) and compared the intensities of the +1 and -1 diffracted groups, as shown in figure 5.5, to derive an error signal proportional to misalignment in X. With gratings of identical pitch on mask and substrate, the useful range would be restricted to +/- a quarter of a pitch around the alignment point with false nulls occurring at misalignments equal to multiples of the pitch. This was avoided by having a deliberate mismatch or vernier effect between the two gratings so that only one null could occur within the width of the target grating. The accuracy of alignment depended on both gratings being symmetrical and non-blazed and remaining so at all photolithographic stages. In the case of the target grating on the wafer this cannot be guaranteed as successive process layers are built up with the consequent risk of systematic alignment offsets.

The major drawback of the above arrangement, which has been widely reported, is the sensitivity of the alignment signal to variations in the gap between mask and

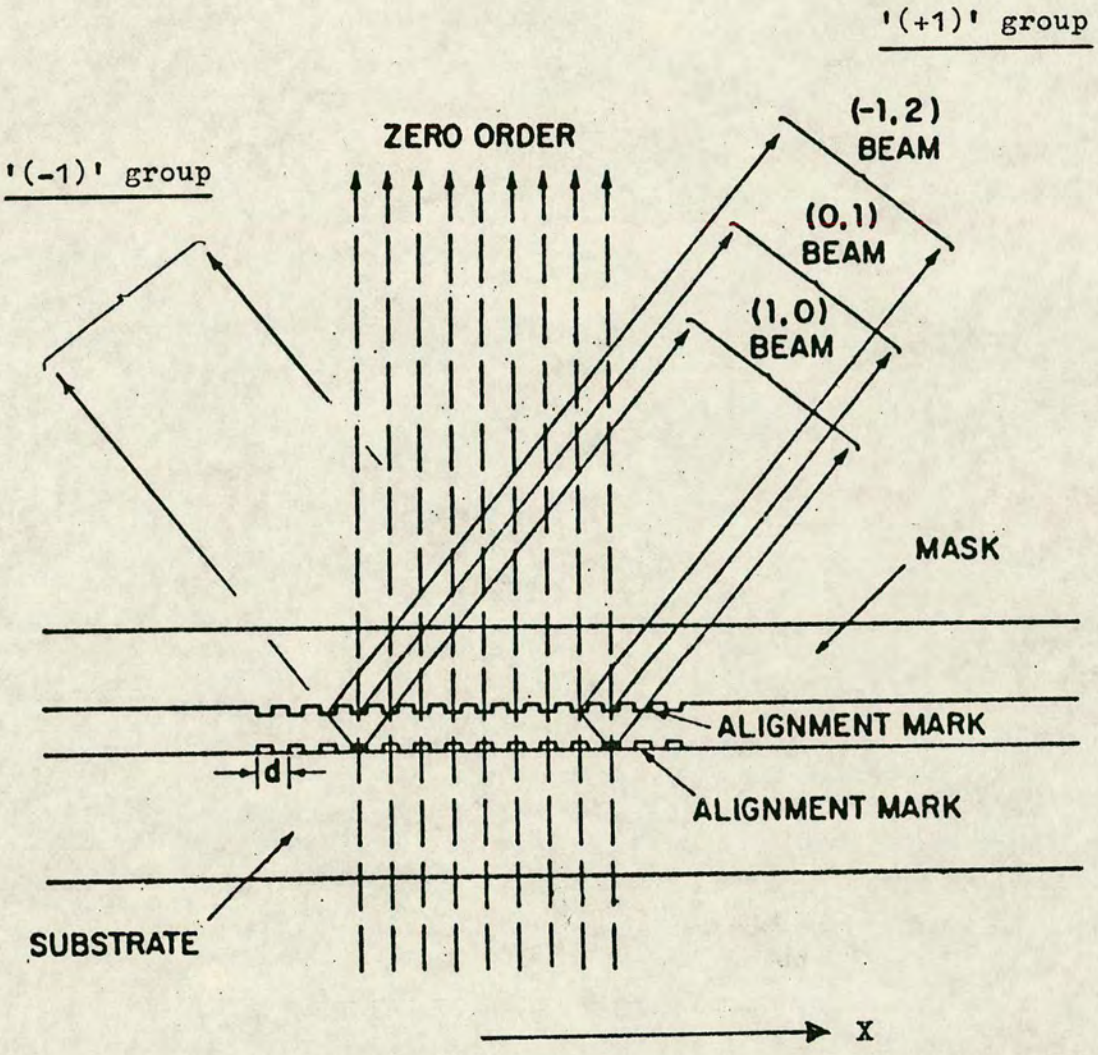

Matching symmetrical gratings are used on both mask and substrate.

Beams emerging in the same direction mutually interfere. Intensities of (+1) and (-1) groups are only balanced at exact superposition of the two gratings.

Figure 5.5 USE OF GRATINGS IN PROXIMITY ALIGNMENT
(after Flanders et al ref. 61)

wafer. Kinoshita et al (1983) [69] have reported that it is possible to derive a signal which varies periodically with the gap between the gratings by monitoring the sum of the +1 and -1 diffracted orders (ΣI) rather than the difference (ΔI). It was found that ΣI reached a maximum at a gap of p^2/λ (where p is the grating pitch and λ is the wavelength of illumination) and that the peak occurred at a lateral displacement of p/2 in the alignment direction, largely independent of minor variations in gap. It was also found that when laser illumination was used the ΣI signal exhibited cyclic variations at gap intervals of 0.3 μm ($\lambda/2$) due to interference effects between mask and substrate, with a longer period variation at intervals of p^2/λ as shown in figure 5.6. It would appear that the intensity sum (ΣI) is a more stable indicator of both gap and alignment than the difference signal (ΔI) which was proposed by Flanders et al [61]. Since it can be used only in proximity alignment its high sensitivity of about 0.01 μm is best suited to X-ray lithography.

5.5.2 Fresnel Zone Targets.

The use of linear Fresnel zones, sometimes called Fresnel Zone Plates (FZP), in proximity alignment has been described by Fay et al (1979) [70], Feldman et al (1981) [71], and Nelson et al (1981) [72]. A linear Fresnel Zone on the mask was designed to have a focal length equal to the mask-to-wafer gap so that an incident plane wave was focussed into a line on the wafer. At its simplest, the

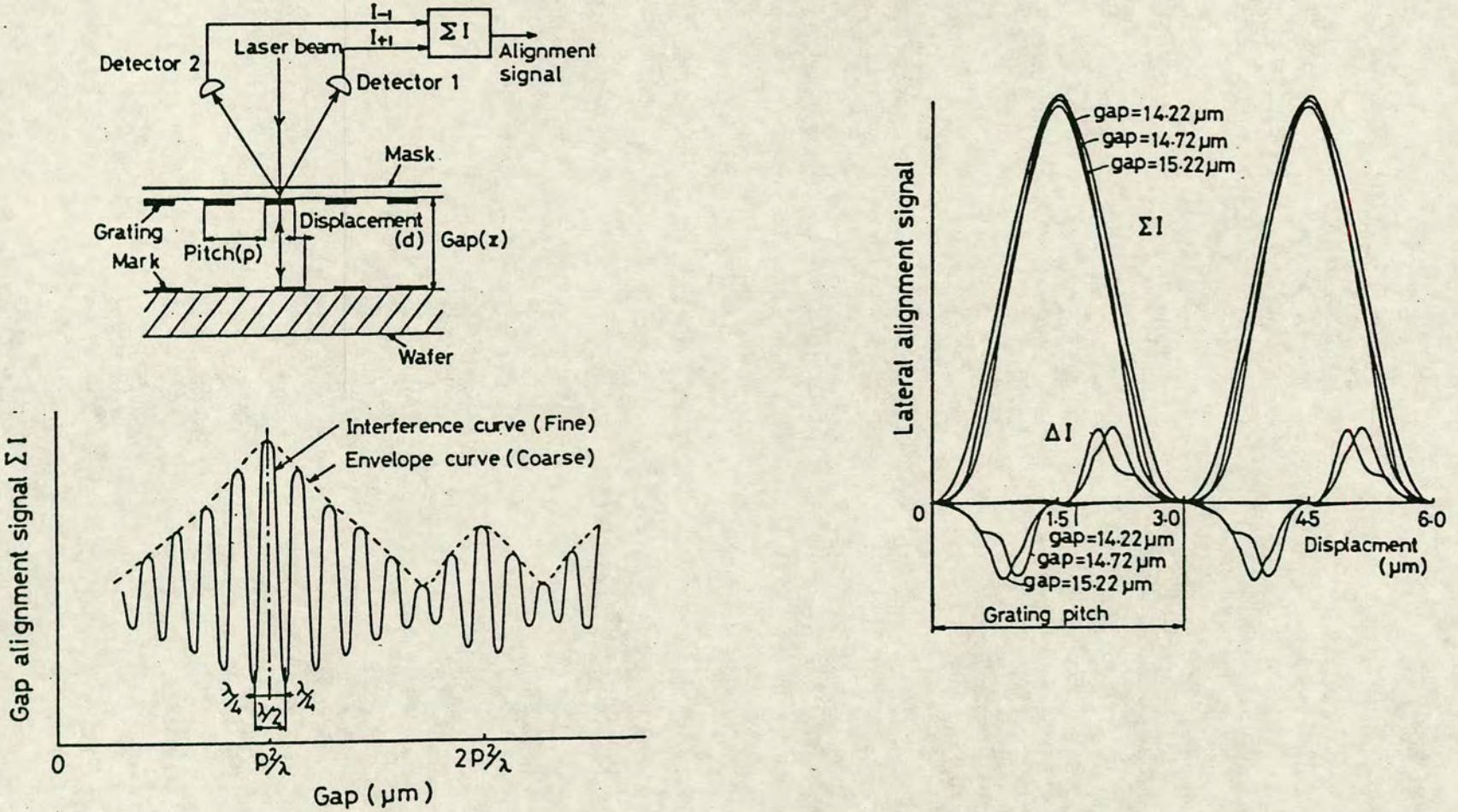

Figure 5.6 SUMMING INTENSITIES OF (+1) & (-1) GROUPS TO CONTROL ALIGNMENT AND GAP
(from Kinoshita et al ref. 67)

wafer target could be a single line or trench but the alignment signal was improved by the use of a dotted line of pits or mesas. These diffracted the light in the yz plane as shown in figure 5.7 with the result that a detector receiving the first diffracted order would produce a correlation signal with a lower d.c. component. The wafer target was modified by Nelson et al [72] to extend the capture range to +/- 1 mm without loss of sensitivity at the alignment point.

The exact converse of the system shown in figure 5.7 is used on the Nikon wafer stepper described by Murakami et al (1985) [79]. The wafer mark in the form of a dotted line is scanned past a laser beam which has been focussed to a line by the main projection lens. The reflected zero order is blocked and the higher diffracted orders are detected in the same way as the correlation signal above.

Circular Fresnel zones behave rather like lenses or spherical mirrors in that they focus an incident plane wavefront into a spot. That property has been exploited by printing circular FZP's as targets on wafers and detecting the position of the diffracted spots using a quadrant photodetector. Feldman et al [71] investigated the contrast and signal to noise ratio which could be achieved using FZP's in typical wafer processing applications. Although the results were encouraging subsequent experience has shown that the alignment signal is particularly sensitive to process variations, to the extent that it has been largely abandoned as a technique

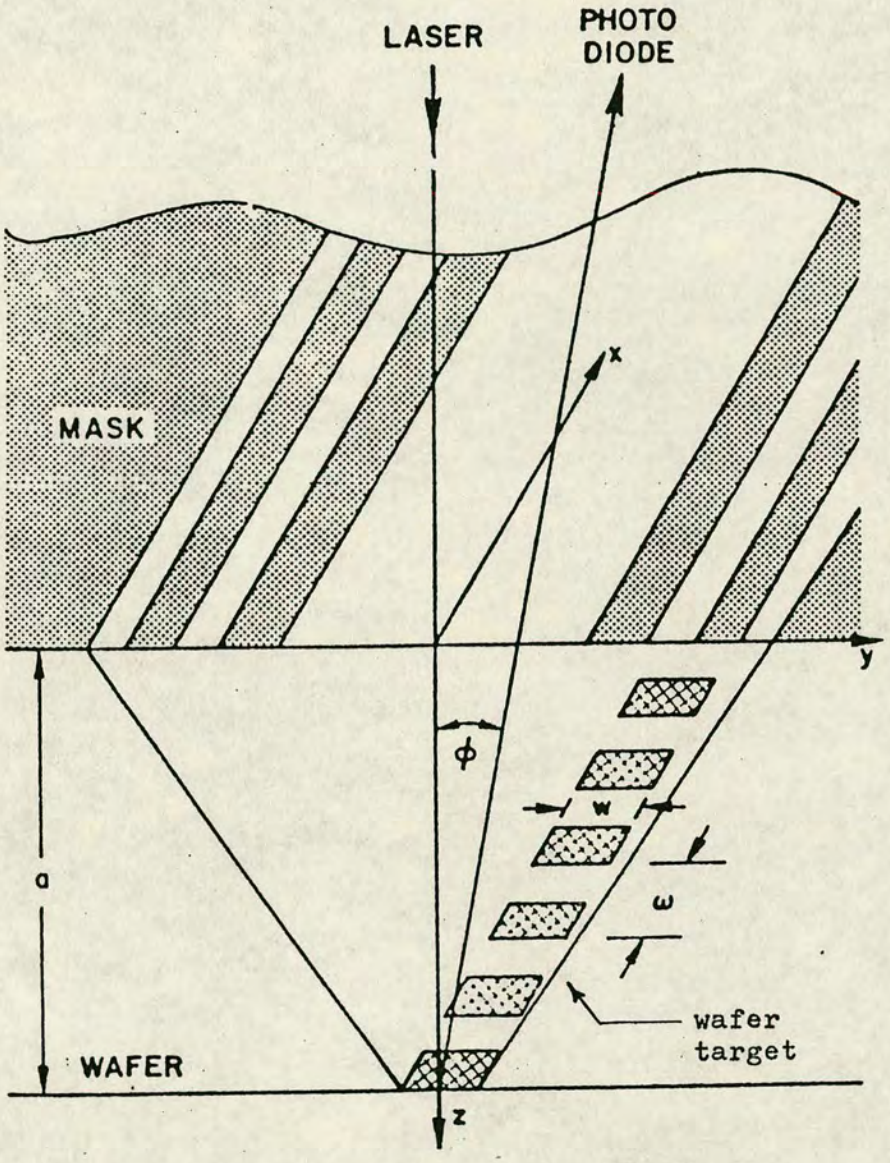

Linear FZP brings laser to a line focus on the surface of the wafer. Target grating on wafer diffracts laser in XZ plane so that first order emerges at angle ϕ given by

$$\phi = \sin^{-1} \frac{\lambda}{\varepsilon}$$

Figure 5.7 USE OF A LINEAR FZP WITH A PERIODIC WAFER TARGET (from Nelson et al ref. 72)

on optical wafer steppers, although it is still used on some X-ray aligners where the choice of illuminating and viewing optics is less restricted.

5.5.3 Use in Projection Systems.

The principles described above can also be applied in equipment where an image of the mask is projected onto the wafer by an optical system. A moiré technique for real-time observation of overlay performance on 1:1 scanning projection aligners has been described by Brunner and Smith (1984) [73] but the major applications have been on wafer steppers. Figure 5.8 shows the arrangement first described by Bouwhuis and Wittekoek (1979) [74] which formed the basis of the Philips/ASM-L wafer stepper as described in later papers by Wittekoek (1980) [75], Wittekoek et al (1985) [76], and van der Brink et al (1986) [77]. The basic concept is similar to the original scheme of Flanders et al with sections of phase grating on the wafer and similar gratings on the reticle. The zero diffracted order is blocked and only the first diffracted orders are allowed to recombine at the detector. An electronic polarisation modulator is used to scan the wafer mark at 50 kHz to permit a.c. coupling and phase sensitive detection of the signal. A similar system was described by Dubroeucq et al (1980) [78], where linear Fresnel zone plates were used instead of gratings.

Since the depth of focus on the main projection lens of a wafer stepper is of the order of a few microns,

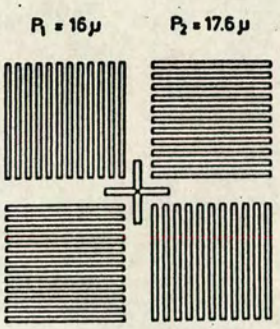

Alignment gratings on silicon. Each grating is about 200 × 200 microns. Two gratings with different periods are necessary to increase the capture range.

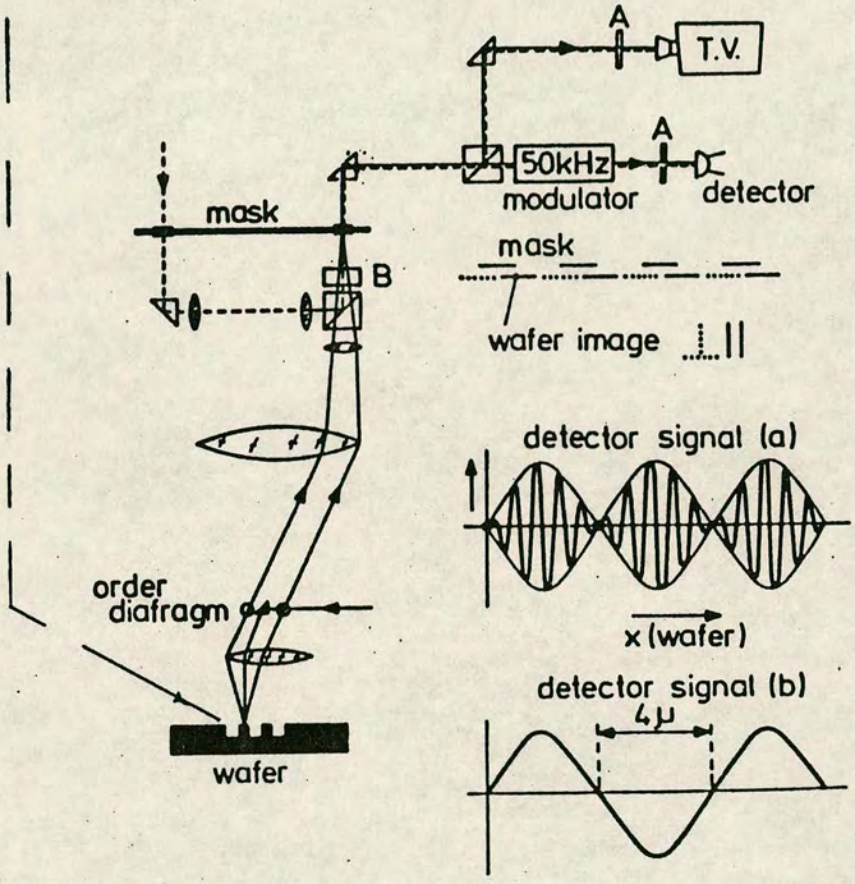

Optical arrangement for auto alignment. "B" is the birefringent plate splitting the wafer image. Signals "a" and "b" are, respectively, before and after phase sensitive detection.

Figure 5.8 PHILIPS / ASM - L AUTO ALIGNMENT SYSTEM
(from Wittekoek ref. 75)

automatic control is essential and hence the gap sensitivity which plagued this technique on proximity aligners is no longer a problem. The sensitivity of the ASM-L system to process variations has been analysed theoretically [76] and subsequent experience has confirmed that the automatic alignment system will operate on substrates with reflectivity as low as 0.15%. It does however rely on the resist being transparent at the alignment wavelength which in this case is 633 nm.

5.5.4 Holographic Configurations.

The principle of holographic reading of gratings has been applied to a wafer stepper by Nomura et al (1985) [80], (1986) [81]. In the simplest configuration shown in figure 5.9, a fine-pitch pattern is generated holographically by the intersection of two coherent laser beams at the wafer surface. The interference between this projected pattern and the lines already etched on the wafer produces moiré fringes with a period equal to the pitch of the grating. The projected pattern is formed in space and is insensitive to height or gap changes but in the form shown it is not directly referenced to the reticle plate. A later development [81] has achieved direct reticle referencing on a 5x stepper with an alignment sensitivity of 5 nm and an overlay accuracy of 100 nm, 3 sigma. If good tolerance to process variations can also be demonstrated, this is potentially one of the most sensitive alignment systems yet devised.

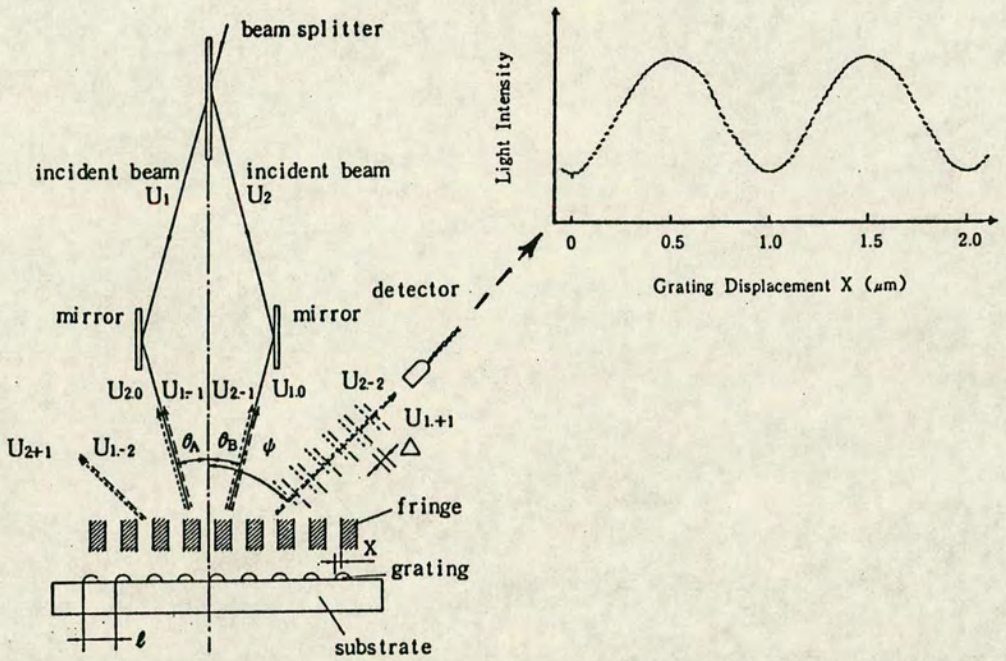

Configuration of new interferometric alignment technique superposing interference fringe of two conjugate beams in a space and a grating on a substrate.

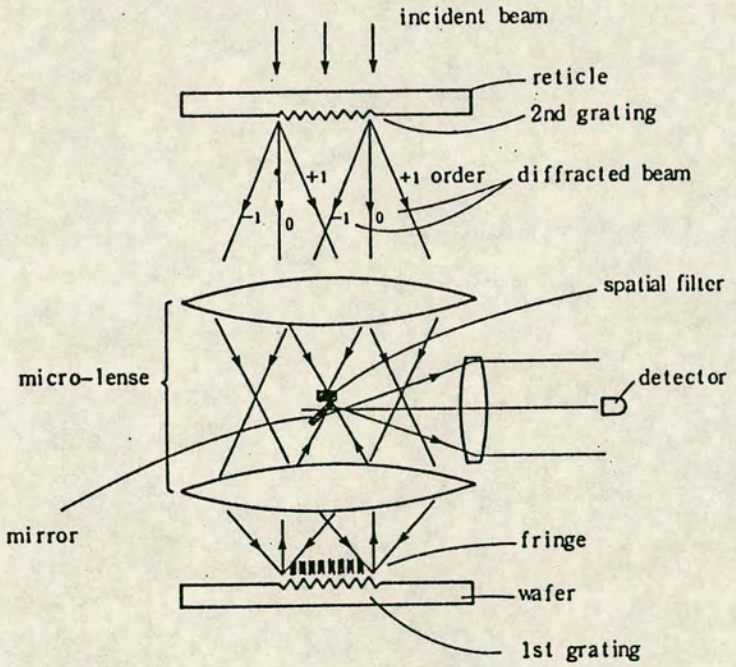

Schematic configuration of optical system for alignment between 1st grating on a wafer and 2nd grating on a reticle.

Figure 5.9 HOLOGRAPHIC ALIGNMENT SYSTEM
(from Nomura et al ref. 80)

5.6 Conclusion.

This chapter has reviewed the use of moiré fringe techniques in microfabrication equipment, with special emphasis on mask to wafer alignment. The evolution of the various optical methods has been outlined and the limitations of each method have been pointed out. The use of gratings and periodic structures has been shown to give advantages over direct viewing, and the holographic approach is looking promising.

There is, however, one limitation common to all the systems described in that they all operate in a static or quasi static mode, i.e. with the wafer stationary or moving only very slowly near the exposure site. The use of a continuously moving stage in conjunction with 'flash' exposure would give enormous gains in throughput but a completely new approach to field by field alignment will be required, {Markle (1984) [55]}. This problem will be addressed in chapter 8.

CHAPTER 6: EXPERIMENTAL TRANSDUCERS USING REFLECTION GRATINGS ON SILICON.

6.1 Outline.

The basic aim was to investigate the optical properties of reflecting gratings which might be produced on silicon using microfabrication techniques and then measure the performance of such gratings as displacement transducers.

6.2 One-Dimensional Linear Gratings.

6.2.1 Plane Amplitude Gratings.

A plane reflecting grating was designed and fabricated as a reference for subsequent comparison with gratings having a vee-groove profile. This was a one-dimensional linear grating with a line structure of 10 lines per mm, i.e. 50 μm lines and 50 μm spaces. The relatively coarse line structure was chosen so that diffraction effects would be insignificant and geometrical effects would pre-dominate.

The reflecting lines were formed by etching a layer of AlSiCu alloy which had been sputter coated onto a film of silicon nitride. The metal was about 1000 Å thick to ensure good reflectivity whilst the silicon nitride film was 1050 Å thick to create destructive interference of the reflected light and thus ensure low reflectivity from the

spaces between the lines. A matching index grating was generated on a high resolution photographic plate.

The reflecting grating and index grating were mounted on an optical bench as shown in figure 6.1 with facilities for mechanical adjustment of gap, parallelism of the grating lines and micrometer-controlled displacement along the measurement axis, i.e. at right angles to the lines. The source and detector fibres were mounted in the focal plane of the aspheric collimator lens such that the chief rays subtended an angle of 39 degrees at the grating. The positions of the fibres were optimised using a plane mirror in place of the grating and then comparative measurements of the reflected light intensities were made.

Results.

Condition	Intensity (volts)	
Illuminator switched off	0.016	
Matt black paper in place of wafer	1.20	*
Plane silicon nitride surface	1.56	
Plane ALSiCu surface	7.30	

* It is worth pointing out that this reflection from the faces of the index grating (which are parallel to the reflecting grating) contributes to a d.c. level which is the major factor in limiting the modulation achieved in reflecting reading heads.

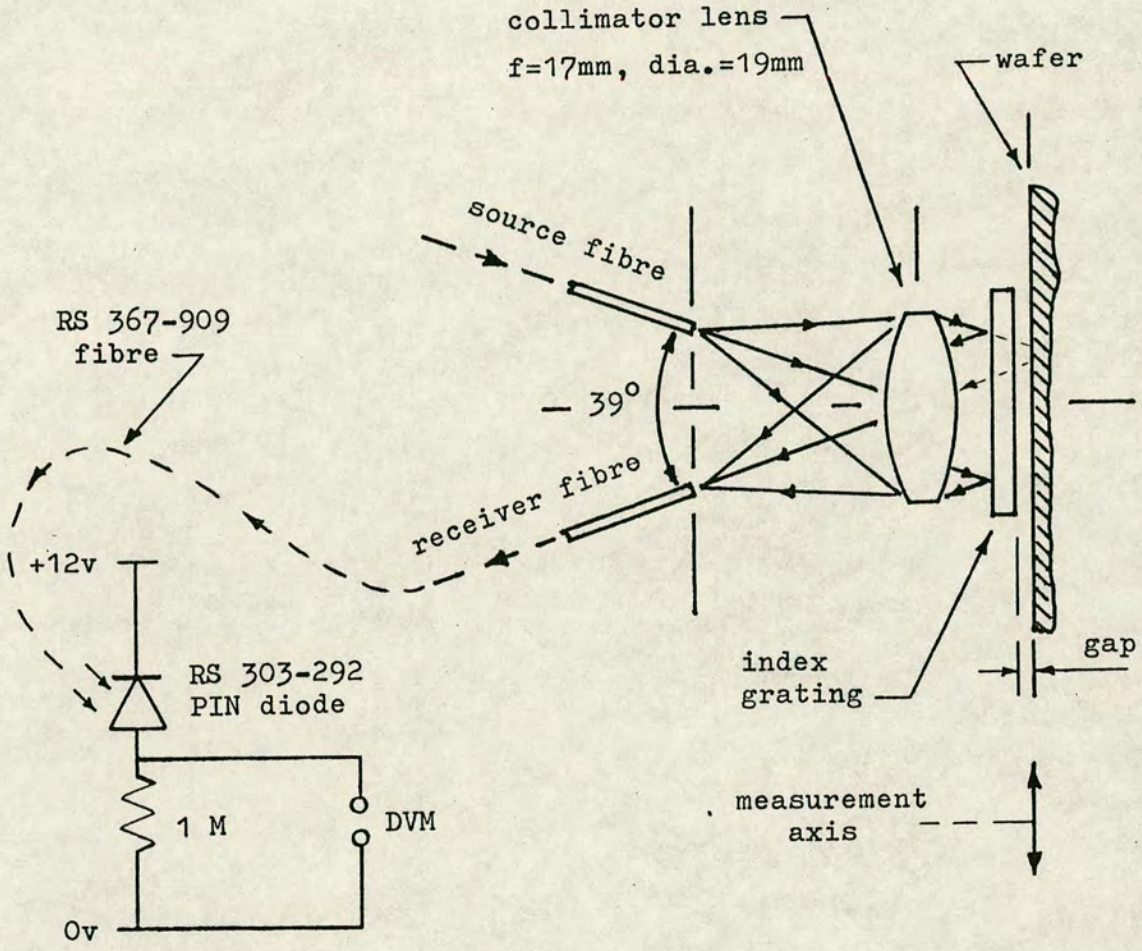

Optical components were mounted on an 'Ealing Mini-Bench' to provide the appropriate mechanical degrees of freedom.

Figure 6.1 REFLECTING READING HEAD FOR PLANAR GRATING

Fringe Contrast.

The best contrast of 64% was measured at zero gap between index grating and wafer, decreasing linearly to 43% at a gap of 1 mm. With the configuration shown in figure 6.1 the displacement (fringe) signal was extremely sensitive to cross-talk from gap variations. This arose because the lines of the index grating were not being projected across the gap at right angles to the axis of measurement and hence a variation in gap caused a spurious change in intensity, equivalent to a displacement along the measurement axis. Rotation of the fibre assembly by 90 degrees about the optic axis cured the problem.

6.2.2 Vee-Groove Gratings.

Diffraction gratings are frequently ruled with a vee-groove profile in order to improve their efficiency in a particular diffracted order. Such gratings are said to be 'blazed' for a particular order when the angle of deviation due to direct reflection from the face of the groove coincides with the diffraction angle for that order.

Consideration of the optical properties of the reflecting vee-grooves defined by the (111) planes of silicon revealed another interesting property as shown in figure 6.2. An incident ray will undergo a double reflection and will emerge at an angle of 39 degrees to

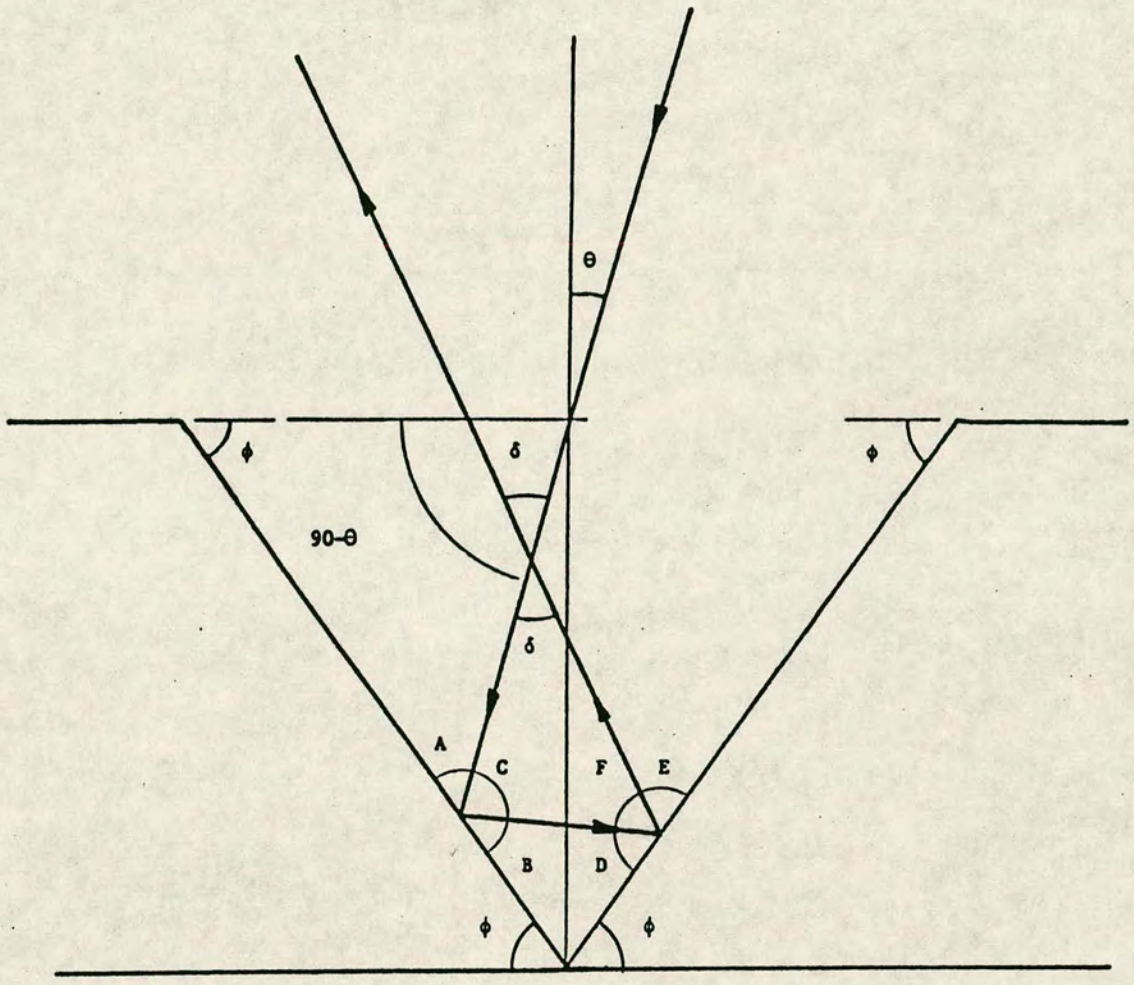

Note 1. $A = B = 180 - \phi - 90 + \theta = 90 - \phi + \theta$

2. $C = 180 - 2(90 - \phi + \theta) = 2(\phi - \theta)$

3. $D = C = 180 - (90 - \phi + \theta) - (180 - 2\phi) = 3\phi - \theta - 90$

4. $F = 180 - 2(3\phi - \theta - 90) = 2\theta - 6\phi + 360$

5. Incoming ray is deviated through an angle δ

$\delta = 180 - (2\theta - 6\phi + 360) - 2(\phi - \theta)$

$\delta = 4\phi - 180$

6. For silicon, $\phi = 54.74^{\circ}$, hence $\delta = 38.96 \equiv 39^{\circ}$

Figure 6.2 DOUBLE REFLECTION FROM A VEE GROOVE - THE GENERAL CASE.

its direction of entry. Further, this angle of deviation is, to first order, independent of the angle of incidence and thus the sides of the vee-groove can be regarded as a constant deviation mirror in one plane. The angle of the reflected ray is independent of any rotation of the mirror about an axis parallel to the vee-groove.

This property was used to improve the modulation achieved by a reflecting reading head. Figure 6.3 shows an arrangement similar to that used for the previous measurements on a plane grating, but in this instance the optic axis of the collimating lens was at about 9 degrees to the normal to the gratings. This angle ensured that any direct reflections from the surfaces of the gratings would not reach the detector and would not contribute to the dark level signal.

The vee-groove gratings were fabricated as follows:

1. Deposit a 1050 Å film of silicon nitride on wafer.
2. Print and etch 10 lines/mm grating in nitride film.
3. Etch vee-grooves to completion using hot KOH solution.
4. Sputter coat a 1000 Å layer of AlSiCu.
5. Align and print same grating as (2) to clear flat areas.
6. Etch metal from flat areas.
7. Strip photoresist.

The use of silicon nitride as a masking layer during etching of silicon with hot KOH solution had been developed by Gundlach [95].

The resulting vee-groove pattern is shown in cross-section in figure 6.3.

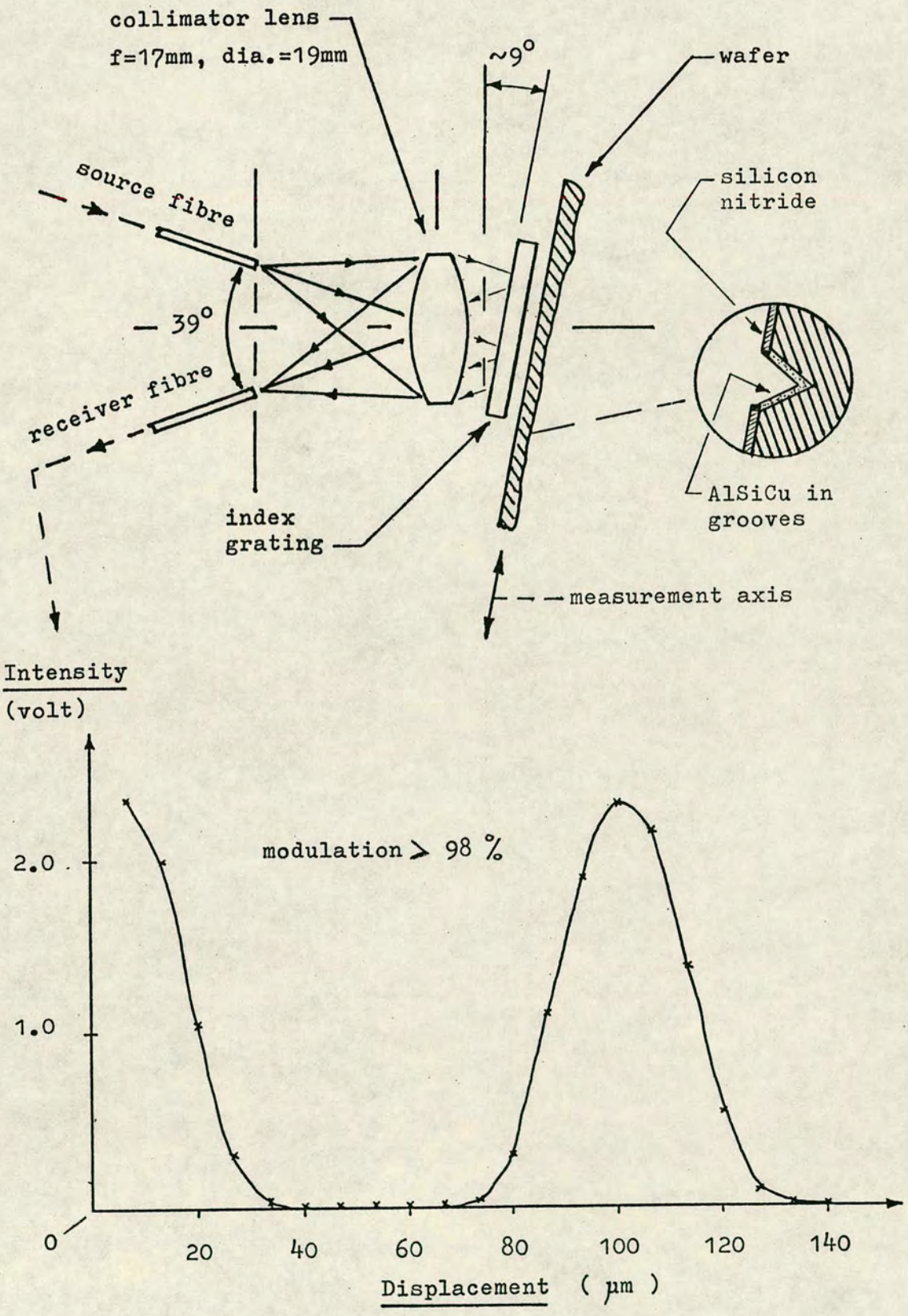

Figure 6.3 REFLECTING READING HEAD FOR VEE GROOVE GRATING

Modulation Results.

The fringe contrast was measured at a gap of 0.13 mm between the gratings, with the lines set parallel as before. The dark level was less than 1% of the peak, indicating a fringe modulation in excess of 98%. The reflected intensity as a function of displacement in the measurement direction (figure 6.3) showed a marked asymmetry which could not be explained by any mismatch between the mark-to-space ratios of the index grating and the scale grating. It was due to the fact that light undergoing a double reflection could reach the detector only when the top of the vee-groove was largely clear. Unlike the case of the plane reflecting grating, half-masking of the vee-groove by an opaque bar on the index grating would block more than half the reflected light, hence the short region of 'light' and the longer region of 'dark.'

6.3 Two-Dimensional XY Gratings.

6.3.1 Plane Gratings.

A two-dimensional version of the plane linear grating described above was fabricated. It consisted of an array of reflecting areas of AlSiCu, each 50 μm square, at a pitch of 100 μm on a field of silicon nitride. Fringe contrast, measured with a matching index grating in an arrangement similar to figure 6.1, was 48% at zero gap

and fell to 23% at a gap of 1 mm. Again, the direct reflections from the index piece contributed to a significant dark level.

6.3.2 Vee-profile XY Grating.

By etching an array of 50 μm square windows in a film of nitride followed by etching of the silicon to completion in hot KOH solution, an array of pits was created in the surface of the silicon. The sides of the pits were bounded by (111) planes as in the case of the vee-grooves. The same fabrication process was used to metallise the sides of the pits and the planar areas of the field were left as bare silicon nitride.

Fringe contrast, measured in an arrangement similar to figure 6.3, was 93% at zero gap.

The measurements were repeated using an adjacent area of the same wafer where the metal had not been removed from the planar areas of the field. Fringe contrast at zero gap was 92%, falling to 76% at a gap of 1 mm. This result confirmed the benefits of excluding the direct reflections from the detector and also indicated that there was no need for the second photolith and etch stage to remove the metal from the field.

Since the grating could be metallised all over, it could be mass produced at lower cost from a master by a casting process, or by a mechanical stamping process followed by metallisation, as in the case of diffraction gratings and compact discs. This aspect was not pursued.

6.4 An XY Reading Head.

6.4.1 Design Considerations.

This reading head was designed to derive phase and quadrature signals for both the X and Y directions from an array of reflecting pits, taking advantage of the experience gained from single channel measurements. The layout is shown in figure 6.4. The index grating consisted of four windows, symmetrically arranged around the optic axis, with a quadrature phase relationship between the lines on opposite windows. This arrangement ensured that slight rotation of the reading head around the optic axis would not introduce significant quadrature errors. A single source and collimator lens provided illumination, normal to the grating surface, to all four windows.

The reflected illumination from the array of pits left the surface as four distinct rays, two in the XZ plane at +/- 39 degrees to the optic axis and a similar pair in the YZ plane. Direct reflections from the plane surfaces returned along the optic axis. Detectors were arranged at +/- 39 degrees to the optic axis to monitor the reflected light from each of the windows. Each detector used a short focus lens to gather the light from the window and couple it into an optical fibre.

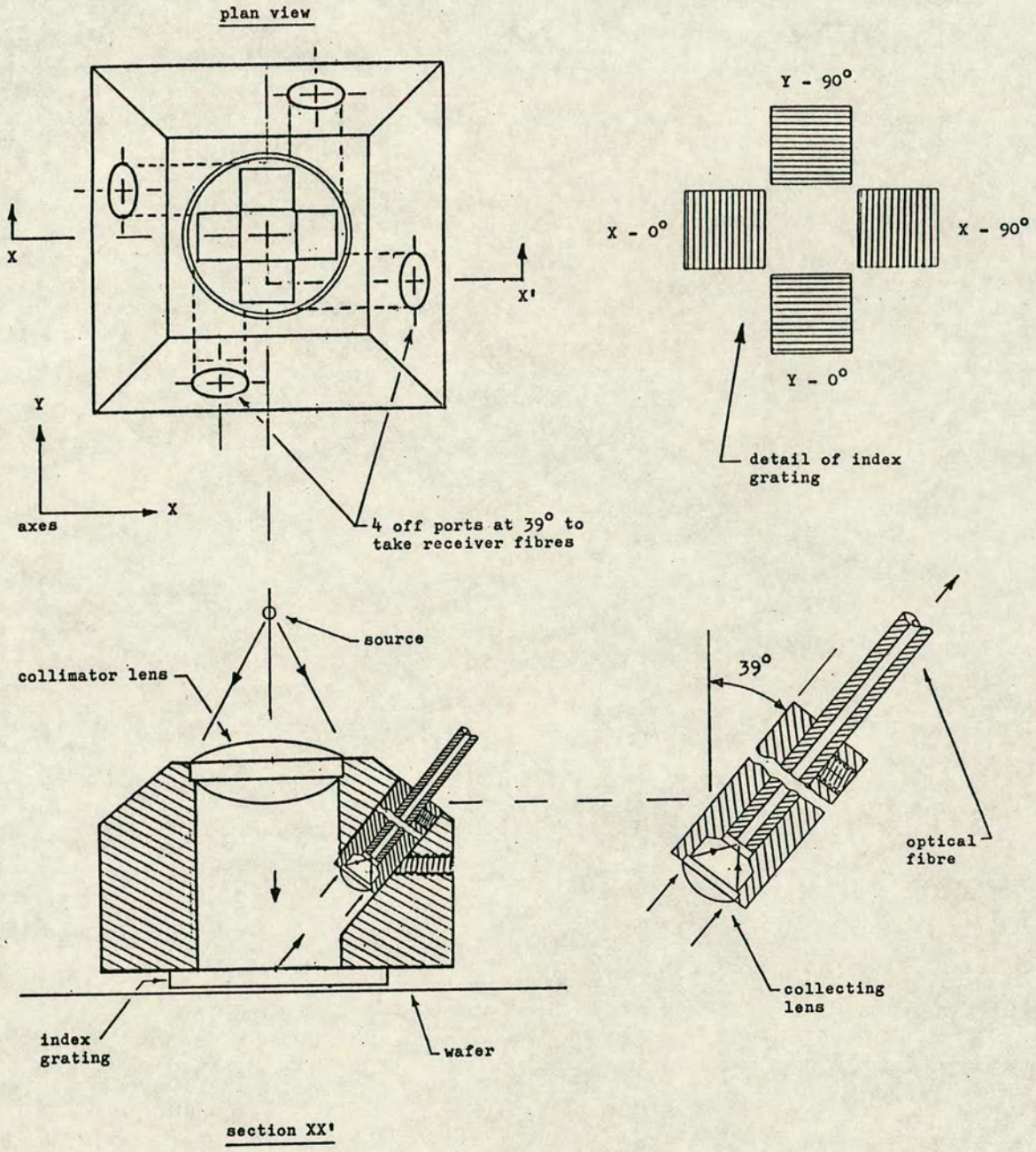

Figure 6.4 TWO - DIMENSIONAL (XY) READING HEAD

6.4.2 Modulation Results.

The maximum reflected intensity measured by the four detectors was the same within +/- 4% and the fringe contrast on the four windows was equally well matched with a maximum of 97%, falling to 79% at a gap of 1 mm. There was no trace of cross-talk between the four channels.

The mark-to-space ratio on the index grating was made 41:59 instead of 50:50 to give a symmetrical output signal. Figure 6.5 is a plot of the output of the phase and quadrature channels for the Y axis as a function of displacement.

6.5 Conclusion.

The measurements on plane gratings showed that the careful choice of film thickness could give low reflectivity from the spaces between the lines but the major contribution to the d.c. signal at the photodetector was the un-wanted reflections from the index grating. The use of vee-groove gratings confirmed the constant deviation properties which were used to eliminate the d.c. level and thus achieve good modulation. The compact design of XY reading head with optical fibre links performed well and could form the basis of an XY transducer in which the straightness of the axes, the orthogonality and the accuracy would be determined purely by the quality of the two-dimensional grating. The

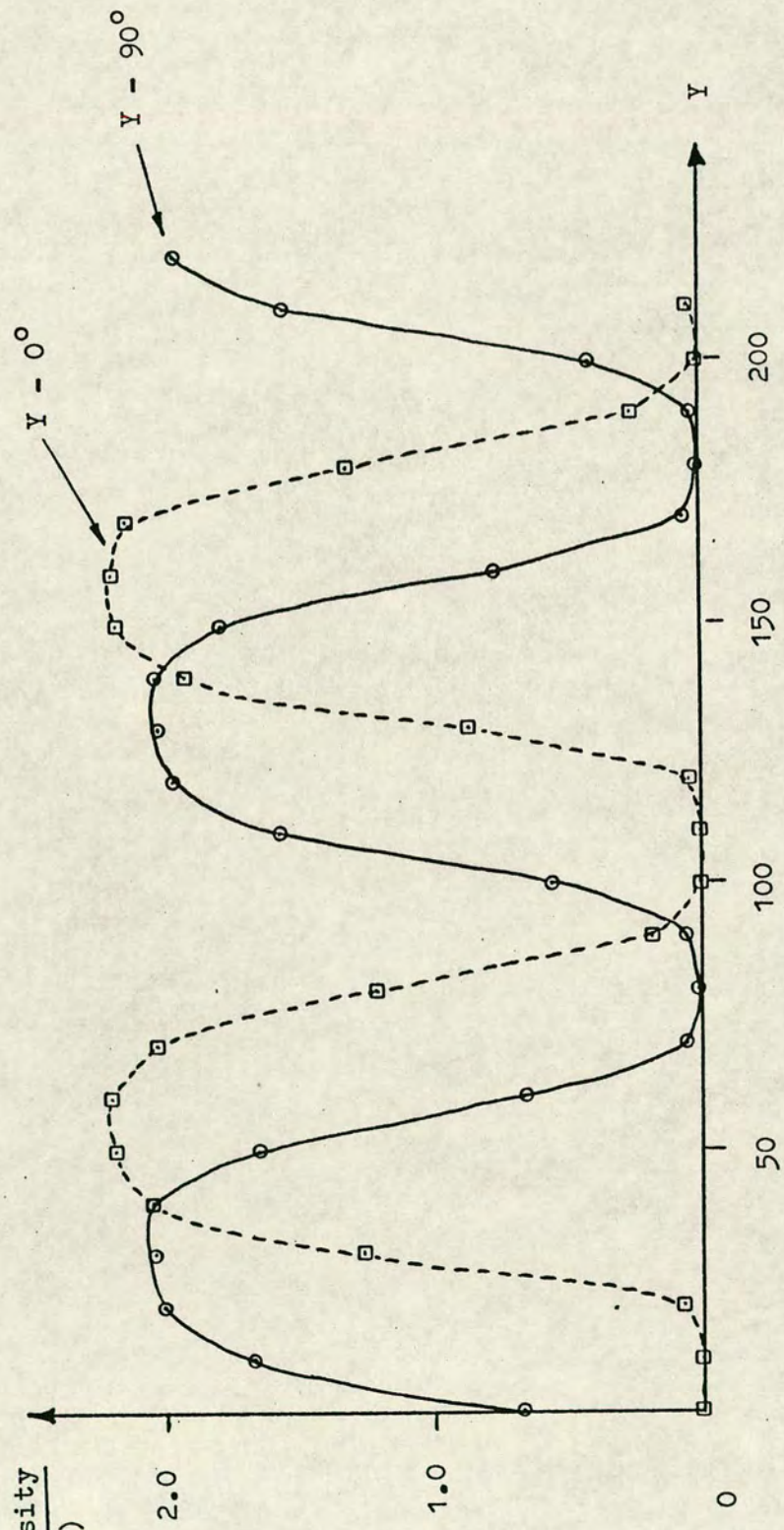

Figure 6.5 INTENSITY MODULATION FROM XY READING HEAD - Y AXIS SIGNALS

optical properties of vee-grooves could be used to advantage in achieving good contrast of alignment targets on wafers if the targets were etched as deep grooves in the silicon at the start of the process. This will be investigated in chapter 8.

CHAPTER 7: EXPERIMENTAL ABSOLUTE POSITION ENCODERS.

7.1 One-Dimensional Absolute Position Encoder.

7.1.1 Outline.

The basic aim was to investigate whether a single track scale could be produced on which both absolute and incremental information could be encoded and which could be read by either a specialised absolute reading head or by a moiré fringe reading head or both. This would allow a common scale to be used for both types of transducer. A combined hybrid reading head could be designed to give fine resolution by moiré fringe interpolation in incremental mode, with absolute position updates as and when required.

7.1.2 Design Considerations.

The code chosen was a PRBS as described by Jones & Zia [86]. It was realised that the simplest optical implementation of the code would be as opaque bars on a transparent substrate which could be viewed in transmission. The bars and spaces of the absolute code would be relatively coarse and the spaces, instead of being clear, would contain a fine-pitch linear grating. The moiré fringes generated between the fine pitch grating and a suitable index grating would be much broader than the bars of the absolute code so that the fringe detectors

would not be perturbed by the presence of the code bars.

However if, say, a 1 in the code appeared as an opaque bar and in a particular section of scale there were a majority of 1's, the area available for the fine-pitch grating would be reduced and the moiré fringes would be obliterated. For this reason each bit of the code was implemented as a bar and a space as already discussed in chapter 4 and shown in figure 4.2 so that when the coded pattern was superimposed onto a fine-pitch linear grating the overall transmitted light intensity would be reduced by a constant 50%, irrespective of the proportion of 0's and 1's in the code.

7.1.3 Choice of Pitch.

The dimensions of the code bars and the pitch of the linear grating are determined mainly by the dimensions of the photodetectors and the optical arrangement in the reading head. Linear arrays of photodiodes are readily available and a standard 512 element array with a diode spacing of 25 μm was used in these experiments. There are advantages in choosing the width of the code bars to be several times the pitch of the photodiodes to ease the problem of edge detection, but if the bars were too wide their presence might perturb the signal from the moiré fringe detectors. By arranging that the overall length of the diode array exceeds the minimum n bits of the code by, say, 2 bits some immunity from debris is gained by the provision of two extra samples of adjacent n-bit words. It

is also possible to determine the position of the edges of the bars relative to the end of the array to within +/- 1 diode, thereby establishing the absolute position to the nearest diode instead of to the nearest bit in the code.

The uncertainty of +/- 1 diode in absolute position can be removed by referring to the moiré fringe pattern generated by the fine pitch grating. It is essential, therefore, that the pitch of the grating is not less than the diode spacing and ideally should be twice the diode spacing to ensure an unambiguous readout. The other constraint is that each space in the absolute code pattern should correspond to an even multiple of the grating pitch and hence contain an even number of grating lines and spaces.

Thus the diode spacing is the major consideration in choosing the pitch of the fine grating and the length of the diode array and/or the width of the code bars can be chosen to achieve the required range of measurement.

7.1.4 Experimental Reading Head.

The arrangement is shown diagrammatically in figure 7.1. Since the diode array had a pitch of 25 μm the grating pitch was 50 μm (i.e. a 25 μm line and 25 μm space or 20 lines per mm.). The bars of the PRBS code were 200 μm wide so that one bit of the code corresponded to 400 μm and hence the widest opaque bar which would occur at a 0 to 1 transition would be 400 μm. Each bit of the PRBS corresponded to 16 photodiodes. A section of the combined

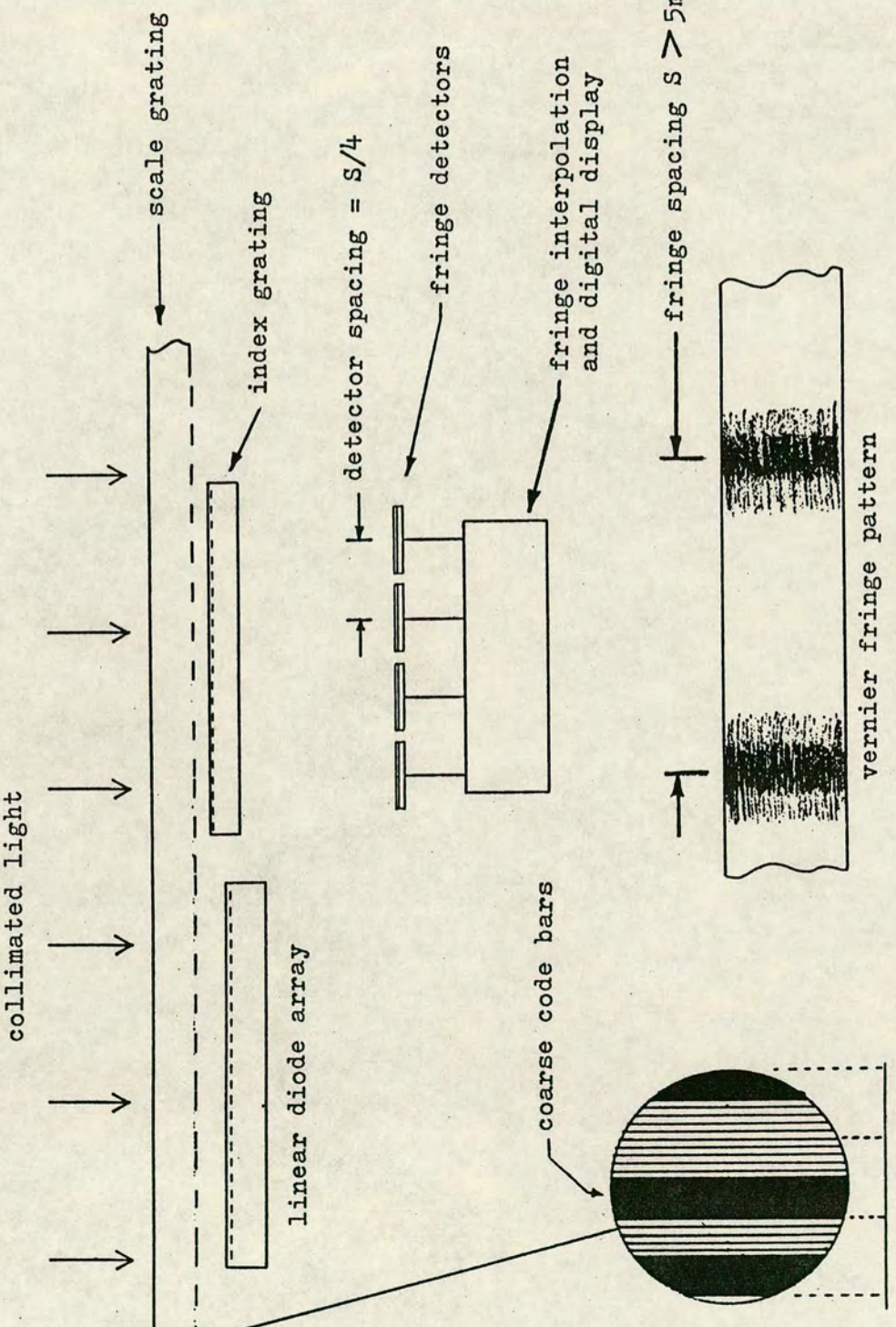

Figure 7.1 EXPERIMENTAL ABSOLUTE + INCREMENTAL READING HEAD

scale pattern is also shown in figure 7.1.

Moiré fringes were generated using a vernier index grating with a pitch of 50.5 μm giving a fringe spacing of 5 mm. A wider fringe spacing would be desirable for use with 4 discrete photodetectors as shown in figure 7.1, but in practice the fringe pattern was examined using the same 512 element diode array for which 5 mm was an appropriate spacing. The scale and the index grating were produced on high resolution photographic plates using a computer controlled optical pattern generator.

The illumination was supplied by a tungsten lamp via an optical fibre which acted as the source for an aspheric collimating lens. The fibre core diameter was 1 mm and the focal length of the lens was 17 mm giving a divergence or angle of smear of 1/17 radian. In some circumstances this can be a drawback but it can be used to good effect in two ways. Firstly, it ensures that the fine lines of the grating pattern are not detected by the linear diode array and secondly, it can be used to eliminate the effect of the code bars on the fringe detectors when they are spaced well away from the index grating. The code bars are completely smeared out whilst the broader moiré fringes are still detectable.

7.1.5 Experimental Results.

Detection of Code Bars.

The presence of a glass window on the linear diode

array prevented operation at anything less than about 1 mm spacing between the scale and the array. The traces in figure 7.2 confirmed that the maximum usable gap was about 2.5 mm when the angle of smear was 1/17 radian. Larger gaps reduced the modulation. It is interesting to note that at the minimum working gap, the fine lines of the grating were just visible on the output signal.

Detection of Vernier Fringes.

The index piece had a pitch of 50.5 μm with a working aperture of 6 mm. The fringe pattern was examined using the same linear diode array. Figure 7.3 shows the movement of the vernier fringe as the scale was displaced by one whole pitch of 50 μm in steps of 10 μm. The edges of the index grating are visible as dark bars: the difference in dark level between the two sides of the array was not noticed until after the traces were taken and was found to be caused by ambient light. The gap between the scale and the index grating was about 0.1 mm and the fringe contrast or modulation was about 60%.

With a scale to detector gap of only 2.5 mm, the 200 μm wide code bars are clearly visible within the envelope of the vernier fringe. In this instance the bars were at regular intervals corresponding to a series of 1's in the code. If the spacing of the vernier fringes were chosen to match the length of the diode array, the output signal could be put through an electronic bandpass filter centred on the fringe frequency and thereafter compared in

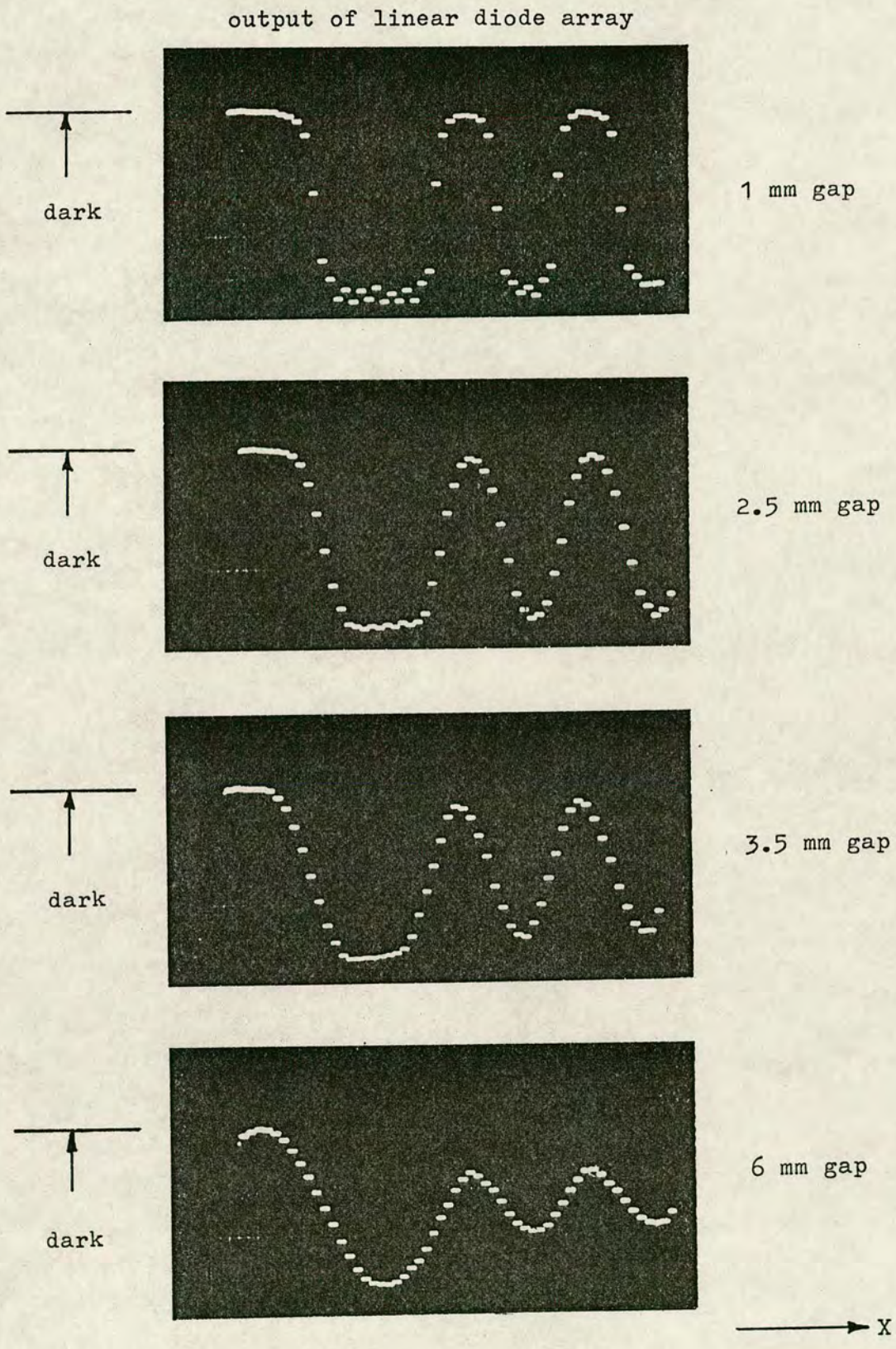

Figure 7.2 PROJECTION OF CODE BARS ACROSS GAP

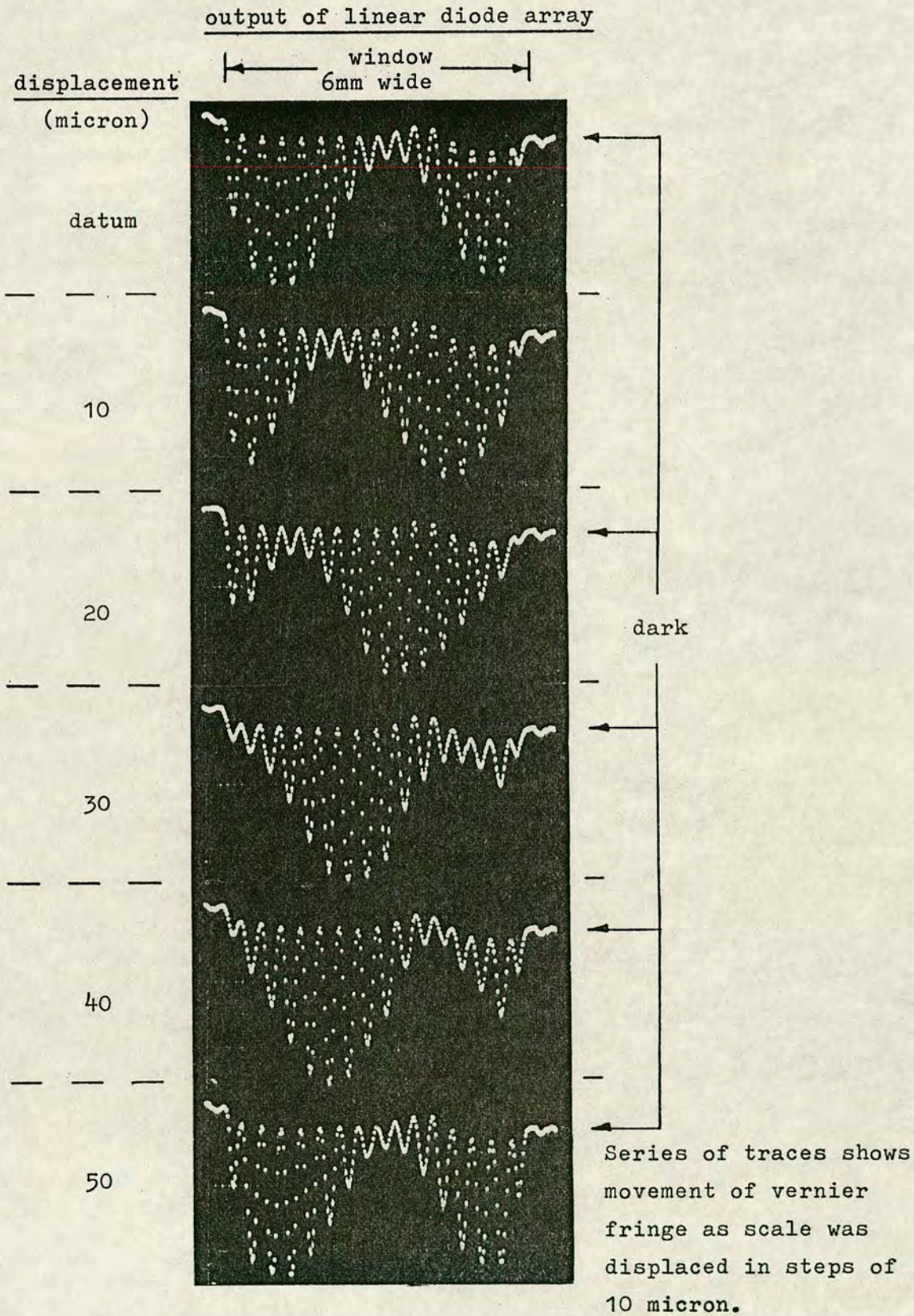

Figure 7.3 DETECTION OF VERNIER FRINGES

phase with the array scan signal to determine the fringe position. This is a well proven method which has been reviewed in chapter 3, [35], and it was not pursued experimentally.

When the array was moved about 25 mm away from the index grating, the bars were smeared out but at the expense of a loss of intensity on the detectors. It then became clear that a better signal could be obtained by adopting the configuration in figure 7.4 where the detectors were arranged across the scale and the fringes were generated by a skewed index grating. With the linear diode array spaced 25 mm away, the signal showed no trace of the code bars and the efficiency of the detectors was improved by introducing a 19mm diameter perspex rod as a cylindrical lens in front of the array.

7.1.6 Decoding of PRBS Signals.

A decoding scheme was devised and a custom diode array with an on-chip correlator was designed by W.Chow (1986) [88] as a M.Sc. project.

7.1.7 Conclusion.

The experimental results confirmed that reliable detection of coded patterns using a linear diode array is feasible and that the introduction of coded patterns onto a linear grating can be tolerated by a suitably designed moiré fringe reading head. The fringe signals can be

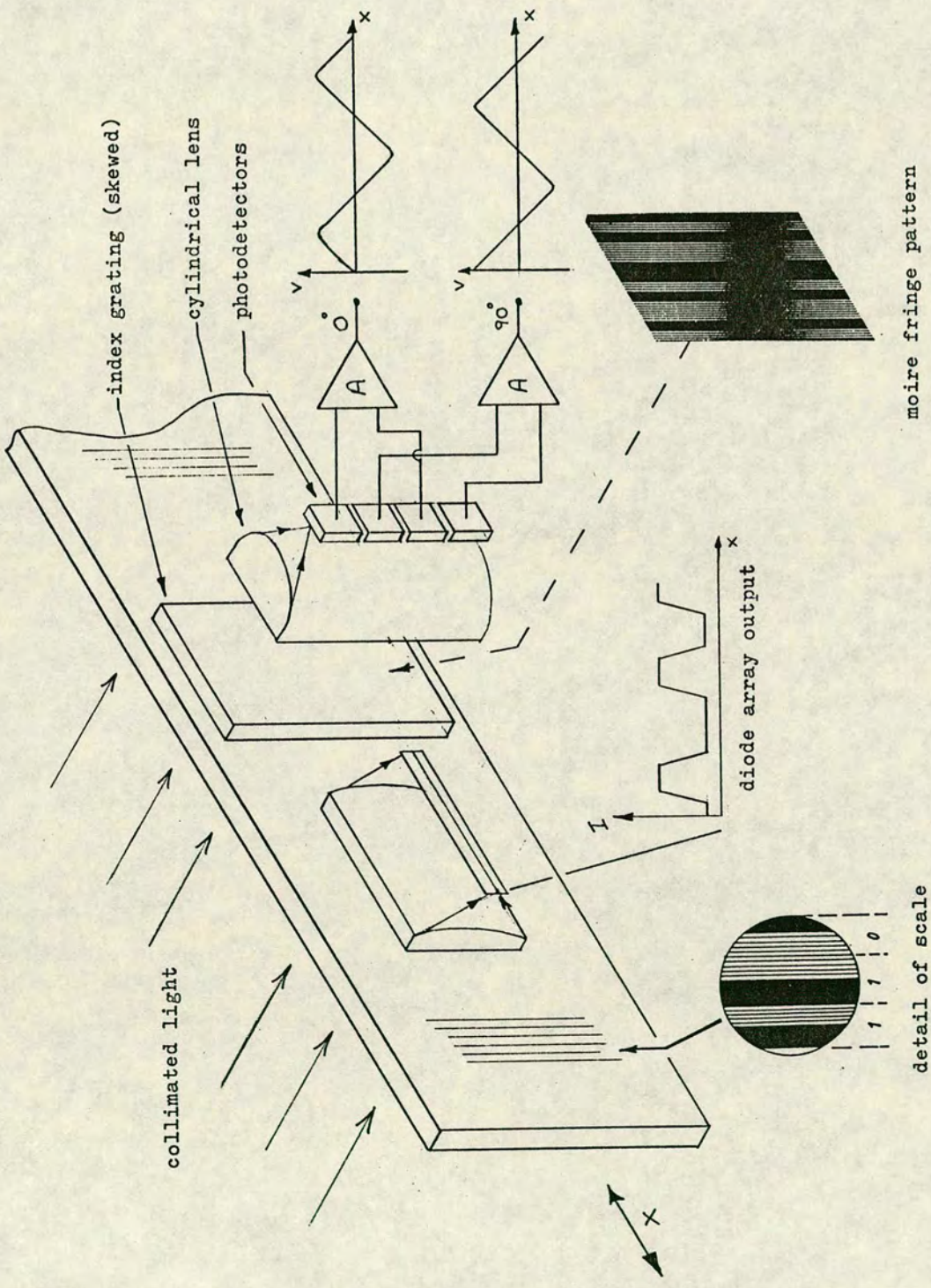

Figure 7.4 COMBINED ABSOLUTE + MOIRE FRINGE READING HEAD

interpolated by up to a factor of 100, giving a digit size of 0.5 μm with the grating chosen. With a PRBS bit size of 400 μm, an array of 256 diodes could sample 16 bits, to provide a working sample of 14 bits and a total range of 6553 mm.

7.2 Two-Dimensional Position Encoder.

7.2.1 The Pattern.

It was realised that the coding implementation adopted for the linear position encoder described previously could be applied in two dimensions by superimposing two linear patterns at right angles on a common substrate. An example is shown in figure 7.5. An XY position is found by decoding an n bit sample from a row and from a column.

Again, the position resolution may be improved by having the detectors much smaller than the pattern elements or by using a fine pitch grid in the spaces between the elements, as in the linear case. This grid may be read using an index grating with fringe detection and interpolation to give position resolution which is much better than the limit set by the size of the detectors.

7.2.2 Reading the Pattern.

A convenient 2-dimensional array of detectors was

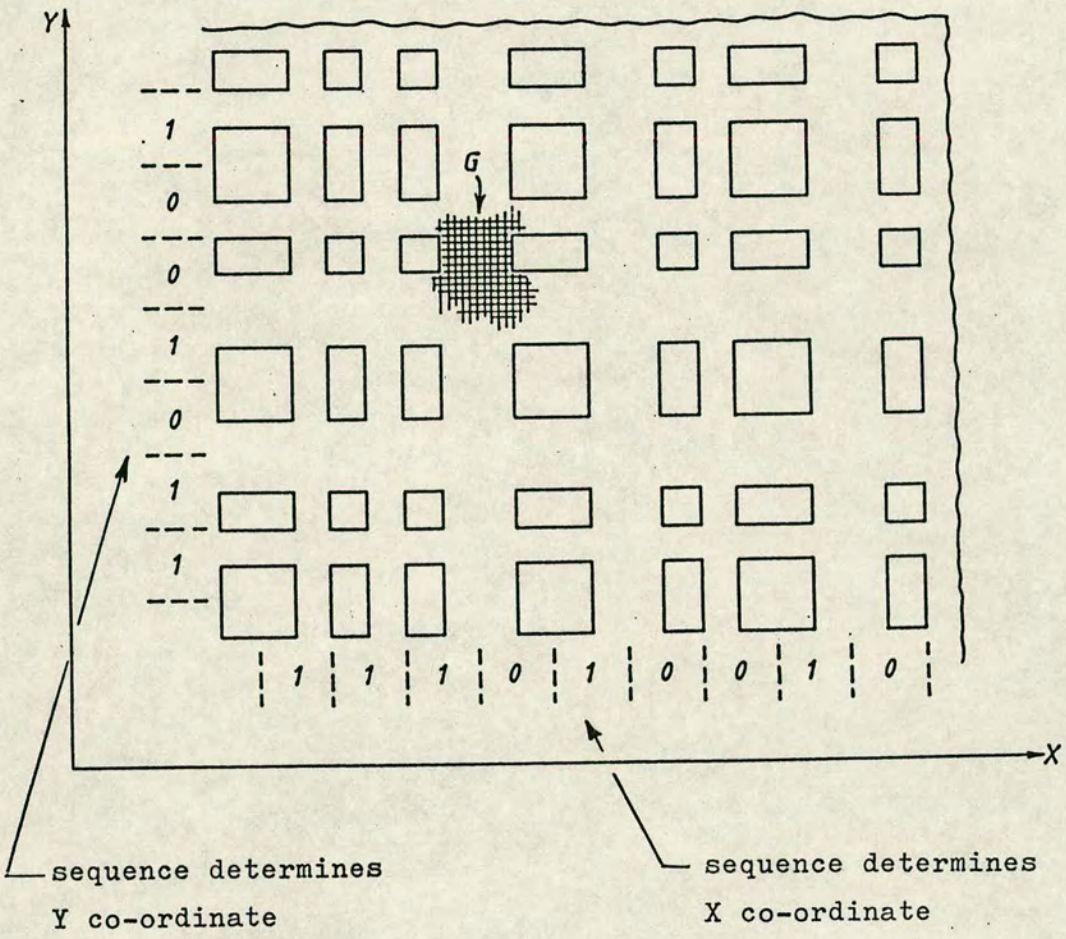

G = fine-pitch grid (optional)

Figure 7.5 XY POSITION ENCODER PATTERN

available in the form of an 'Robot-Eye' miniature camera [89] which used a RAM chip with a transparent lid as the image sensor and a BBC computer to decode and display the binary image. Unfortunately the pixel spacing on the chip was 8.6 μm by 6.8 μm which imposed an awkward constraint on the choice of pitch for the grid and the PRBS pattern. Although the image array was 256 by 256 elements, there was a gap across the middle which meant that it was best regarded as a pair of 128 by 256 element arrays.

7.2.3 Small-scale Implementation.

It was decided to generate patterns on which the X and Y pitches were in the same ratio as the pixel spacing on the array, thus ensuring that the image data would appear the same in the X and Y directions. A computer controlled optical pattern generator was used to produce a small-scale pattern on a photographic plate. The fine grid had pitches of 86 μm in X and 68 μm in Y whilst the PRBS pattern superimposed on it had equivalent pitches of 430 μm in X and 340 μm in Y, i.e. there was a 5:1 ratio between the pitch of the PRBS and that of the fine grid. This proved to be an unfortunate choice: the resulting plate had a very non uniform appearance due to the unequal numbers of clear spaces which were left between the elements of the PRBS pattern, with for example a 0 to 0 transition leaving 2 spaces clear whilst a 1 to 0 transition left 5 spaces clear. Figure 7.6 shows the result.

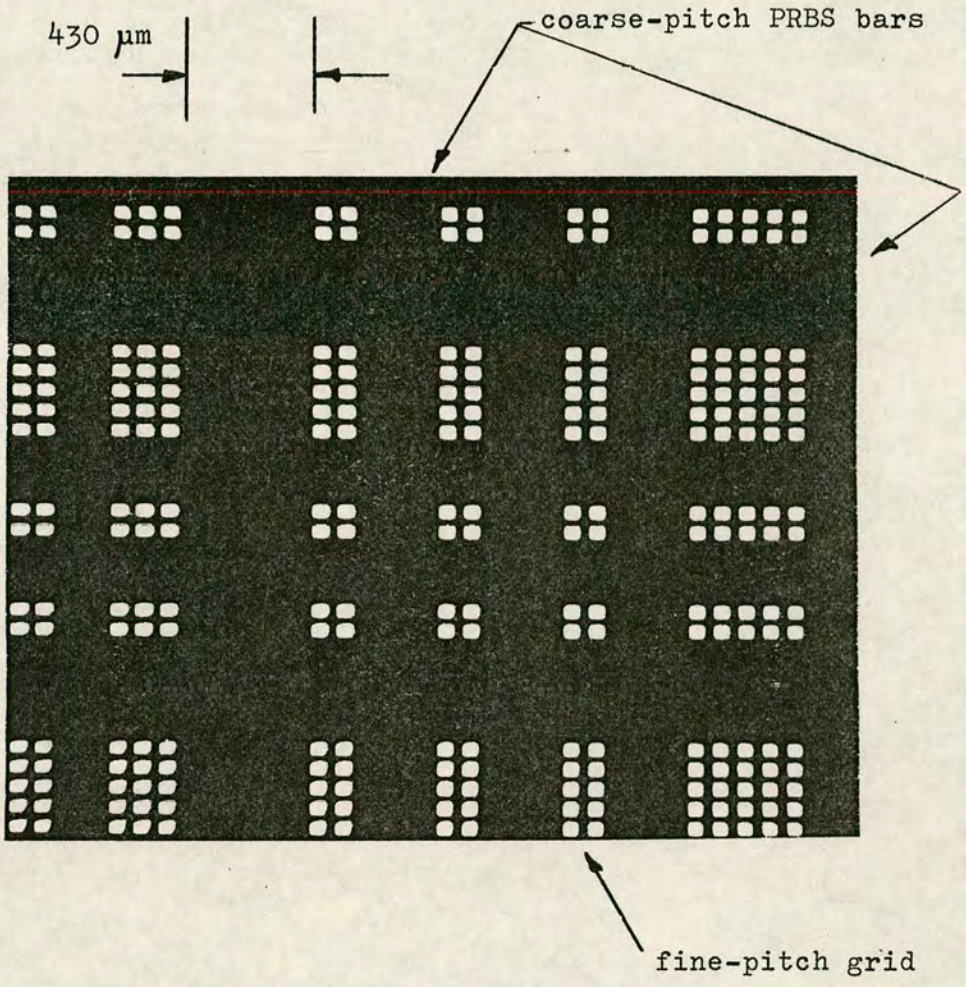

Small - scale implementation with 5:1 ratio between the pitch of the PRBS pattern and the pitch of the fine grid.

Ratio of 5:1 causes uneven numbers of spaces to occur between the blocks of the coarse-pitch PRBS pattern, leading to the uneven overall appearance shown.

Figure 7.6 PRBS CODED PATTERN ON A FINER GRID WITH 5:1 PITCH RATIO

Another pattern was generated with a pitch ratio of 6:1 giving PRBS pitches of 516 μm in X and 408 μm in Y. A PRBS of order 8 gave a maximum range of about 131 mm in X and 104 mm in Y. The index piece shown in figure 7.7 had a clear viewing window in a dark field to sample 10 bits in X and Y with sections of linear grating on two sides to generate vernier fringes from the fine grid. These short sections of grating had pitches of 84.30 μm in X and 66.65 μm in Y to give vernier fringe spacings of 4.35 mm in X and 3.43 mm in Y. Thus the fringe spacing was approximately 50 times the grating pitch and extended over the same number of pixels as the 8 bits of the PRBS.

The patterns were viewed in transmission by the 'Robot-Eye' camera using a lens of 24 mm focal length, in an optical bench arrangement which produced a de-magnification of 7.5:1. This caused the viewing window for the PRBS to be imaged onto an area 80 pixels square.

Unfortunately, it was difficult to obtain a satisfactory binary image in which both the PRBS pattern and the vernier fringes were clearly displayed relative to a common intensity threshold. Several different patterns were tried in which, for example, the field or polarity of sections of the pattern were reversed, and the best of these is shown in figure 7.8. This pattern produced vernier fringes with a dark level which matched the dark level of the PRBS elements, but the results of using the binary imager for fringe detection were still disappointing.

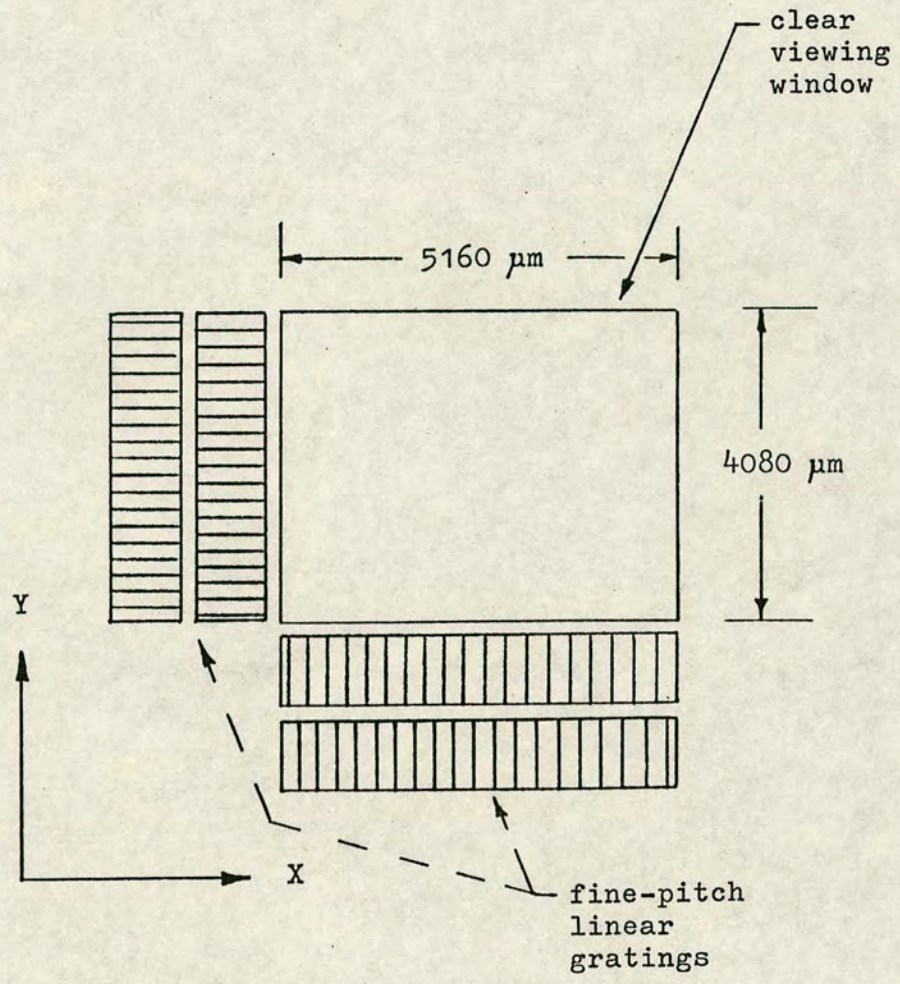

Clear viewing window samples PRBS coded pattern.

Sections of linear grating generate vernier fringes when superimposed on fine-pitch grid. Adjacent sections of linear grating are 180° out of phase to facilitate interpolation within the pitch of the grid.

Figure 7.7 INDEX PIECE FOR USE WITH CODED PATTERN + FINE GRID

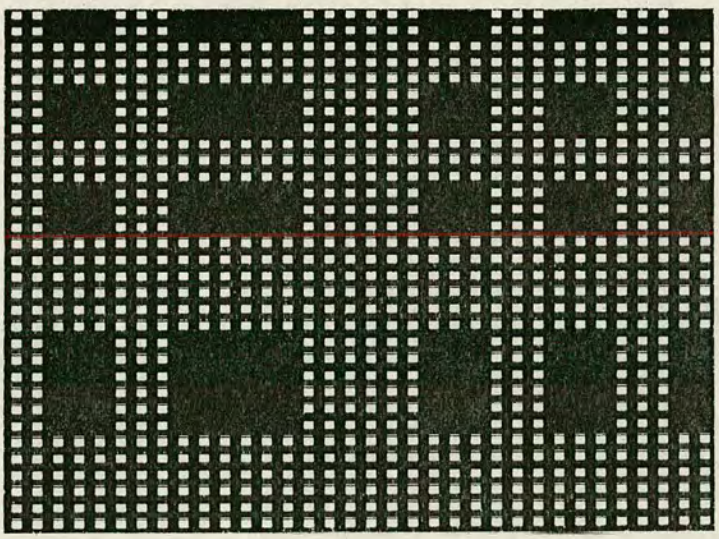

combined PRBS pattern + grid

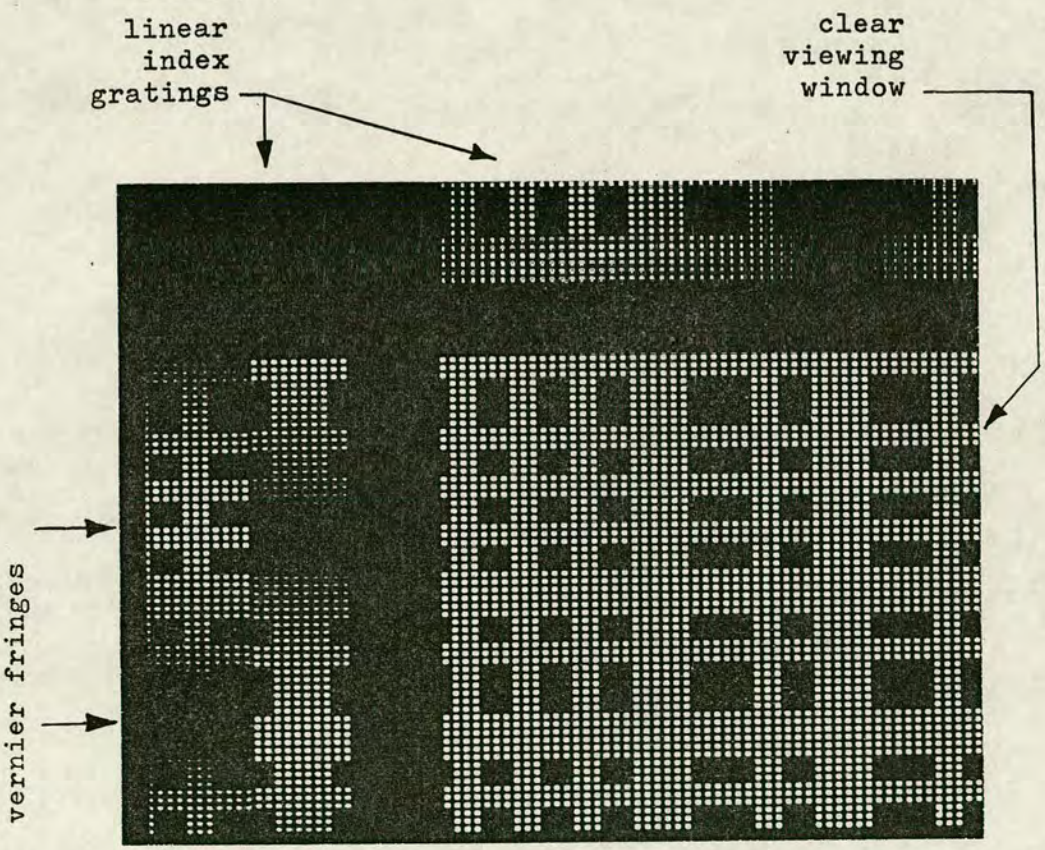

Figure 7.8 PRBS CODED PATTERN + FINE GRID WITH 6:1 PITCH RATIO

7.2.4 Conclusion.

The binary imager could be used to obtain data from a two dimensional position encoder with a potential resolution of +/- 1 pixel but it proved to be unsuitable for detecting moiré fringe patterns. To combine both methods in a single reading head would require a separate set of linear, analogue fringe detectors as in the case of the linear encoder.

7.3 Applications in Wafer Alignment.

Two-dimensional coded patterns can also be used as global alignment targets on wafer steppers. The alignment strategy on existing equipment has been outlined in chapter 5.

7.3.1 The Problem.

In general, a pair of global marks is printed and etched on the wafer when the first layer is patterned and at each subsequent patterning stage these marks are used for initial alignment of the wafer in θ, X, and Y. After mechanical pre-alignment of the wafer, the optical alignment system must be capable of 'capturing' the global mark within its field of view and measuring its X, Y position. The tolerances on pre-alignment are such that the viewing optics must have a wide field of view (perhaps up to 1 mm in diameter) or the global mark must be large,

or both. The use of zoom lenses would introduce unacceptable X,Y errors and thus ultimate sensitivity of alignment is often sacrificed in favour of a wide field of view and a high capture rate.

7.3.2 Coded Patterns as Alignment Marks.

The key benefit of a mark in the form of a two-dimensionsal coded pattern of the type shown in figure 7.5, lies in the fact that the capture range is proportional to 2^n whilst the field of view need only be n bits wide, where n is the order of the sequence. The dimensions of the pattern elements must be compatible with the wafer patterning process so that they can be clearly defined in the first instance and remain clearly visible at all stages throughout the process. A dimension of 5 μm for an element is reasonable for most current processes, implying that each bit of the PRBS would occupy an area 10 μm square. If n is chosen to be 8, the capture range would be more than 2.5 mm, whilst the field of view of the alignment system could be restricted to 100 μm in diameter. If the video camera could resolve 500 pixels in X and Y, each pixel would be equivalent to 0.2 μm on the surface of the wafer. Thus capture of the mark would be guaranteed and it would only be necessary to capture two video frames, one from each side of the wafer, to establish its orientation and position to within +/- 0.2 μm.

An additional benefit of this approach would be the

elimination of the off-axis microscope and the associated uncertainty in the offset or 'baseline' between its optic axis and that of the main projection lens. Instead, the high magnification, through-the-lens microscope used for field by field or die by die alignment could be used to capture these global marks with direct referencing to the reticle. Apart from the obvious gain in accuracy, there would be a time saving of several seconds per wafer due to the reduced number of stage iterations, and of course the overhead time spent on regular calibration of the baseline would disappear.

7.3.3 Survival of the Marks.

Since each mark has a high level of redundancy, local defects and imperfections are unlikely to cause errors. In the unlikely event of a gross defect larger than 100 μm in diameter appearing in the field of view, the stage could be programmed to translate by, say, 100 μm in one axis before repeating the alignment procedure.

The visibility of the marks throughout a process sequence can be established for certain only by experimental trials. There are basically three mechanisms which contribute to the visibility of an alignment mark. First, it may have a different reflectivity from the surroundings and thereby alter the amplitude of the reflected light, appearing either lighter or darker against its background. Second, it may have a different refractive index or be of a different thickness than the

surrounding material and thereby alter the phase of the reflected light giving phase contrast. Third, it may have a topographical shape such as a trench or mesa with edges which scatter light and thus the edges may appear dark or light depending on the type of illumination.

The experimental trials could have been done on an optical bench using sample wafers but it was more convenient and more realistic to use a wafer stepper with real time through-the-lens viewing and a video capture and analysis system. The method and results will be fully described in section 8.5.3.

7.4 A Co-ordinate Position Indicator for Large-scale Industrial Application - 'COPILIA'

7.4.1 Outline.

A two-dimensional absolute position encoder could have applications in other fields. It was realised that the patterns described above could be scaled by about three orders of magnitude to give a range of 100's of metres with a sensitivity of a few millimetres. This could form the basis of an automatic navigation system for Automated Guided Vehicles (AGV's) where the ceiling of the working area could be patterned and the vehicle could carry an upwards-looking TV camera. An appropriate application area might be in semiconductor cleanrooms where there is a continuous ceiling, an increasing need to introduce automated transfer of wafers and where the

disruption and contamination of installing a buried wire guidance system is out of the question.

7.4.2 Laboratory Demonstration.

An automated guided vehicle in the form of a turtle controlled by a BBC computer was fitted with an upwards-looking 'Robot-Eye' camera. A section of two-dimensional PRBS pattern of order 8 was fabricated with a pitch of about 5 mm. As before, the pitches chosen were in the same ratio as the pixels on the camera: approximately 6 mm in X and 4.7 mm in Y. This pattern was applied to an illuminated ceiling. To simplify decoding, the dimensions of the pattern were chosen such that a sample of 10 bits on the pattern would be imaged onto 60 pixels in the camera.

A computer program to drive the turtle to any specified XY position, to interrogate the camera, decode the image and display the achieved position was written and tested by W. Alexander and S. Anderson (1986) [89]. It was written in FORTH and the time taken to decode the image was 7 seconds. The program assumed that the pattern was aligned parallel to the image raster of the camera: no attempt was made to accommodate image rotation. A sample screen dump is shown in figure 7.9.

The experiment demonstrated the benefits of this approach. The turtle could be switched off and on again or it could be carried 'blind' to any point in the work area and, after 7 seconds, it would establish its correct

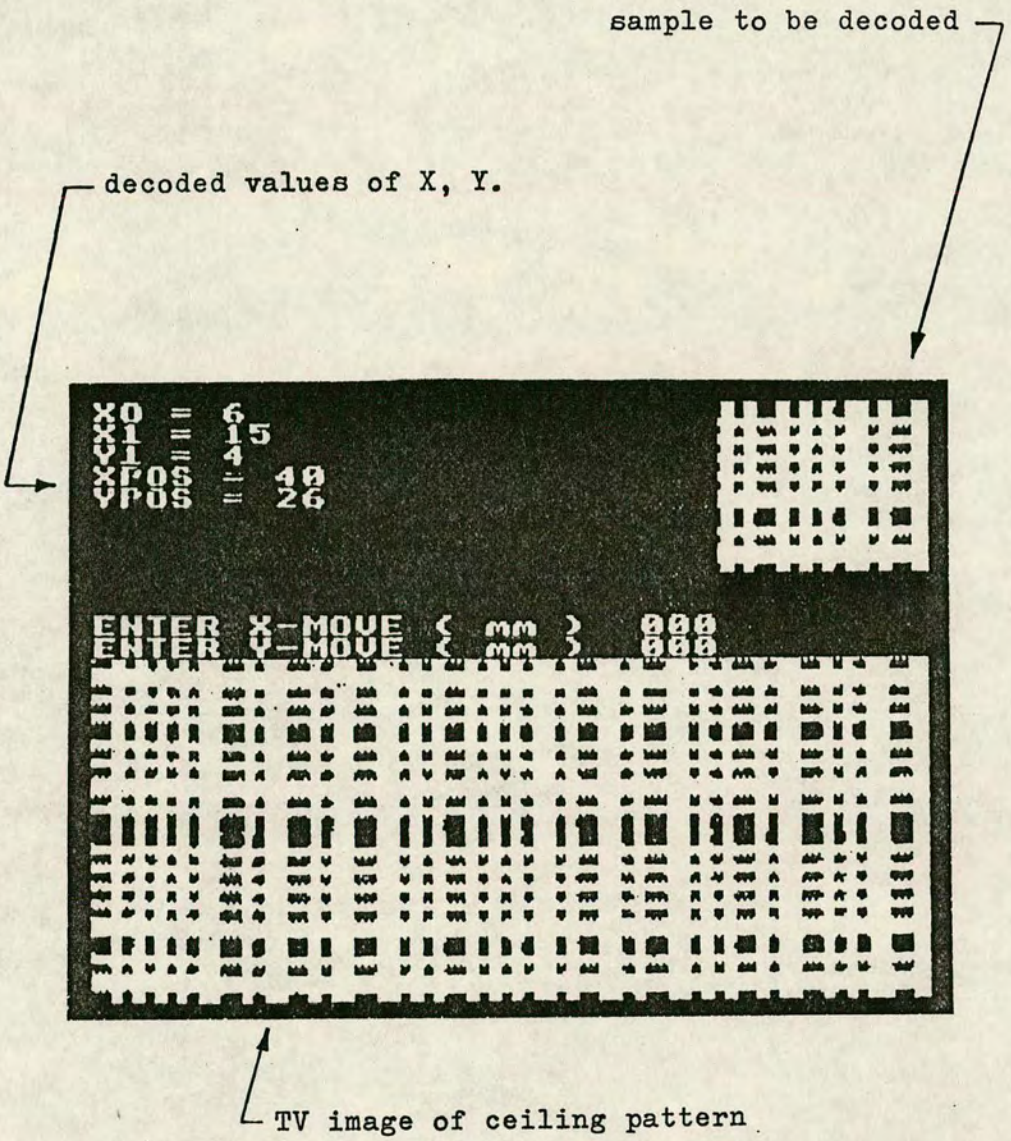

Figure 7.9 SCREEN DUMP FROM AGV PROGRAM

position by referring to the pattern on the ceiling. It is expected that the decoding time will be significantly reduced when a more appropriate microcomputer system is used.

7.4.3 Reference Grid Pattern.

Experience also confirmed that the full two-dimensional pattern could be replaced by a series of coded tapes arranged on a square grid as shown in figure 7.10, since the decoding procedure merely selected a row and a column from the image of the full pattern. The intersection points on the grid would have to be fitted with blanking plates as shown.

Two other requirements of the reference grid are important: it must be possible, by inspection of the local pattern, to distinguish X from Y and (+) from (-) in each axis, irrespective of the position or orientation of the AGV. This could be done in several ways. The X and Y tapes could be produced from a single long PRBS with, for example, the X tapes coming from the first half of the sequence and the Y tapes from the second half. After decoding the X and Y co-ordinates would be identified from their position in the sequence. Alternatively, the tapes for one axis could have an additional feature such as a continuous black band along one edge, as in figure 7.10. This would serve 3 functions:

1. To identify the X and Y axes

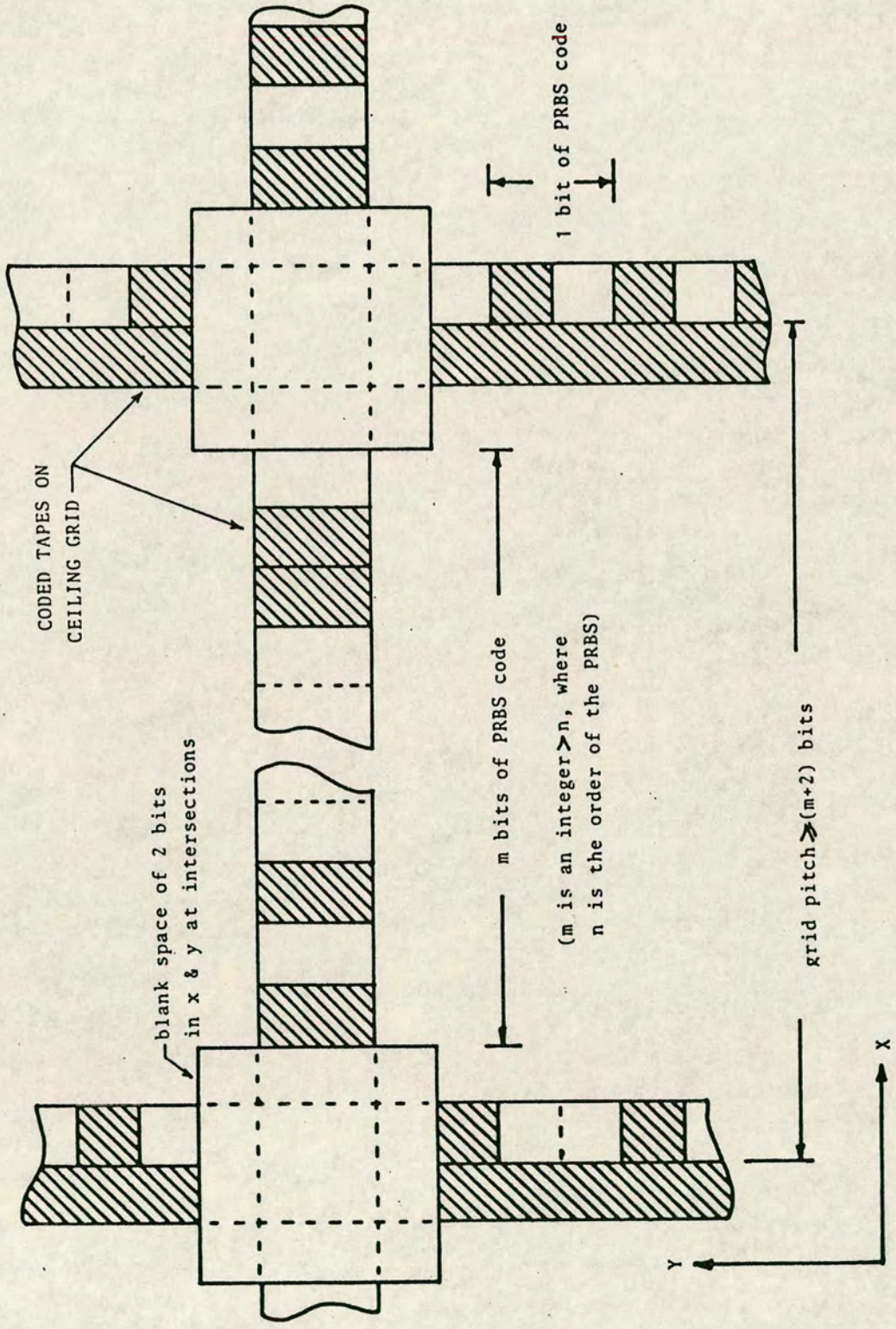

Figure 7.10 CODED TAPES ON CEILING GRID

2. To define the (+) and (-) directions

3. To provide a continuous edge from which the orientation or heading of the AGV could be measured.

There may be other means of achieving the above functions by careful design of the coded pattern to provide directional information. For example, it may be possible to compare successive n-bit groups on the basis that only the sequence in the (+) direction will match the stored code, but these methods have not been investigated.

7.4.4 Dimensions, Resolution and Range.

If the tapes were installed on a 600 mm grid to be compatible with a ceiling support framework as shown in figure 7.11 and if one bit of the PRBS pattern occupied 25 mm on the tape, a sequence with n=16 would give a total range of approximately 1.6 Km within which any position could be determined by reading a 400 mm section of coded tape.

The field of view of the camera would need to be about 900 mm to cater for the worst case 45 degree orientation of the pattern as shown in figure 7.11. If the camera could resolve 500 pixels across its image field, each pixel would correspond to a distance of about 2 mm on the grid. Similarly the angle of the edge of the tape, giving the orientation or heading of the AGV, could be determined to within about 0.1 degree.

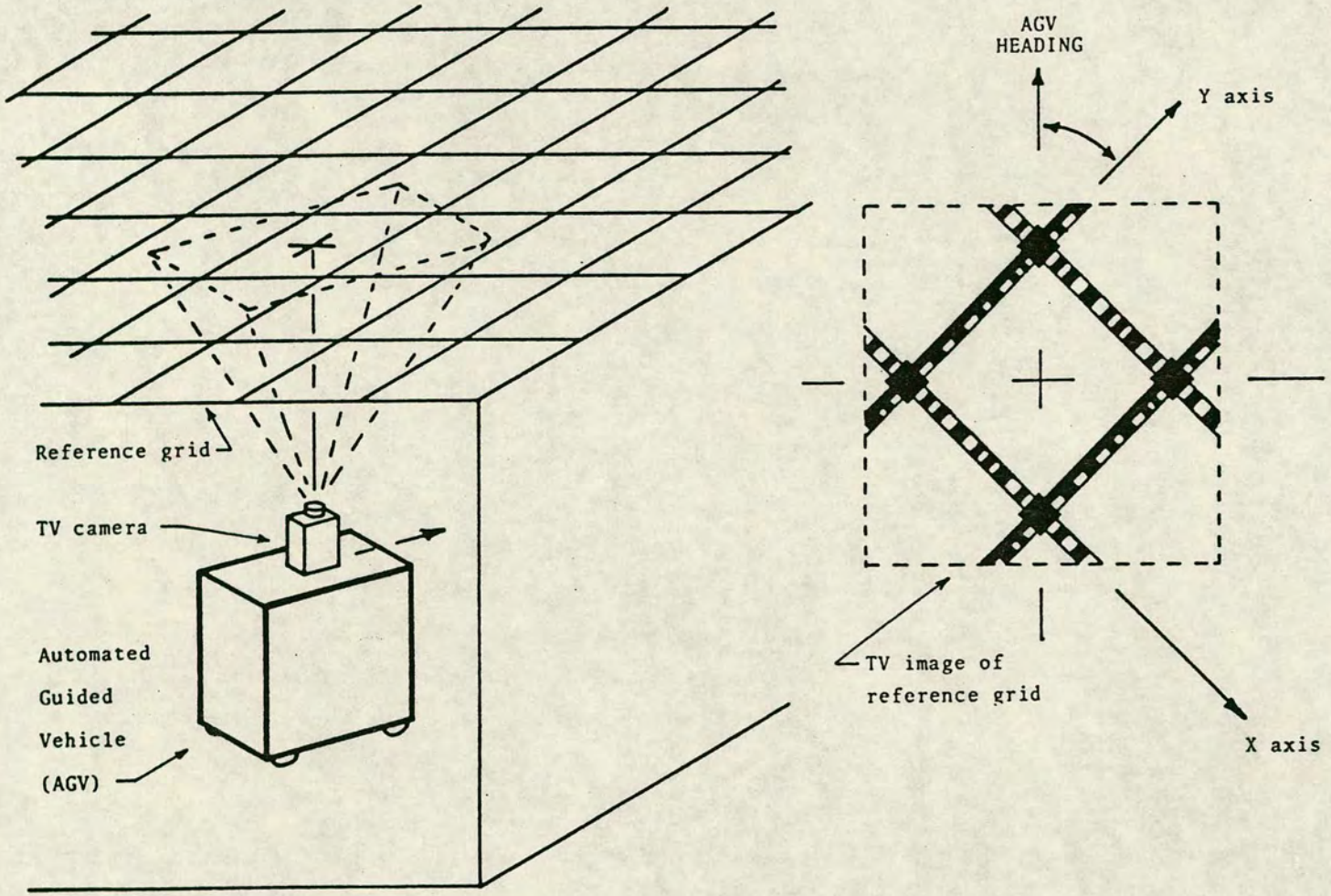

Figure 7.11 IMAGE ROTATION - AGV HEADING

7.4.5 Image Rotation and Zoom.

Although the image could be rotated and zoomed by mechanical adjustment of the camera, the same effect can be achieved electronically by modifying the drives to the scanning raster of a vidicon camera tube. Such a system has been described by Green (1985) [90]. By restricting the scanning raster, a 5:1 zoom ratio can be achieved, thus offering a position resolution of about 0.4 mm in the above example. A conventional optical zoom lens could produce higher magnification at the image plane but it would require modification of the ceiling grid in the areas where higher positioning accuracy might be required. This could take the form of areas of chequer board pattern or the full two-dimensional PRBS pattern might be used. The final position would then be determined by locating the feature nearest to the optic axis when the lens was zoomed.

Software methods of image rotation are widely used in robot vision but they are likely to be much slower and they have not been pursued.

7.4.6 Conclusion.

The laboratory demonstration served to illustrate the principle of the proposed navigation system which has a number of advantages. It is capable of meeting the required accuracy and repeatability in the positioning of

AGV's in an industrial environment, using a passive reference pattern which could be installed at low cost wherever a suitable surface was available. When combined with a dead-reckoning capability in the AGV, the system could tolerate large gaps or omissions in the reference pattern as it is an absolute system. The cost of the on-board TV camera and microcomputer would be modest in relation to the cost of the AGV, perhaps £1000 on a vehicle costing tens of thousands.

The systems described in this chapter are the subject of a provisional UK Patent Application [91]. The patent rights have been assigned to British Technology Group.

CHAPTER 8: A DYNAMIC ALIGNMENT SYSTEM FOR WAFER STEPPERS.

8.1 Outline.

When the use of pulsed excimer lasers as exposure sources for wafer steppers was reviewed in chapter 2, the possibility of operating in a flash-on-the-fly mode with a continuously moving stage was mentioned. This would give an enormous increase in the throughput of wafer steppers by exposing a whole row of dice in little more than the time taken to step the stage and expose a single field on present equipment. It was pointed out, however, that a completely new approach to the problem of die by die or field by field alignment would be required to achieve the overlay tolerances which have been predicted for the 1990's.

This chapter analyses the alignment requirements of flash-on-the-fly operation, describes an alignment system based on two-dimensional gratings and presents the results of experiments using two-dimensional grating patterns on a wafer stepper.

8.2 The Requirement.

The tolerances on layer to layer registration or overlay have already been reviewed. These tolerances are determined by the design rules and the process, i.e. they are dictated by the requirements of the product. Any future alignment system will have to meet the requirements

of products having critical dimensions of 0.5 μm and overlay tolerances of +/- 0.15 μm (3 sigma), {Broers (1985) [58]}. This implies that the alignment system must have a sensitivity of at least 50 nm and preferably better than 25 nm. It must achieve these tolerances whilst coping with the variations in reflectivity and contrast of the alignment marks which inevitably arise as successive process layers are deposited on the wafer.

When operating in a flash-on-the-fly mode, one axis of the wafer stage, say the X axis, will be scanned continuously whilst the Y axis will remain stationary until the end of a row when it will step across by the appropriate distance to the start of the next row. It would be possible to expose the sites 'blindly' by triggering the flash at the appropriate X co-ordinates in a manner analagous to the 'blind stepping' mode of operation on current equipment. However, better overlay accuracy will be obtained if the exposure co-ordinates of each site are adjusted to take account of wafer distortion and local pattern misplacement. This means that minor adjustments have to be made to the Y position of the wafer stage as it is scanned in X to ensure that it is in the correct position or 'on track' before the flash is fired. These local adjustments would typically be less than 2 μm. The alignment system must therefore provide a signal which gives advanced information on the Y co-ordinate of the next exposure site to allow the necessary Y axis adjustment to be made before the flash occurs.

The X position at which the flash occurs is equally

important but the problem is transformed to a question of timing accuracy. There will be a latency period between application of the trigger pulse to the excimer laser and the occurrence of the flash, typically 1 μs with a spread of +/- 2 ns, [96]. In addition, there will be phase lags in the alignment and detection circuits which generate the trigger pulse, all of which contributes to an uncertainty of position in the X direction. The systematic delays in the system can be allowed for, provided the scan velocity is known, by advancing the trigger pulse to the laser. Again advanced information is required from the alignment system to define the X co-ordinate of the next exposure site from some distance ahead to allow time for the calculation and application of the appropriate phase advance to the trigger pulse.

Clearly the bandwidth of the alignment system must be compatible with the scan velocity of the stage. This will be determined by mechanical considerations such as the moving mass and the limitations of the servo drives. The flash duration is so short that its effect on the pattern can be ignored: even at a velocity of 1 m/s it would amount to only a 10 nm broadening of the lines in the X direction. The wafer stages on current equipment are capable of velocity in excess of 150 mm/s with acceleration in excess of 1000 mm/s^2 to produce rapid stepping from one site to the next. The scan velocity is likely, therefore, to be of the order of 100's of mm per second. A scanning stage has recently been designed with a maximum velocity of 660 mm/s [92].

To summarise, the alignment system must operate in a dynamic, continuous manner to provide advanced knowledge of the Y and X co-ordinates of each exposure site together with a measure of the relative velocity between the projected reticle pattern and the reference pattern on the wafer. It must operate through the main projection lens with direct referencing of the wafer pattern to the reticle. It is envisaged that the alignment control circuit will operate in conjunction with a conventional XY stage measuring system which would give the machine a blind step capability in the event of failure of the field by field alignment system. A possible control scheme is shown in figure 8.1.

8.3 Possible Alignment Patterns.

The above requirements imply some form of continuous or pseudo-continuous pattern to provide a tracking error signal for the Y axis together with a velocity signal and a means of identifying the X co-ordinate of the next exposure site. The pattern should preferably be confined to the scribe channels which are about 150-200 μm wide. At its simplest the pattern might take the form of a single continuous line parallel to the scan direction with cross markers at regular intervals as indicators of X position. By imaging the line onto photodetectors a Y axis error signal could be derived and a separate detector with a slit to match the cross markers could detect the X positions. However, this approach

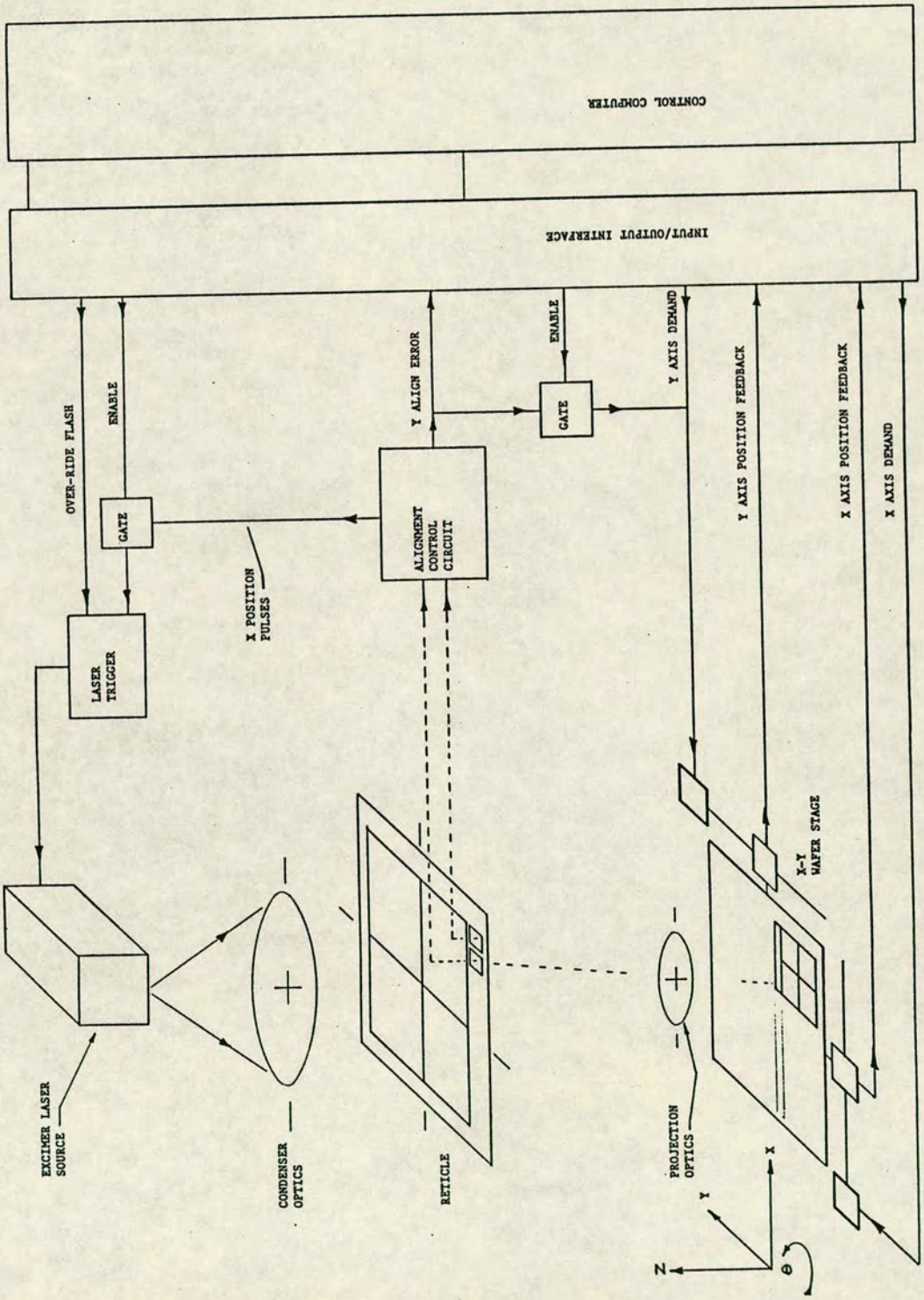

Figure 8.1 'FLASH-ON-THE-FLY' WAFER STEPPER CONTROL SCHEME

would be subject to the problems of d.c. coupled analogue circuits as well as being sensitive to debris and asymmetry of the line image.

As an alternative, a periodic or grating pattern could be used to provide an a.c. signal as the stage is scanned. The grating pattern would provide a signal from a larger area of wafer, averaged over a large number of lines and would thus be less sensitive to local errors, debris and minor imperfections. An XY grating of the type previously described could be imaged onto two short sections of linear grating, one in the X direction and one in the Y direction. As the stage scanned, these would give periodic moiré fringe signals in the X direction but the fringes in the Y direction would be virtually static. Some additional modulator or scanner would have to be incorporated to allow a.c. coupling of the Y signal.

A more elegant solution is to rotate the above pattern through 45 degrees to produce a chevron grating as shown in figure 8.2. When two such gratings are superimposed, the fringe pattern is sensitive to relative displacement in both the X and Y directions and if one grating is scanned past the other in the X direction each half of the chevron will produce a periodic fringe signal with a frequency of v/p where v is the velocity and p is the pitch of the grating in the X direction. The phase difference between these two signals is directly related to the Y offset between the centre lines of the gratings. An offset in the Y direction equal to p/4 would produce a phase difference of 180 degrees between the chevron

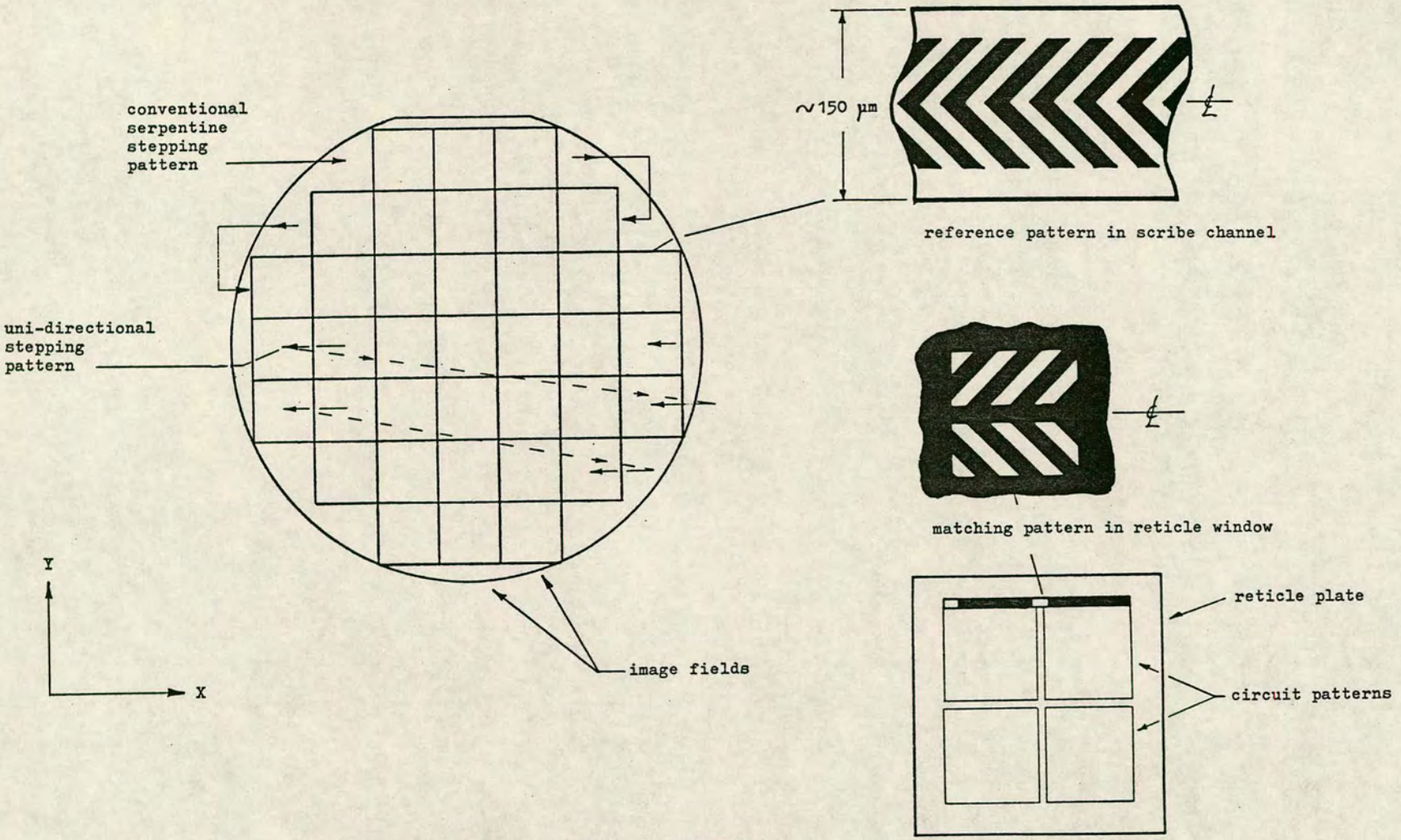

Figure 8.2 CHEVRON GRATING ALIGNMENT PATTERNS

fringes. This means that, for example, a Y offset of only 14 nm on gratings with p=10 μm would produce a phase difference of 1 degree. Phase comparison to better than 1 degree is a well established technique. The frequency of the fringe signals at a scan velocity of, say, 500 mm/s would be 50 kHz.

8.4 Optical Arrangements.

At the first photolithographic stage in the fabrication process, the reference pattern would be printed along one edge of the exposure field over a length of several millimetres and preferably over the entire length of the exposure field. The reticle for each subsequent layer would have two viewing windows containing short sections of linear grating with an associated illumination and detector system. Figure 8.3 shows one possible configuration in which these components are mounted above the viewing windows on the reticle to avoid any intrusion into the space between the reticle and the main projection lens. The position of these windows on the reticle in relation to the die pattern depends on the exposure strategy. Ideally, the position should be chosen to maximise the duration of the alignment signal prior to exposure. If, for example, exposures are to be made only when the stage is scanning from left to right, the windows would be on the leading corner of the field. If, however, bi-directional exposures are to be made the windows would be in the middle of the side and would provide an

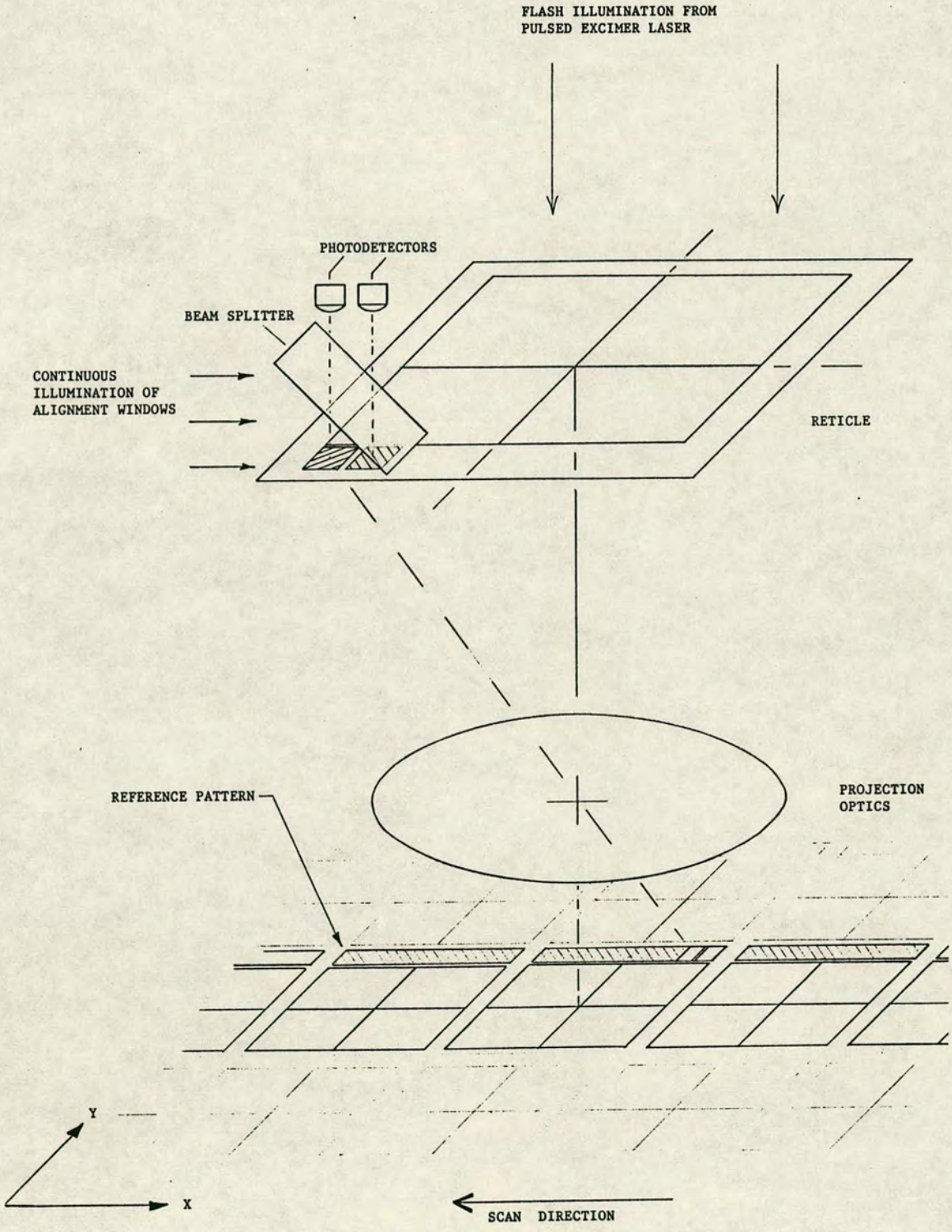

Figure 8.3 OPTICAL ARRANGEMENT OF ALIGNMENT DETECTORS

alignment signal during the scan of half the length of the exposure field.

With a chevron grating as the reference pattern each viewing window and photodetector must be less than half the width of the scribe channel. An alternative reference pattern is shown in figure 8.4. A chequer board may be regarded as a superposition of two linear gratings where each grating consists of rows of individual squares at 45 degrees to the scan axis. When it is interrogated through two separate full-width windows, one having lines at +45 degrees and the other having lines at -45 degrees to the scan axis, the signals would be equivalent to those derived from a chevron grating.

The use of separate full-width windows would also facilitate any arrangements to block the zero diffracted order and detect only the first orders as is already done on some existing equipment. By blocking the zero diffracted order, 100% modulation of the fringes is guaranteed but the amplitude of the signal is greatly reduced and is still affected by variations in reflectivity of the substrate.

8.5 Experimental Work on Chevron Gratings.

A series of experiments was undertaken to prove the feasibility of using chevron gratings as alignment patterns on a typical MOS process. The contrast of the patterns was measured at each of the photolithographic stages under worst-case conditions.

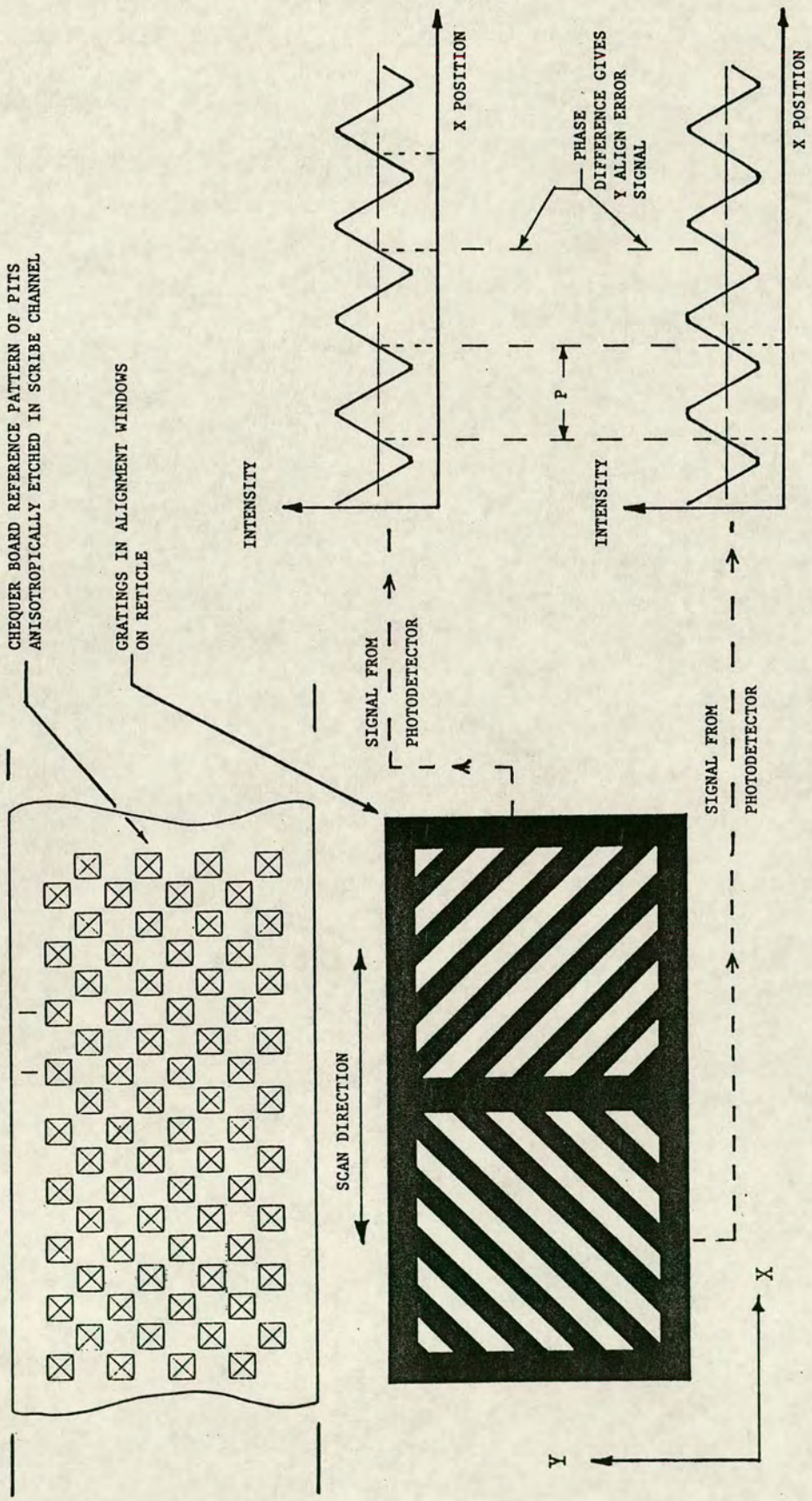

Figure 8.4 CHEQUER BOARD REFERENCE PATTERN

8.5.1 Reticle Patterns.

Test reticles were designed with arrays of chevron gratings and viewing windows. Three different line structures were included, with pitches in the X and Y directions of 5 μm, 10 μm and 20 μm. Thus the chevrons had nominal line widths of 1.8 μm, 3.5 μm, and 7.0 μm. Each stripe of grating was several millimetres long. Chequer board patterns were also included with dimensions to match the chevron gratings, laid out so that matching pairs of chequer board and grating could be overlaid by a simple offset of the wafer.

8.5.2 Processing of Test Wafers.

It was known that alignment targets which had been etched at level 1 (active area) showed poor contrast at later stages in the process. It was decided, therefore, to investigate the benefits of a 'zeroth' layer reference pattern. The chequer board mask was used to define an array of windows in a film of silicon nitride. Etching to completion in hot KOH solution as before produced an array of pits whose sides were bounded by (111) crystal planes.

It had already been confirmed that these pits would reflect normally incident light at +/- 39 degrees to the optic axis and these reflections had been used in an XY reading head. It was now intended to use this property the other way round to guarantee good contrast. Since the

main projection lens on the stepper had a numerical aperture (NA) of 0.32 corresponding to a cone angle of 19 degrees, reflections from the sides of the pits would be outwith the acceptance angle of the lens and hence the pits would appear black against the direct reflection from the planar areas of the field. Observation of etched pits with a microscope using a range of objectives had shown that the pits appeared completely dark when viewed with an objective of low NA and, although some light became visible at NA = 0.4, detailed viewing of the sidewalls required an objective with NA greater than 0.8.

After pit etching, the wafers had the chevron gratings etched at level 1, followed by a sequence of typical n-MOS layer depositions. Details of the process are given in Appendix 1. In some processes it may be possible to ensure that the alignment marks are cleared of deposited material by exposure and etching, but this cannot always be guaranteed and hence these process conditions were deliberately chosen to produce the worst case viewing conditions by burying the alignment marks under successive process layers. At each photolithographic stage, a wafer was removed from the batch and coated with photoresist to simulate the alignment conditions which would be encountered by a wafer stepper at that stage of the process.

8.5.3 Measurement of Contrast.

The test wafers were evaluated using an Optimetrix 10X wafer stepper. The optical system is shown diagrammatically in figure 8.5. The key features which were of use in this experiment were the real-time through-the-lens viewing via a fixed beamsplitter and TV camera and a means of storing and analysing data from the video system. The video data could also be transferred to another computer for plotting and analysis of intensity profiles using routines devised by Maxwell [93]. The viewing and exposure wavelengths were the same - the g-line of the mercury spectrum, 436nm.

8.5.4 Results - Contrast of Reference Patterns.

The video system which normally captures the die by die alignment marks was used to take line scans across the various samples of chevron gratings and chequer board pits. The intensity profiles were digitised and then hard copy plots of intensity against horizontal position were obtained. The magnification of the optical system between wafer and screen was about 1000X: this produced a clear image of the wafer patterns, with a 10 μm feature occupying about 50 pixels on the video plot.

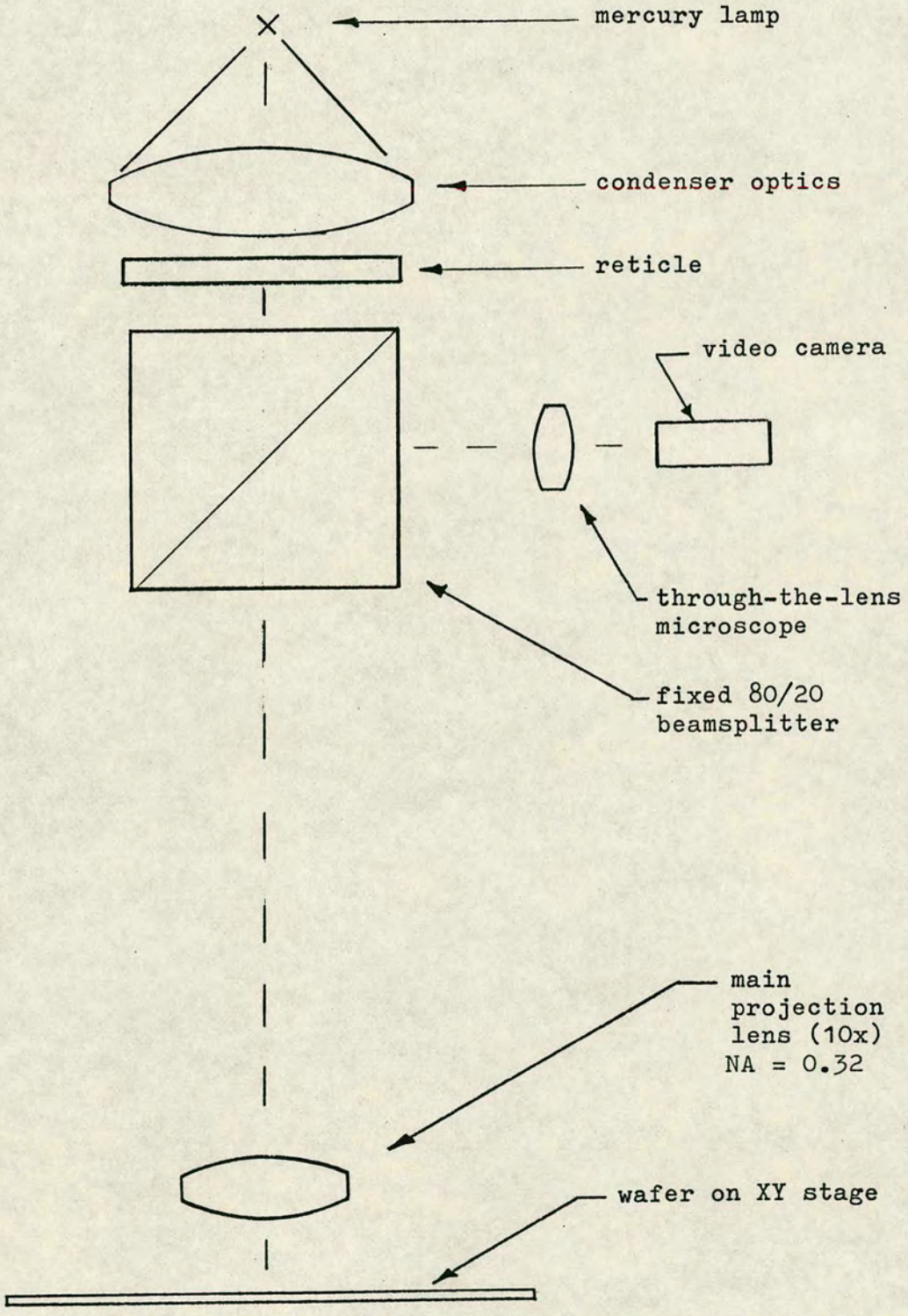

Figure 8.5 'OPTIMETRIX' WAFER STEPPER - OPTICAL SYSTEM

Details of the process layers on each of the test wafers are summarised below:-

Wafer No.	n-MOS Stage	Process Layer
1	Zero - N/A	N/A - bare silicon
2	1-active area	nitride
3	3-buried contact	field oxide
4	4-poly silicon	poly silicon
5	6-contact	pyrolytic oxide
6	7-metal	aluminium-silicon

NOTES.

1. The light field reticle which was used to define the chevron gratings at n-MOS stage 1 had dark areas to mask the chequer boards so that they remained covered in nitride during field oxidation.

2. The build up of layers listed above was cumulative so that e.g. on wafer 6 the marks were covered by all the previously deposited layers plus AlSi and then a layer of photoresist.

The video plots of the chequer board patterns are shown in figures 8.6 and 8.7. It was found that the smallest chequer board pattern with 2.5 μm square pits did not exhibit satisfactory contrast as the pits were so small that they filled up and became 'planarised' by the deposition of material. The larger pits (5 μm and 10 μm) showed good contrast on all the test wafers and the visual observations were confirmed by the video plots.

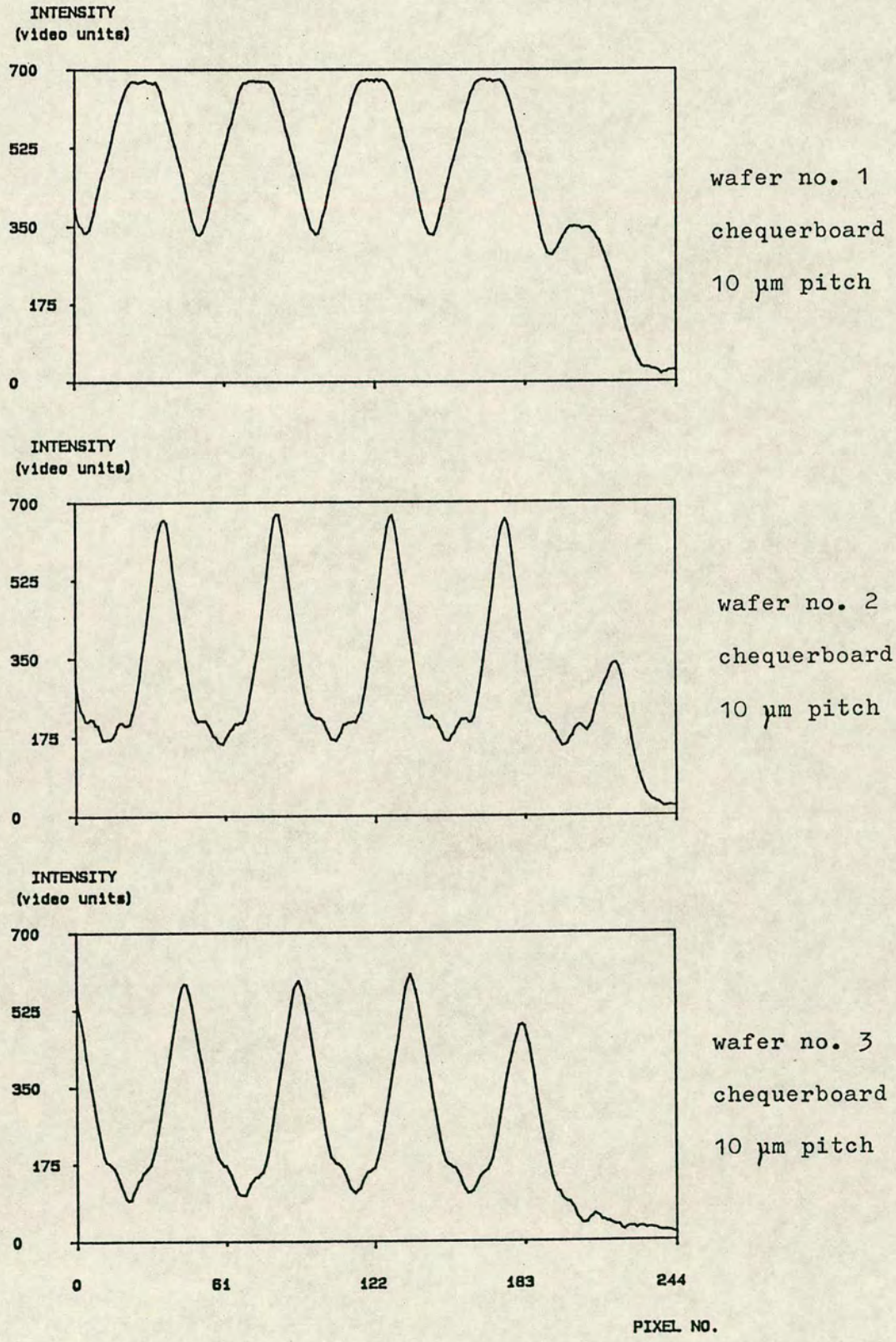

Figure 8.6 VIDEO INTENSITY PLOTS OF CHEQUER BOARD IMAGES

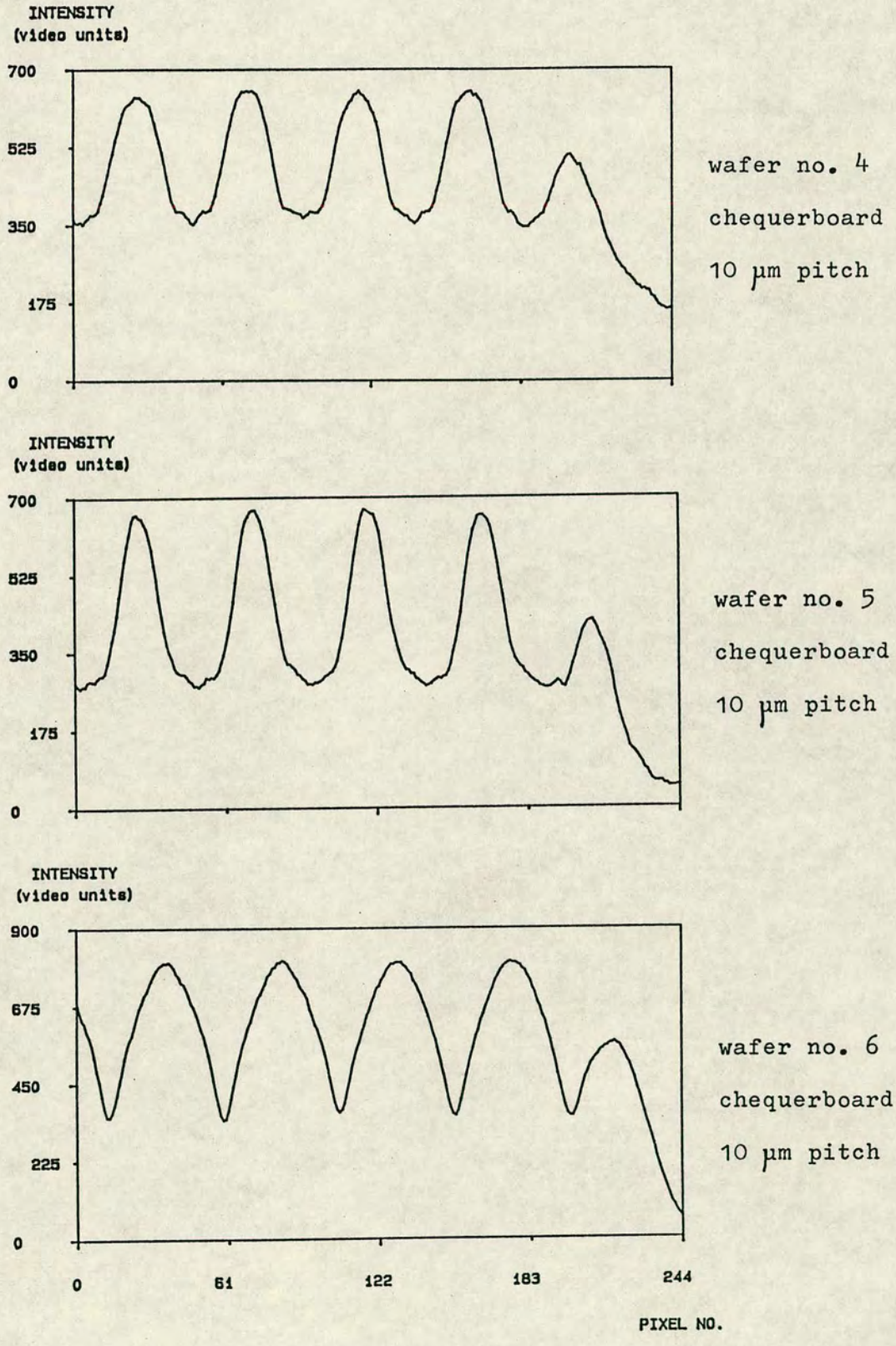

Figure 8.7 VIDEO INTENSITY PLOTS OF CHEQUER BOARD IMAGES

The planar chevron gratings which had been etched at level 1 were less satisfactory. In addition to a lack of contrast, the grating pattern was corrupted by the appearance of interference fringes near the edges of the grating lines. This produced additional bands of dark and light areas which sometimes looked like a grating of half the nominal pitch. The effect was due to variations in the thickness of the layer of resist (or of the underlying layer if it too was transparent) producing fringes when viewed in monochromatic light. This is a well known phenomenon on all steppers which use monochromatic illumination of the alignment marks and it has been investigated by Maxwell [93]. Figure 8.8 shows video plots from wafers 3, 4, and 5 where the fringing was very noticeable on the 5 μm chevron (10 μm pitch in X,Y).

8.5.5 Measurement of Fringe Contrast.

The wafers were moved in X and Y on the stage of the stepper until the image of the viewing windows was projected onto the appropriate reference pattern. The resulting fringes were surprisingly easy to use as a visual alignment aid. Using a chevron grating with a pitch of 10 μm in X and Y, it was possible to adjust the position of the stage in the cross-track direction to within about 0.25 μm of the correct position simply by observing and 'balancing' the intensity of the two sides of the fringe pattern. When moved off track by a quarter of the grating pitch, one half of the chevron would go to

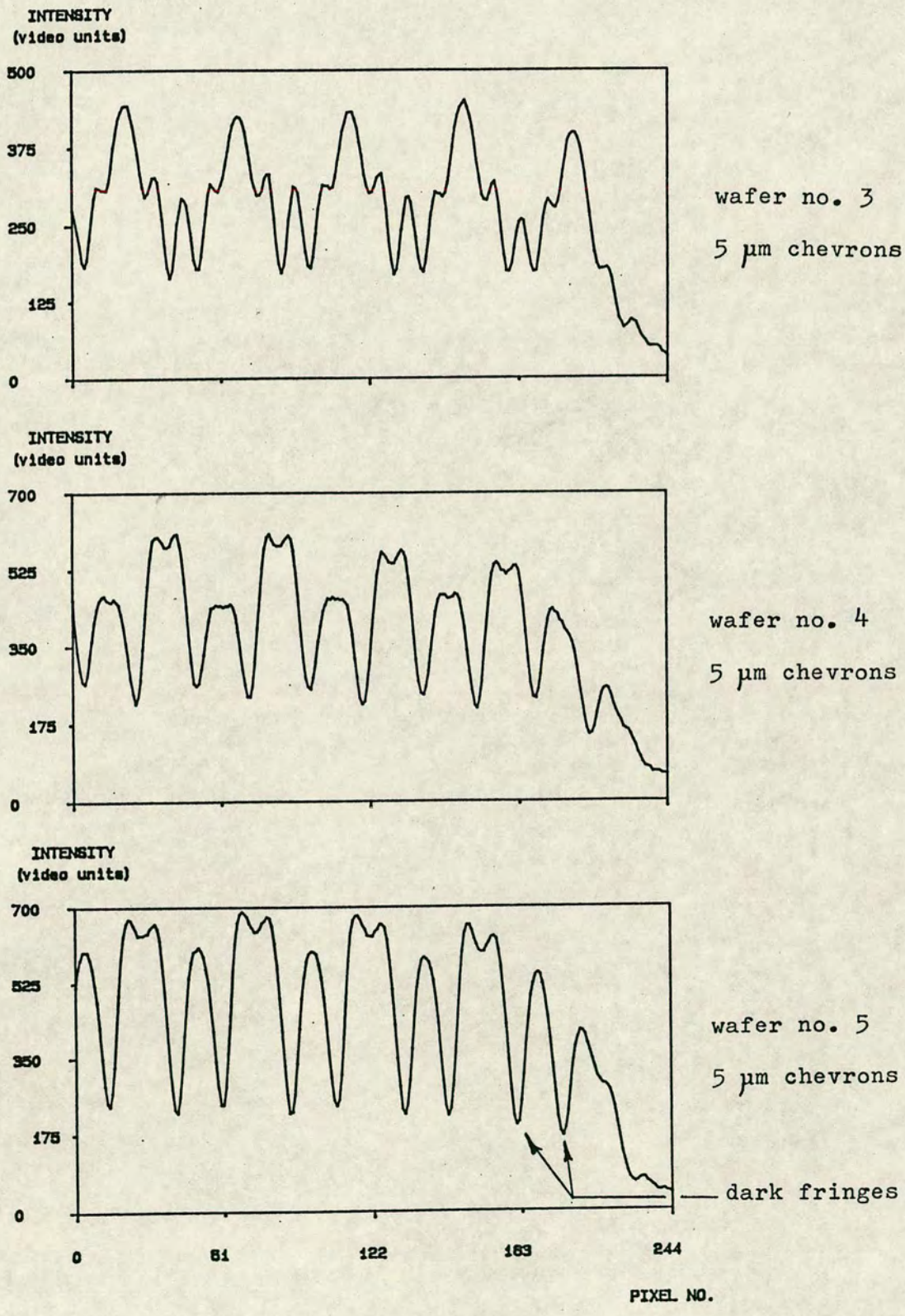

Figure 8.8 SEVERE FRINGING ON CHEVRON IMAGES

its maximum brightness whilst the other would go to a minimum, thereby giving an indication of the fringe contrast.

Ideally, the fringe contrast should have been measured by mounting photodetectors in the conjugate image plane of the reticle, in place of the on-axis viewing system. This could not be done without partial dismantling and interference with the optical column of the stepper and this was considered unwise in view of the cost of the equipment (about $800K) and the fact that it was in daily use providing a fabrication service to other users. Instead, intensity plots were taken using the on-axis viewing system with the chevrons adjusted for 180 degree phase difference between the two halves as mentioned above. Two measurements were taken, one with +180 degrees offset, the other with -180 degrees offset so that the maximum and minimum intensity achieved by each window was recorded.

To simulate the effect of a photodetector of larger area, the intensity plots were integrated using a separate computer program and the integrated values of intensity were used to calculate the fringe contrast which had been achieved.

8.5.6 Results.

The fringe contrast generated by the chequer board pattern of 5 μm pits (10 μm pitch) was measured with the following results:-

Wafer No.	n-MOS Stage	Fringe Contrast
1	Zero - N/A	N/A
2	1-active area	32 %
3	3-buried contact	44 %
4	4-poly Si	30 %
5	6-contact	26 %
6	7-metal	33 %

The results from the chevron gratings which had been etched at level 1 were much poorer and they were difficult to measure because of the multiple maxima and minima caused by the interference fringes. Comparative figures for the 10 μm pitch chevron grating were:-

wafer 3 fringe contrast = 14%

wafer 4 " " = 9 %

8.5.7 Conclusion.

The experimental results confirmed that chevron gratings are a viable means of deriving alignment signals from wafers. The chequer board patterns which were

etched as pits at level zero gave good contrast throughout the process.

The planar chevron gratings which were etched at level one were severely affected by intra layer interference effects which would have corrupted any alignment signal derived from the fringes. These fringe signals could be improved by blocking the zero order and allowing only the first diffracted orders to reach the photodetectors but this was not possible on the present equipment.

CHAPTER 9: CONCLUSIONS AND FURTHER WORK.

9.1 Conclusions.

In this thesis the techniques of optical sensing of mechanical position have been reviewed in chapters two and three. The fabrication of gratings on silicon has been investigated and the problem of mask to wafer alignment in photolithography has been analysed in chapter five.

The feasibility of encoding absolute position by superimposing a relatively coarse-pitch coded pattern on a linear grating of finer pitch has been demonstrated in chapter seven and it has been shown that such a combined scale could form the basis of a hybrid transducer. It could be read by an array of photodiodes for absolute position determination, or by a suitable design of moiré fringe reading head for incremental operation with fringe interpolation to give finer resolution, or by a combination of the two types of reading head in a single unit.

A two-dimensional position encoder has been designed, fabricated and demonstrated in the laboratory. It was initially intended for use in small-scale instruments where a resolution of 1 micron and a range of up to 200 mm would be appropriate and this has been shown to be feasible.

The principle of a large-scale position encoder appropriate to the navigation of automated guided vehicles by reference to coded patterns on the ceiling has been demonstrated in the laboratory. A patent application has

been filed [91]. The patent rights have now been assigned to BTG and an initial market survey by independent consultants has been funded. Their report on the possible application to AGV navigation was basically favourable. The next phase in the development will require collaboration with an industrial partner and this is being investigated by BTG and Unived Technologies Ltd.

The benefit of using small sections of two-dimensional coded pattern and an associated reading head to establish the global alignment of silicon wafers has been discussed. In chapter eight, the detection of two-dimensional patterns of appropriate dimensions with a video camera has been demonstrated using a wafer stepper in a simulation of the worst-case build up of process layers.

In chapter six, the techniques of microfabrication were used to produce gratings on silicon for use in displacement transducers. The optical properties of vee-groove gratings have been used to good advantage in the design of a miniature XY reading head which has been shown to be capable of intensity modulation approaching 100%. Other applications of vee-groove gratings have been identified. The University of Edinburgh Quantum Fund is backing the development of a prototype Fetal Heart Monitor. This requires a lightweight, non-contacting microdisplacement transducer to sense the movement of the abdomen caused by the fetal heartbeat. An optical approach using vee-groove gratings as constant deviation mirrors is being evaluated.

The alignment requirements of a 'flash-on-the-fly' wafer stepper have been analysed in chapter eight and a dynamic alignment system based on two-dimensional grating patterns has been devised. The grating patterns have been fabricated on silicon on a series of test wafers and the contrast of the moiré fringe signals has been measured under realistic process conditions on a wafer stepper. A patent application has been filed [92].

9.2 Further Work on Chevron Gratings.

The work on chevron gratings is being pursued and developed for use in the next generation of wafer steppers and this could lead to considerable improvements in overlay accuracy and throughput. The next phase will include measurements of chevron signals on test wafers at realistic scan speeds to assess the signal processing requirements. However, the potential benefits of the alignment system can only be exploited by a complementary design of wafer stage which is capable of making the rapid local corrections in the cross-track direction during a high speed scan. Informal discussions with Professor S. Salter of the Department of Mechanical Engineering and Mr A. Gundlach of the Edinburgh Microfabrication Facility have led to collaboration on the mechanical design of a scanning stage with a dynamic correction capability. This work is well advanced and calculations have shown that computer control of trajectory is entirely feasible at scan speeds in excess of 500 mm/second. The combination

of trajectory control with a novel mechanical drive and guidance system will enhance the positioning repeatability and hence the overlay accuracy which can be achieved. The target specification is a standard deviation of 25 nm when operating on 200 mm diameter wafers.

The ability to measure deviation from a straight line or to measure X and Y overlay errors from a single axis scan could be applied the other way round, i.e. in the monitoring of stepper performance and in the 'matching' of a series of wafer steppers. The problem of matching steppers arises because it is desirable to have all the steppers in a production area interchangeable so that any layer of any product can be printed on any stepper. This gives maximum flexibility of production scheduling and allows for downtime on equipment.

A description of the current methods of matching steppers and a proposed alternative approach using chevron gratings is given in Appendix 2. In essence, the stepper under test would be used to print a chequerboard pattern on a wafer. This wafer would then be mounted on a step-and-scan stage where a relatively simple optical system would be used to interrogate the chequerboard pattern and thus produce a wafer map of XY placement accuracy and uniformity of critical dimensions.

To summarise, the combination of chevron grating measurement and computer control of stage trajectory could form the basis of an instrument for measuring and matching the performance of wafer steppers or it could be incorporated into the next generation of wafer stepper as

a dynamic alignment system.

Following a presentation on the dynamic alignment system to the UK Stepper Users Group, an invitation was received from a major electronics company to join a consortium of European organisations who are collaborating on a possible Esprit II project. After technical discussions, a proposal to develop a prototype stage and alignment system has been submitted to the companies concerned and it has been agreed that it will be included in the final project proposal under Esprit II.

APPENDIX 1: PROCESS SCHEDULE FOR TEST WAFERS.

EDINBURGH MICROFABRICATION FACILITY

N-CHANNEL SILICON GATE VLSI

BATCH NUMBER: 656 START DATE: 27/8/86
MASK SET: DALN stepping pitch 6.0 mm. Framing 5.6 mm
STARTING MATERIAL: 14-20 ohm.cm.(100) P-type, 3in.Dia.
No. OF WAFER STARTS: 8

INITIAL CLEAN

10 min. boil in 2:1, Sulphuric acid:Hydrogen peroxide in Teflon jig
D.I water wash
Dip 3 min. in 10% HF in Polypropylene jig
Wash and spin dry

INITIAL OXIDE

Furnace No.1, 950oC, idling on oxygen
Preset gas flows as follows:

Oxygen	20%	(1.5 l/min.)
HCl	15%	(0.15 l/min.)
Hydrogen	10%	(1.7 l/min.)

Load wafers into furnace with Oxygen only flowing.
5 min.Oxygen + HCl
10 min.Oxygen + HCl + Hydrogen
5 min.Oxygen

Measure oxide thickness:

SILICON NITRIDE DEPOSITION

Furnace No.3, 800oC
Preset flows:Dichlorosilane,30 cc/min. Ammonia,90 cc/min.
Deposition time: min. (aim for 500 Angstroms)
Pressure during deposition: mTorr

Measure Si3N4 thickness:

1st PHOTO (POSITIVE RESIST) LAYER No. dacb

HMDS vapour box prime for 30 min.
Spin HPR 204 at 6000 rpm for 30 secs
Soft bake at 105oC for 30 min in static oven

Align and expose for secs. (Stepper)
Develop in 1 vol LSI 2 Developer, 3 vols DI water at 30oC for 60 secs
Inspect for proper development.

Measure resist image: microns. SQUARES MUST NOT TOUCH!

Hard bake at 130,oC for 30 min. in static oven
Inspect for proper baking

4:1 ETCH

Immerse in 4:1, Ammonium Fluoride soln.(40%w/v) : HF
Etch time: 30 secs
Wash and spin dry

SILICON NITRIDE RIE ETCH

RIE etch to clear patterns

RESIST STRIP

Immerse in Fuming Nitric Acid 10 min
Wash and spin dry
Inspect for removal of resist.

Measure etched image: microns

KOH SILICON ETCH

Pre-heat solution of 40% W/V Potassium hydroxide in water to 85oC.
Immerse wafers in etch until pits are of required depth. (Approx. 5 min)
Wash in DI water to 10 Mohm.cm. and spin dry

REMOVE ONE WAFER & LABEL No.1

SILICON NITRIDE WET ETCH

Heat Orthophosphoric Acid to 165oC
Immerse wafers on Teflon jig for 1hr or until nitride removed.
Wash and spin dry

INITIAL OXIDE

Furnace No.1, 950oC, idling on oxygen
Preset gas flows as follows:

Oxygen	20%	(1.5 l/min.)
HCl	15%	(0.15 l/min.)
Hydrogen	10%	(1.7 l/min.)

Load wafers into furnace with Oxygen only flowing.
5 min.Oxygen + HCl
5 min.Oxygen + HCl + Hydrogen
5 min.Oxygen

Measure oxide thickness:

SILICON NITRIDE DEPOSITION

Furnace No.3, 800oC
Preset flows: Dichlorosilane,30 cc/min. Ammonia,90 cc/min.
Deposition time: min. (aim for 1000 Angstroms)
Pressure during deposition: mTorr

Measure Si3N4 thickness:

2nd PHOTO (POSITIVE RESIST) LAYER No. daln

HMDS vapour box prime for 30 min.
Spin HPR 204 at 6000 rpm for 30 secs
Soft bake at 105oC for 30 min in static oven

REMOVE ONE WAFER & LABEL No.2

Align and expose for secs. (Stepper)
Develop in 1 vol LSI 2 Developer, 3 vols DI water at 30oC for 60 secs
Inspect for proper development.
Hard bake at 130 degrees for 30 mins in static oven.
Inspect for proper baking

4:1 ETCH

Immerse in 4:1, Ammonium Fluoride soln.(40%w/v) : HF
Etch time: 30 secs
Wash and spin dry

SILICON NITRIDE RIE ETCH

RIE etch to clear patterns

RESIST STRIP

Immerse in Fuming Nitric Acid 10 min
Wash and spin dry
Inspect for removal of resist.

Measure etched image: microns

PRE-DIFFUSION CLEAN

Dip in 10% HF for 15 secs.
Wash and spin dry.

FIELD OXIDE

Furnace No.7, 950oC, idling on oxygen
Preset gas flows as follows:
Oxygen 24.5% (1.22 l/min.)

Hydrogen	20%	(2.0 l/min.)
HCl	10%	(0.1 l/min.)

Load wafers into furnace with Oxygen only flowing.
5 min.Oxygen + HCl
0.5 hours Oxygen + Hydrogen + HCl
2.25 hours Oxygen + Hydrogen
5 min.Oxygen

Measure oxide thickness:

OXIDE ETCH

Immerse in 4:1, Ammonium Fluoride soln.(40%w/v) : HF for 15 secs.
Wash and spin dry

SILICON NITRIDE WET ETCH

Heat Orthophosphoric Acid to 165oC
Immerse wafers on Teflon jig for 0.5 hr or until nitride removed.
Wash and spin dry

OXIDE ETCH

Immerse in 4:1, Ammonium Fluoride soln.(40%w/v) : HF to dewet scribelines
Wash and spin dry

Measure etched image: microns

3rd PHOTO (POSITIVE RESIST) LAYER No. daln

ONE WAFER ONLY (No.3)

Pre-spin bake,
furnaceNo.1, 950oC, Nitrogen 20% (2 l/min), 5 min.
Spin HPR 204 at 6000 rpm for 30 secs
Soft bake at 105oC for 30 min in static oven

PRE-DIFFUSION CLEAN WAFERNo. 4 - 8

Dip in 10% HF for 15 secs.
Wash and spin dry.

SACRIFICIAL OXIDE

Furnace No.1, 950oC, idling on oxygen
Preset gas flows as follows:

Oxygen	20%	(1.5 l/min.)
HCl	15%	(0.15 l/min.)
Hydrogen	10%	(1.7 l/min.)

Load wafers into furnace with Oxygen only flowing.
5 min.Oxygen + HCl
5 min.Oxygen + HCl + Hydrogen
5 min.Oxygen

Measure oxide thickness:

10% HF DIP

Dip in 10% HF for 15 secs.
Wash and spin dry.

GATE OXIDE & ANNEAL

Furnace No.1, 950oC, idling on oxygen
Preset gas flows as follows:

Oxygen	20%	(1.5 l/min.)
HCl	15%	(0.15 l/min.)
Hydrogen	10%	(1.7 l/min.)

Load wafers into furnace with Oxygen only flowing.
38 min.Oxygen + HCl
15 min.Nitrogen

Measure oxide thickness:

POLY-SILICON DEPOSITION

Furnace No.4, 600oC
Preset flows: Silane,60 cc/min.
Deposition time: 40 min. (aim for 4000 Angstroms)
Pressure during deposition: mTorr

Measure poly-silicon thickness:

PHOSPHORUS DEPOSITION (SOLID SOURCE)

Furnace No.5, 850oC, idling on Nitrogen
Preset gas flows as follows:

Nitrogen	50	(2.0 l/min.)

Insert wafers at 4 ins./min.
20 min. ramp at 8.1oC/min. to up 1000oC
15 min. soak
20 min. ramp at 8.1oC/min. down to 850oC
Remove wafers at 4ins./min.

PHOSPHORUS DEGLAZE

Immerse for 30 secs. in 10% HF (1 vol HF, 9 vols DI)
Wash and spin dry

POLY OXIDE

Furnace No.1, 950oC, idling on oxygen
Preset gas flows as follows:

Oxygen	20%	(1.5 l/min.)
HCl	15%	(0.15 l/min.)
Hydrogen	10%	(1.7 l/min.)

Load wafers into furnace with Oxygen only flowing.
5 min.Oxygen + HCl
10min.Oxygen + HCl + Hydrogen
5 min.Oxygen

4th PHOTO (POSITIVE RESIST) LAYER No. daln

WAFER No. 4 ONLY

Spin HPR 204 at 6000 rpm for 30 secs
Soft bake at 105oC for 30 min in static oven

REFLOW PYRO DEPOSITION NO PHOSPHINE WAFER 5 - 8

PWS 2000 Hotplate at 430oC, in right hand rest position.
Preset SPEED: 750 NOTE DIFFERENT SPEED FROM USUAL
Preset gas flows as follows:
Nitrogen(02),80 (4.0 l/min):Nitrogen(SiH4),60 (2.9 l/min)
5%Silane,110 (1.3l/min): Oxygen,60 (0.65l/min)
Water flow, 100

Include one fresh 14-20 ohm.cm. P-type test wafer per batch.

Place up to 6 wafers onto hotplate as close as possible
to centre.
Press button <-- to deposit
When hotplate stops, remove wafers to steel worktop with
Bernoulli tweezer
Reload with fresh wafers and press button -->
Continue with whole batch.

Measured thickness:

NOTE: Proceed immediately to First Reflow

FIRST REFLOW
FURNACE No. 2 (02)
Temperature: 1000oC NOTE LOWER TEMPERATURE
Idling ambient: Oxygen

Preset gas flows as follows:

Oxygen	50	(2.0 l/min.)

20 min. furnace time

DENSIFICATION OF REFLOW PYRO

Furnace No.7, 950oC, idling on oxygen
Preset gas flows as follows:
Oxygen 28% (1.4 l/min.)
Hydrogen 20% (2.0 l/min.)
Load wafers into furnace with Oxygen only flowing.
5 min.Oxygen
15 min.Oxygen + Hydrogen
5 min.Oxygen

NOTE: Proceed immediately to resist spin for contact photo.

5th PHOTO (POSITIVE RESIST) LAYER No. daln

WAFER No. 5 ONLY

Spin HPR 204 at 6000 rpm for 30 secs
Soft bake at 105oC for 30 mins in static oven

PHOSPHORUS DEPOSITION (SOLID SOURCE)

WAFER No. 6 - 8 ONLY

Furnace No.5, 850oC, idling on Nitrogen
Preset gas flows as follows:
Nitrogen 50 (2.0 l/min.)

Insert wafers at 4 ins./min.
20 min. ramp at 8.1oC/min. to up 1000oC
15 min. soak
20 min. ramp at 8.1oC/min. down to 850oC
Remove wafers at 4ins./min.

PHOSPHORUS DEGLAZE

Immerse for 30 secs. in 10% HF (1 vol HF, 9 vols DI)
Wash and spin dry

PRE-ALUMINIUM EVAPORATION CLEAN

Dip 20 secs. in reflow etch:
25 vols Ammonium Fluoride soln.(40%w/v),1 vol HF
Wash and spin dry

ALUMINIUM EVAPORATION (Al-Si)

Load wafers on palettes and load into Balzers BAS 450 coater.
Pump system to 5e-6 or better with Meissner trap.
Close shutter
Throttle pump and admit argon at 2e-3.
Set integrator at 9500, Range 3 (Aim for 1 micron)
Run up Aluminium/Silicon target to 6 kW.
Open shutter until integrator times out.

Warm up Meissner and chamber.
Vent system and remove wafers.

6th PHOTO (POSITIVE RESIST) LAYER No. daln

WAFER No. 6 ONLY

Spin HPR 204 at 4000 rpm for 30 secs
Soft bake at 105oC for 30 min in static oven

END OF PROCESS.

APPENDIX 2: MATCHING OF WAFER STEPPERS.

The Requirement.

The problem of matching steppers arises because it is desirable to have all the steppers in a production area interchangeable so that any layer of any product can be printed on any stepper. This gives maximum flexibility of production scheduling and allows for downtime on equipment, but it also implies that the performance of all the XY stages and optical systems must lie within a fairly narrow tolerance band.

When steppers are being operated in 'blind step' mode with only global alignment of the wafer, matching is a time-consuming problem. First, the XY stages must be checked for repeatability and then for accuracy to ensure that the XY stepping grid of all the machines is within the required tolerance band. Second, the size and shape of the image produced by each machine, i.e. magnification and distortion, must be measured to ensure that the overlay tolerance within each exposure field is acceptable. Third, the global wafer alignment system and reticle alignment system must be checked for offsets and image rotation relative to the XY grid, see figure A2.1. Finally, the exposure system must be checked for accuracy of dose and uniformity over the image field. When steppers are being operated in die by die alignment mode the matching of the XY stages is not important but it is still necessary to measure the image magnification and

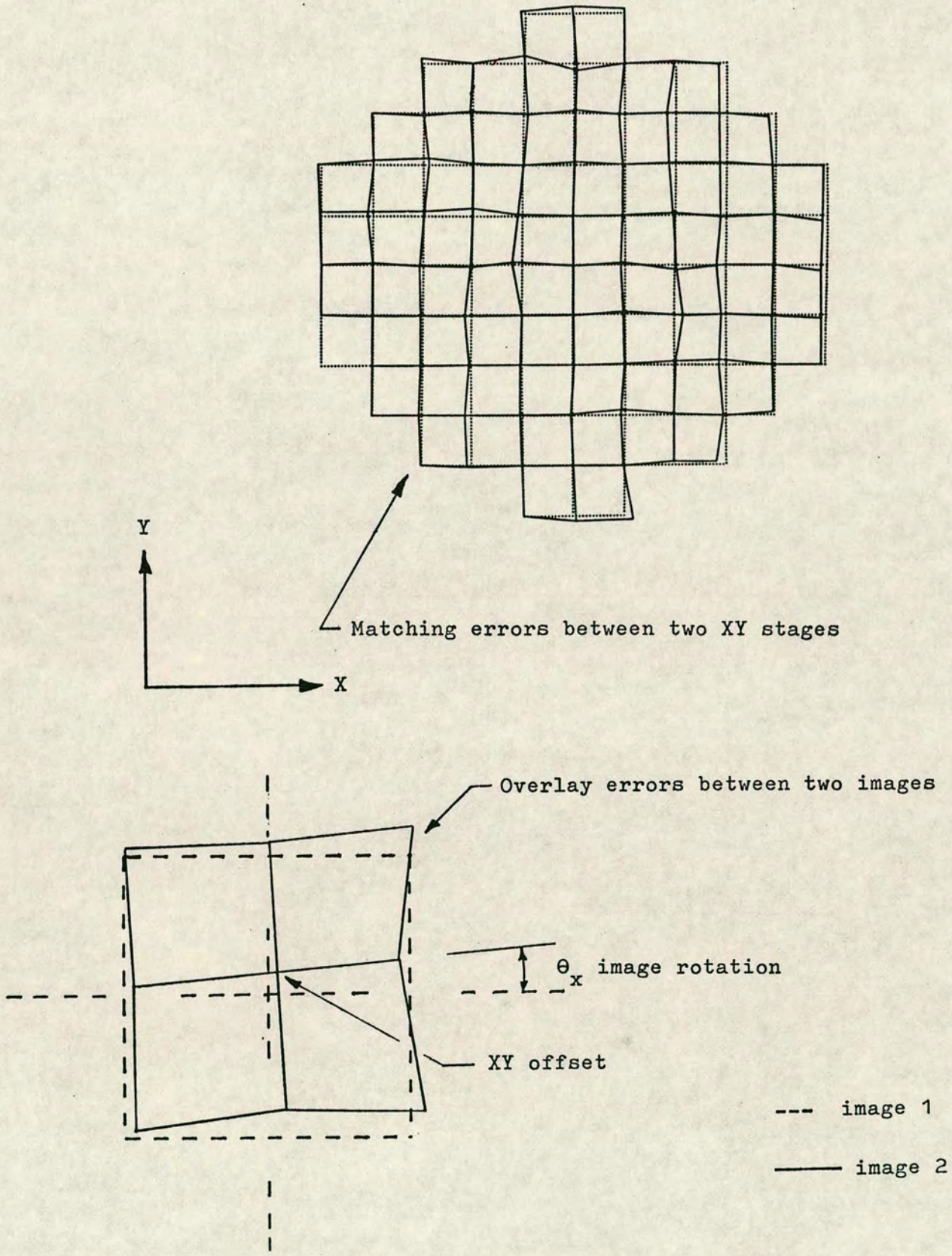

Figure A2.1 MATCHING OVERLAY ERRORS BETWEEN TWO STEPPERS

distortion on each machine and to calibrate any systematic offsets in the die by die alignment system.

Current Methods of Matching.

Test reticles are available to enable measurements of XY misalignment, magnification, distortion, and image rotation to be made manually by printing a matrix of interlocking vernier patterns and reading them using an optical microscope, [97]. These verniers can, with care, be read to +/- 50 nm but it is a time-consuming process since a large number of readings have to be taken and averaged to get a meaningful result. As an example, consider the measurement of magnification and distortion. In the usual procedure, a square image is projected onto the wafer and stepped and repeated at a pitch which exactly matches its nominal size. Verniers at the corners and in the middle of the sides are thus caused to enmesh and any departure from nominal can be read optically, see figure A2.2. This test uses the blind step grid generated by the XY stage as a reference or standard against which the size and shape of the image is compared. The measurements are thus subject to random variations due to the repeatability errors of the XY stage and hence it is essential to take vernier readings from at least 10 and preferably more than 50 sites, depending on the stage repeatability.

The other measurements associated with matching of image shape and placement are essentially similar,

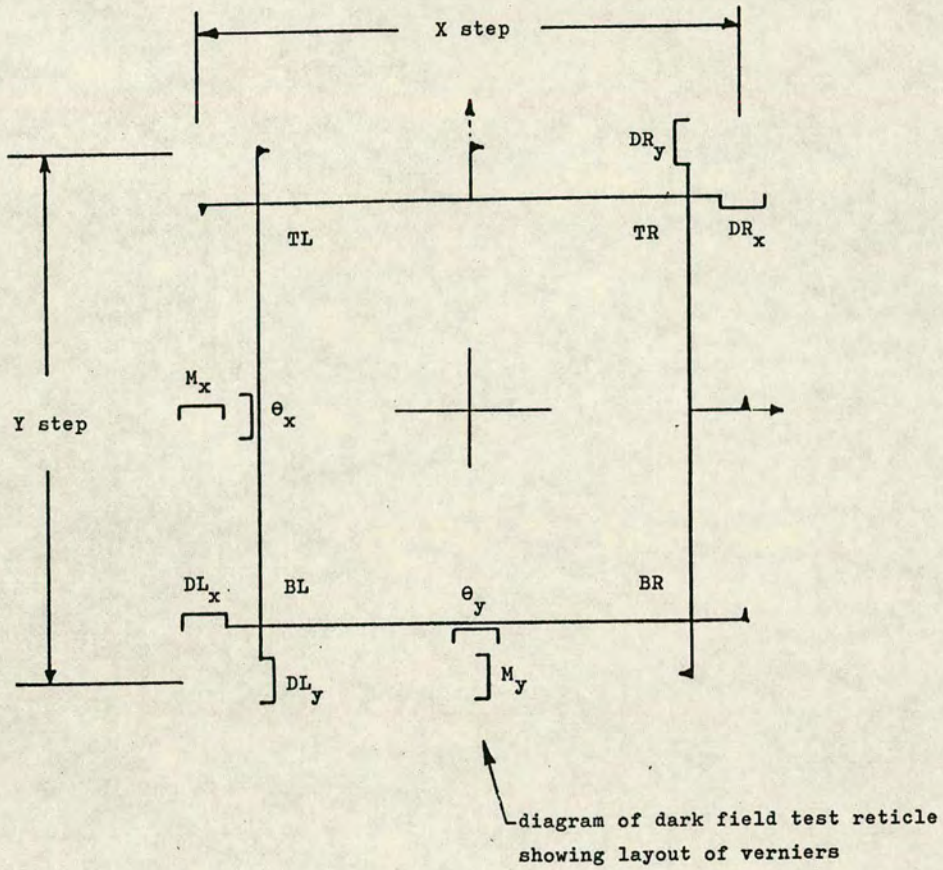

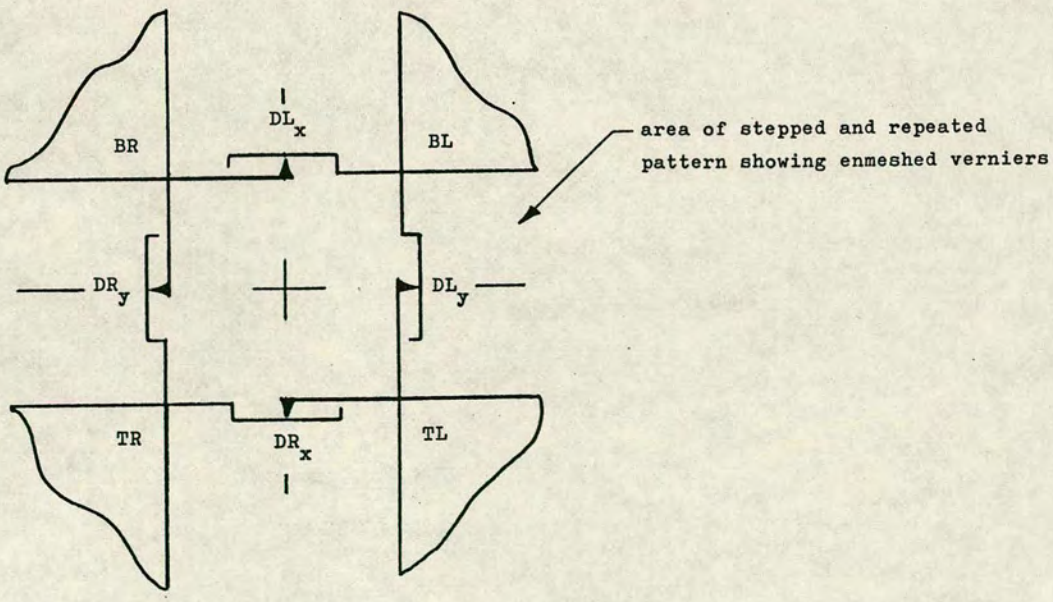

Figure A2.2 USE OF A VERNIER TEST RETICLE

involving XY error measurements at a number of points within each image field such as the centre, along the major axes and along the diagonals.

These measurements have been automated in the interests of speed and accuracy. Three approaches are now in use:

1. If the vernier patterns are replaced or supplemented by 'block-in-a-box' structures, the X and Y errors can be established using an automatic linewidth measuring system to compare the clearances at each side of the block in the box.

2. If the block-in-a-box structure is replaced by a pair of alignment marks suitable for the die by die alignment system, the stepper can be used to inspect the developed resist pattern and measure the X and Y errors using its own die by die alignment system, [98]. Clearly, checks have to be included to calibrate the alignment system in order to ensure the validity of this approach. A number of wafer steppers now offer some sort of self checking 'metrology package' of this type to assist with matching.

3. Suitable test patterns can be etched in an electrically conducting layer such as poly-silicon to allow testing on an automatic prober. This approach was developed by Perloff [99] as the basis of the 'Prometrix' instruments for stepper evaluation. The advantages of electrical testing are its speed and sensitivity and the ability to measure several parameters simultaneously at each site, using hardware which is relatively inexpensive.

Software is available to convert the mass of data into an understandable form. The main disadvantage is the need to deposit a suitable layer of material and then etch it for each test, a process which introduces delay and potential uncertainty to the results. Also, the choice of substrate material is restricted and it is not possible, therefore, to measure the effect of different substrate materials on the control or uniformity of linewidth.

An Alternative Approach.

It would be possible to characterise a wafer stepper by optical inspection of suitable test patterns which had been exposed and developed in a layer of photoresist. This could be done on any substrate material. The test pattern would have to provide a sensitive indication of both XY placement and variation of critical feature size over the image field and would have to be suitable for automatic inspection.

A chequerboard pattern of squares in the range 2 - 5 micron is a suitable test pattern. It has been established that such a pattern is a very sensitive indicator of variations in feature size within an exposure field and across a wafer, [100]. By measuring the reflected light from a developed resist pattern, a map showing small variations in linewidth can be produced, based on a known relationship between the reflected intensity and the size of the squares in the chequerboard. (To first order, a 5% change in linewidth would produce a

10% change in reflected intensity.) Work is in hand to produce an automatic linewidth monitor based on this principle.

Information on XY placement can be obtained by interrogating the chequerboard pattern using two short sections of linear grating, or a chevron grating with lines at +/- 45 degrees to the X and Y axes, as previously described. The detector would take the form of a microscope or similar optical system having a field of view of about 1 mm diameter with an illuminator, index gratings and photodetectors to provide the output signals from the moiré fringes and a measure of the reflected intensity. The wafer would be mounted on a high speed step-and-scan stage with a laser interferometer XY measuring system and computer control of the scan trajectory. After global alignment and levelling, the wafer would be scanned and the signals would be sampled at appropriate intervals to produce a wafer map of reflected intensity and XY placement information. The errors would be processed to provide magnification, distortion, rotation and XY position information relative to the XY grid generated by the step-and-scan stage. Thus, unlike the existing methods which compare one stepper with another, the step-and-scan stage would be used as a standard or reference against which all test wafers would be measured.

The stability and repeatability of such a stage would be crucial to the success of this approach. The long-term stability would be ensured by the choice of

materials, the design and the environmental isolation of the instrument. The stability of laser interferometers in this type of measurement is well known and automatic wavelength compensation would be applied. Known systematic errors would be removed by continuous dynamic control of the scan trajectory and isolation of the wafer stage from all other perturbing forces by an outer guard stage. The repeatability of the XY stage should be better than +/- 25 nm (1 sigma).

The absolute accuracy of the XY stage is of less importance, but it would be essential to include a means of calibrating the systematic errors on a regular basis. If the stability of the laser interferometer as a standard were accepted, the XY scale accuracy would not be in doubt but it would still be necessary to establish the systematic geometrical errors of the stage mechanism. To do this, the wafer stage would have a means of indexing the wafer in steps of 90 degrees in the XY plane. A test wafer would be scanned four times in quick succession, being indexed by 90 degrees between scans. The results would be processed to extract the systematic errors of the stage, on the assumption that the shape of the test wafer remained constant during the four scans. Although a 'special' wafer with an etched chequerboard could be used for this test, any wafer with an overall chequerboard pattern would suffice. Alternatively, the pattern could be etched into the surface of the wafer chuck itself. Since an entire 200 mm wafer could be scanned on a grid of, say, 5 mm in less than 60 seconds, the instrument

could be used during maintenance and adjustment of steppers to provide rapid evaluation of performance.

The measurement of alignment offsets requires measurement of the relative XY placement of two sets of images: the first printed as level 1 to which the second is aligned and exposed. A test reticle in the form of a swatch of chequerboard pattern with the appropriate alignment marks would be printed on alternate sites as level 1. After development and/or etching, the wafer would be aligned and the intermediate sites would be exposed as level 2. The combined pattern would then be scanned as described above to measure the XY position of every image and hence the relative misplacement of the alternate images would be calculated.

Thus the combination of a relatively simple optical system and a step-and-scan stage with computer control of trajectory could form the basis of an instrument for evaluating and monitoring the performance of wafer steppers. The ability to measure and map variations in critical dimensions across wafers would also be of benefit in general process development by providing information on uniformity of layer deposition, patterning and etching.

REFERENCES

1. RAYLEIGH, Lord (1874) Phil Mag 47, 81, p193
2. MERTON, T. (1949) "On the production and ruling of diffraction gratings."
   Proc. Roy. Soc. A 201, p187-191, Oct. 1949
3. ROBERTS, P.W. (1950) "A method for the summation of irregular movements."
   J. Sci. Instrum. 27, p105-106, Apr. 1950.
4. DEW, G.D., & SAYCE, L.A. (1951) "On the production of diffraction gratings I: the copying of plane gratings."
   Proc. Roy. Soc. A, 207, p278-284, June 1951.
5. WILLIAMSON, D.T.N., SHEPHERD A.T., & WALKER, G.S. (1953) Brit. Pat. No. 760,321
6. SHEPHERD, A.T., WALKER, G.S. (1955)
   Brit. Pat. No. 810,478.
7. GUILD, J. (1956) "The Interference Systems of Crossed Diffraction Gratings:Theory of Moiré Fringes." Oxford: Clarendon Press.
8. GUILD, J. (1960) "Diffraction Gratings as Measuring Scales" London: Oxford University Press.
9. BERGER, L. (1984) "Grating interferometry for positioning the X-Y stages of a wafer stepper."
   Proc. SPIE, Int. Soc. Opt. Eng. (USA) 503, p130-134.
10. IWOKA, H., & AKIYAMA, K. (1984) "A high resolution laser scale interferometer."
    Proc. SPIE, Int. Soc. Opt. Eng. (USA) 503, p135-139.

11. LUXMOORE, A.R. (Ed.) (1983) "Optical Transducers and Techniques in Engineering Measurement" London: Applied Science Publishers.

12. PURFIT, G.L., WOODWARD, C.A.W., & PETTIGREW, R.M. (1974) "Grating technology developments" Proc. NELEX 74, National Engineering Laboratory, East Kilbride.

13. HUTLEY, M.C. (1982) "Diffraction Gratings" London: Academic Press.

14. MICHELSON, A.A. (1927) "Studies in Optics" Chicago: U.P.

15. BURCH, J.M., PALMER, D.A. (1961) "Interferometric methods for the photographic production of large gratings."
Optica Acta (Internat.) 8, 1, p73-80, Jan.1961.

16. COWAN, J.J. (1984) "The recording and large scale replication of crossed holographic grating arrays using multiple beam interferometry."
Proc. SPIE Int. Soc. Opt. Eng. (USA) 503, p120-129

17. MILNE, A.D., STEVENSON, J.T.M., & MACKIE, R.D.L. (1978) "Optical production of large area patterns for microelectronics."
Proc. Microcircuit Engineering 78, Cambridge, 1978.

18. VARGADY, L.O. (1964) "Moiré fringes as visual position indicators" Appl. Opt. 3, 5, p631-6

19. TORII, Y., & MIZUSHIMA, Y. (1979) "Theory of alignment monitoring by diffraction from superimposed dual gratings" J. Opt. Soc. Am. 68, 12, p1716-31

20. BURCH, J.M. (1963) "The Metrological Application of Diffraction Gratings" in "Progress in Optics" (Ed.E.Wolf) Amsterdam: North Holland

21. SAYCE, L.A. (1972) "Gratings in metrology" J. Phys.E., 5, p193-198, Mar. 1972

22. SHEPHERD, A.T. (1978) "25 years of moiré fringe measurement" Proc. NELEX 78, National Engineering Laboratory, East Kilbride.

23. SHEPHERD, A.T. (1976) Brit. Pat. No: 1,525,049.

24. PALMER, D.A. (1960) "Moiré fringe reading head for use with a fine grating." J. Sci. Instrum. 37, 8, p261-262, Aug. 1960.

25. SAYCE, L.A., & JESPERSEN, K.I. (1970) Brit. Prov. Pat. No: 35141.

26. DEY, J., & JOHANNSMEIER K. (1980) "An advanced step and repeat aligner for VLSI." Proc. Microcircuit Engineering 80, Amsterdam 1980, p211-221.

27. PETTIGREW, R.M. (1977) "Analysis of grating imaging and its application to displacement metrology" Proc. SPIE Int. Soc. Opt. Eng. (USA) 136, p325-332

28. SHEPHERD, A.T., McLAREN, R.R. (1965) Brit. Pat. No: 1,051,744.

29. DAVIES, B.J., ROBBINS, B.C., WALLIS, C., & WILDE, R.W. (1960) "A high resolution measuring system using coarse optical gratings." Proc. IEE, 107B, p624-633

30. BARBER, D.L.A., ATKINSON, M.P. (1959) "Method of measuring displacement using optical gratings." J.Sci. Instrum. 36, 12, p501-504, Dec. 1959.

31. BRYAN, J.B. (1979) "The Abbé Principle revisited: an updated interpretation." Precision Eng. 1, 3, p129-132.

32. De LANG, H., FERGUSON, E.T., SCHOENAKER, G.C.M. (1969) "Accurate measurement of displacements by optical means." Philips Tech. Rev. 30, p149-160

33. SHEPHERD, A.T. Private Communication.

34. RUSSELL, A., PETTIGREW R.M., MESSER, H., ROBERTSON, A.R. (1976) "Recent trends in angular measurement using the optical grating." Proc. NELEX 76, paper no:14, National Engineering Laboratory.

35. McKEOWN, P.A., BENT, R.G., (1979) "Some developments in grating transducer systems." Precision Engineering 1, 1, p19-23

36. BLAIR, D.P., SYDENHAM, P.H. (1982) "Phase sensitive detection as a means to recover signals buried in noise" Instrument Science and Technology, Vol.1, Ed. B.E. Jones: Adam Hilger.

37. JONES, O.C., FORNO, C. (1975) "High frequency moiré fringe interpolation using electro optic crystals." Opt. Eng. 14, 3, p259-62.

38. CHETWYND, D.C. (1987) "Selection of structural materials for precision devices." Precision Eng. 9, 1, p3-6

39. JENKINS, F.A., AND WHITE, H.E. "Fundamentals of Optics" : McGraw Hill.

40. TSANG, W.T., WANG, S. (1975) "Preferentially etched diffraction gratings in silicon."
J. Appl. Phys. 46, 5, p2163-6

41. BASSOUS, E. (1978) "Fabrication of novel 3-dimensional microstructures by the anisotropic etching of (100) and (110) silicon."
IEEE Trans. Electron Devices, ED-25, p1178-85.

42. BEAN, K.E., (1978) "Anisotropic etching of silicon."
IEEE Trans. Electron Devices, ED-25, p1185-93.

43. ALLEN, D.M. (1981) "Anisotropic etching microtechnology" Precision Eng. 3, 3, p161-6.

44. DOANE, D.A. (1980) "Optical lithography in the 1 micron limit" Solid State Technol. 23, 8, p101-14.

45. WATTS, R.K., BRUNING, J.H. (1981) "A review of fine-line lithographic techniques: present and future."
Solid State Technol. 24, 5, p99-105.

46. WITTEKOEK, S. (1980) "Optical lithography for microcircuits."
Proc. Microcircuit Eng. '80, p155-170, Amsterdam 1980.

47. STEVENSON, J.T.M., GUNDLACH, A.M. (1986) "The application of photolithography to the fabrication of microcircuits."
J. Phys. E. Sci. Instrum. 19, p654-667.

48. MARKLE, D.A., (1974) "A new projection printer."
Solid State Technol. 17, 6, p50-53.

49. STOVER, H.L., PERLOFF, D., HASAN, T., HWANG, D., BLOME, G. (1980) "Characterisations of three wafer steppers and user implications."
Proc. Microcircuit Eng. '80, p223-37, Amsterdam 1980.

50. STOVER, H.L. (1981) "Stepping into the '80's with die x die alignment"
Solid State Technology, 24, 5, p112-20.

51. STEVENSON, J.T.M., ROBERTSON, J.M. (1982) "The performance of DSW machines for VLSI research."
Microelectronics Journal, 13, 6, p33-37.

52. MILLER, V., STOVER, H.L. (1985) "Submicron optical lithography: i-line wafer stepper and photoresist technology." Solid state Technology, 28, 1, p127-136.

53. NUHN, M., YAO, S.K., AVRIT, B. (1987) "I-line wafer stepper used for low volume production of 0.5 micron GaAs integrated circuits."
Solid State Technology, 30, 2, p81-84.

54. BIESTERBOS, J., BOUWER, A., v.ENGELEN, G., v.d.LOOIJ, G., v.d.WERF, J. (1987) "A submicron I-line wafer stepper." Solid State Technology, 30, 2, p73-76.

55. MARKLE, D.A. (1984) "The future and potential of optical scanning systems."
Solid State Technology, 27, 9, p159-166.

56. POL, V. (1987) "High resolution optical lithography: a deep ultraviolet laser-based wafer stepper."
Solid State Technology, 30, 1, p71-76.

57. HOLOGRAF, 2366 Walsh Avenue, Santa Clara, CA 95051, USA.

58. BROERS, A.N. (1985) "The submicron lithography labyrinth." Solid State Technology, 28, 6, p119-126.

59. LAURIA, J., KEREKES, T.(1980) "Automatic alignment technique for the 700SLR/800SLR wafer steppers."
Proc. Microcircuit Engineering '80, Amsterdam, 1980.

60. KING, M.C., BERRY, D.H. (1972) "Photolithographic mask alignment using moiré fringe techniques." Applied Optics, 11, p2455-

61. FLANDERS, D.C., SMITH, H.I., AUSTIN, S. (1977) "A new interferometric alignment technique." Appl. Phys. Lett. 31, 7, p426-428.

62. KLEINKNECHT, H.P. (1979) "Diffraction gratings as keys for automatic alignment in proximity and projection printing." SPIE Developments in Semiconductor Microlithography IV, 174, p63-69.

63. LYSZCZARZ T.M., FLANDERS, D.C., ECONOMOU, N.P., DeGRAFF, P.D. (1981) "Experimental evaluation of interferometric alignment techniques for multiple mask registration." J. Vac. Sci. Technol. 19, 4, p1214-1218.

64. LAVINE, J.M., FISH, R.B., WEGER, A.J., SIMPSON, C. (1985) "A direct-reticle-referenced alignment system." SPIE Optical Microlithography IV, 538, p57-69

65. YAO, S-K (1987) "Optical consideration in target alignment using non-actinic wavelength microscope." Presented at SPIE Conference on Microlithography, Santa Clara, CA, USA, March 1987.

66. SUZUKI, A. (1985) "Double telecentric wafer stepper using laser scanning method." SPIE Optical Microlithography IV, 538, p2-8.

67. WILCZYNSKI, J.S. (1979) "Optical step and repeat camera with dark field automatic alignment." J.Vac.Sci.Technol., 16 (6), Nov/Dec 1979, p1929-1933.

68. HERSHEL, R.S. (1979) "Autoalignment in step and repeat wafer printing." SPIE Developments in Semiconductor Microlithography IV, 174, p54-62.

69. KINOSHITA, H., UNE, A., IKI, M. (1983) "A dual grating alignment technique for x-ray lithography." J.Vac.Sci.Technol.B 1(4), Oct.-Dec. 1983, p1276-1279.

70. FAY, B., TROTEL, J., FRICHET, A. (1979) "Optical alignment system for submicron x-ray lithography" J.Vac.Sci.Technol., 16(6), Nov./Dec. 1979, p1954-1958.

71. FELDMAN, M., WHITE, A.D., WHITE, D.L. (1981) "Application of zone plates to alignment in microlithography." J.Vac.Sci.Technol., 19(4), Nov./Dec. 1981, p1224-1228.

72. NELSON, D.A., DIMILIA, V., WARLAUMONT, J.M. (1981) "A wide range alignment system for x-ray lithography." J.Vac.Sci.Technol., 19(4), Nov./Dec. 1981, p1219-1223.

73. BRUNNER, T.A., SMITH, S.D. (1984) "Moiré technique for overlay metrology" SPIE Integrated Circuit metrology II, 480, p164-170.

74. BOUWHUIS, G., WITTEKOEK, S. (1979) "Automatic alignment system for optical projection printing." IEEE Trans. Electron Devices, ED-26, 4, p723-728.

75. WITTEKOEK, S. (1980) "Step-and-repeat wafer imaging." Solid State Technol., 23, 6, June 1980, p80-84.

76. WITTEKOEK, S., van der WERF, J. (1985) "Phase gratings as waferstepper alignment marks for all process layers." SPIE Optical Microlithography IV, 538, p24-31, 1985.

77. van der BRINK, M.A., LINDERS, H.F.D., WITTEKOEK, S. (1986) "Direct-referencing automatic two-points reticle-to-wafer alignment using a projection column servo system."
SPIE Optical Microlithography V, 633, p60-71.

78. DUBROEUCQ, G.M., LACOMBAT, M., SULLEROT, D. (1980) "Double diffraction gratings as keys for high contrast alignment on wafer steppers"
Microcircuit Engineering '80, Amsterdam 1980.

79. MURAKAMI, S., MATSUURA, T., OGAWA, M., UEHARA, M. (1985) "Laser step alignment for a wafer stepper."
SPIE Optical Microlithography IV, 538, p9-16.

80. NOMURA, N., MATSUMURA, T., YONEZAWA, T., KUGIMIYA, K. (1985) "A new interferometric alignment technique with holographic configuration."
Jap.J.Appl.Physics, 24, 11, Nov.1985, p1555-1560.

81. YAMASHITA, K., NOMURA, N., TAKEMOTO, T. (1986) "Holographic nanometer alignment for a wafer stepper."
18th (1986 Int.) Conf. on Solid State Devices & Materials, Tokyo, 1986, p25-28.

82. WHITWELL, A.L. (1973) "Moire techniques ensure unerring positional control."
Design Engineering, Nov. 1973, p45-48.

83. RUSSELL, A. (1966) "An absolute digital measuring system using an optical grating and shaft encoder."
Part 1: Instrum. Rev., 13, June 1966, p234-237.
Part 2: Instrum. Rev., 13, July 1966, p283-286.

84. KENNEDY, C.J., SHEPHERD, A.T., THOMAS, G.I. (1970) British Patent No. 1 284 641

85. SILKIN, L.B. (1976) "Miniature displacement digitiser." Telecomm. & Radio Eng. Part 1, 30, 6, p37-38.

86. JONES, B.E., ZIA, K. (1981) "Digital displacement transducer using pseudo-random binary sequences and a microprocessor." Trans. Inst. M C , 3, 1, Jan-Mar 1981, p13-20.

87. JOHNSTON, J.S. (1983) UK Patent Application No. GB 2 126 444 A.

88. CHOW, W. (1986) "A position recognition custom chip" M.Sc. Project Report MSP44, University of Edinburgh, Sept. 1986.

89. Micro-Robotics EV1 Camera, Micro-Robotics Ltd., 264 Newmarket Road, Cambridge.

90. GREEN, J. (1985) "A new super camera for vision systems" Robotics Age, July 1985, p6-9

91. JORDAN, J.R., MACKIE, R.D.L., STEVENSON, J.T.M. (1987) "Determination of position." UK Patent Appl. No. 8701889.

92. GUNDLACH, A.M., SALTER, S.H., STEVENSON, J.T.M. (1987) "Improved registration method in photolithography and equipment for carrying out this method." Patent Appl. No. PCT/GB87/00444.

93. MAXWELL, G.D. (1987) Ph.D. Thesis to be submitted 1987, University of Edinburgh.

94. ALEXANDER, W., ANDERSON, S. (1986) "Pseudo random binary sequences and absolute 2-D positioning.", Instrumentation and Digital Systems Laboratory Report, University of Edinburgh, Sept. 1986.

95. GUNDLACH, A.M., Private Communication.

96. 'Questek' Excimer Laser, Lambda Photometrix Ltd., Batford Mill, Harpenden, Herts, AL5 5BZ

97. SCHNEIDER, W.C., (1979) "Testing the Mann 4800 DSW Wafer Stepper" SPIE Developments in Semiconductor Microlithography IV, vol 174, 1979.

98. SWANSON, P., ALONZO, G., DEY, J. (1984) "Automatic self-testing of wafer stepper matching." Eaton Corporation, Microlithography Systems Division, Application Note: MS 106.

99. PERLOFF, D.S. (1978) " A four-point electrical measurement technique for characterizing mask superposition errors on semiconductor wafers." IEEE J. Solid State Circuits, SC-13, 4, p436-444.

100. HOLWILL, R.J., STEVENSON, J.T.M., WALTON, A.J., ROBERTSON, J.M. (1986) "Wafer scale etch assessment using single layer test patterns." IEEE VLSI Workshop on Test Structures, Long Beach, California, February, 1986.